AN ABSTRACT OF THE THESIS OF

Sifen Luo for the degree of Doctor of Philosophy in Electrical and Computer Engineering presented on September 15, 1993.

Title: Analysis and Applications of Layered Multiconductor Coupled Slot and Strip-Slot Structures

Redacted for privacy

Abstract approved: _____
Vijai K. Tripathi

Layered multiconductor coupled slot and strip-slot structures are characterized by introducing the full-wave modal analysis as well as the quasi-TEM spectral domain technique. In the modal analysis, the electric and magnetic fields are constructed in terms of modal fields in different regions. Application of the boundary conditions at interfaces for the tangential components of the electric and magnetic fields results in the dyadic Green's function, which interrelates the tangential currents and electric fields at the boundaries of the layered structure. The slot fields and strip currents are expanded in terms of a set of known basis functions with unknown coefficients. Use of the Galerkin method leads to a set of algebraic equations. The non-trivial solutions for the propagation constants are found by setting the determinant of the algebraic equations equal to zero. All the other normal mode parameters including the modal impedances, the field and current eigenvectors are then computed by using the solutions of the propagation constants. In the quasi-TEM analysis, the Laplace equation is transformed to an ordinary differential equation in the spectral domain, the solution of which together with the boundary conditions yields the Green's function which interrelates the potential and the charge distribution at the interfaces of the layered structure. The

charge distribution is expanded in terms of known functions with unknown coefficients which are subsequently evaluated by applying the Galerkin method. Once the charge distribution is found, the quasi-TEM characteristics of the coupled strip-slot structures are readily calculated.

Different impedance definitions proposed in the literature for multiple coupled line structures are discussed. The only useful impedance definition in the design of microwave and millimeter-wave circuits is the one that results in a symmetric impedance matrix for a coupled line structure in a lossless, isotropic, and linear medium. The normal mode impedance definition as based on the reciprocity is used to systematically study the impedance characteristics of various coupled slot structures for the first time, which together with the propagation characteristics are used to compute equivalent circuit models for ideal coupled line structures. The applications of the coupled slot and strip-slot structures are illustrated through design examples of enhanced couplers and power dividers consisting of coupled line multiports. Time domain simulation of coupled multiconductor structures with slotted ground planes is also presented to exemplify the applications of the techniques developed in this thesis to layered interconnects and packaging structures in high-speed circuits. Some novel techniques to reduce the crosstalk noise in those structures are proposed with theoretical examples and experimental results.

ANALYSIS AND APPLICATIONS OF LAYERED MULTICONDUCTOR COUPLED SLOT AND STRIP-SLOT STRUCTURES

by

Sifen Luo

A THESIS

submitted to

Oregon State University

in partial fulfillment of
the requirements for the
degree of

Doctor of Philosophy

Completed September 15, 1993

Commencement June, 1994

APPROVED

Redacted for privacy

Professor of Electrical and Computer Engineering in charge of major

Redacted for privacy

Head of Department of Electrical and Computer Engineering

Redacted for privacy

Dean of Graduate School

Date thesis is presented September 15, 1993

Typed by Sifen Luo

ACKNOWLEDGEMENTS

First of all, thanks go to my major professor, Dr. Vijai K. Tripathi, for his constant encouragement and support.

Thanks are also due to Drs. Stephen M. Goodnick, Henri J. Jansen, Shih-Lien Lu, and Thomas K. Plant for serving on my graduate committee and reviewing the manuscript.

I owe special thanks to my colleague, Jyh-Ming Jong, for his contribution to the experimental work in this thesis.

In addition, I am deeply indebted to my friend, Dr. Guozhong Xie, at World Bank for his invaluable help at the initial stage of my study in the States.

Finally, Thanks are due to my parents, Shiyin and Fazhi Luo, for their encouragement and understanding.

TABLE OF CONTENTS

LIST OF FIGURES

ANALYSIS AND APPLICATIONS OF LAYERED MULTICONDUCTOR COUPLED SLOT AND STRIP-SLOT STRUCTURES

1. INTRODUCTION

In the last two decades, significant progress has been made in the area of very-large-scale-integrated (VLSI) circuit technology. The packing density of transistors and the corresponding decrease in the intrinsic gate delay have been continuously advanced, whereas the minimum feature size of transistors in VLSI circuits has been dramatically reduced. However, the improvement of VLSI system performance has been hampered by the inadequate development in electronic packaging and interconnection technologies. With the advancement of the minimum feature size towards submicron dimension and the integration of a large number of transistors on a single microprocessor, on-chip and chip-to-chip interconnections are increasingly important in determining the operating speed, power consumption, and size of digital systems [1]. In a high-speed digital system, it is necessary to treat the interconnects between circuit elements as transmission lines. Inevitably, reflection, crosstalk, and distortion of pulse signals are of great importance in the interconnection design.

On the other hand, microwave technology has been advancing with the same pace as the VLSI circuit technology. Small and inexpensive microwave integrated circuits (MICs) have replaced once bulky and costly waveguide and coaxial structures in many applications at microwave frequencies [2]. The future development in MIC technology is leaning towards smaller size, lower cost, lighter weight, and higher integration. Therefore, monolithic MICs (MMICs), where all circuit components are

grown on a single substrate, are playing an important role in microwave circuit applications.

The development in VLSI circuits and (M)MICs now is in such a crucial stage that accurate modeling of passive as well as active structures is a must in designing high performance VLSI circuits and (M)MICs. This is due to the fact that tuning a circuit after fabrication is too costly, if not impossible, to be practical. Therefore, a computer-aided design (CAD) tool which provides accurate characterizations of both passive and active components in the circuits is essential in VLSI circuit and (M)MIC design.

Abreast with the progress made in VLSI circuits and (M)MICs, various mathematical techniques [3] and CAD tools have been developed to accurately model the passive and active structures in VLSI circuits and (M)MICs. Among the techniques used in modeling the passive structures, the spectral domain method is one of the most preferred and the most widely used methods in recent years. The method is relatively simple, powerful, and computationally efficient when properly implemented. But it is limited, in general, to well-shaped structures which have only infinitely thin conductors [2]. However, the metalization thickness can be taken into account by using a modified spectral domain method [4, 5] or other methods such as the modal analysis method [6].

Passive structures such as microstrip lines, coplanar waveguides, fin lines, and slot lines have been widely studied [7, 8], but the available results for the coupled slot and the coupled strip-slot structures are either inadequate or unsuitable to fully characterize the structures from a circuit designer's point of view. It is therefore necessary to have a further study on the coupled slot and the coupled strip-slot structures.

Modal analysis is introduced in Chapter 2 to formulate solutions for a coupled strip-slot structure. In the analysis, the method of separation of variables is employed to solve the scalar Helmholtz equation for the x-component of the electric and magnetic fields. The other components of the electric and magnetic fields are derived from the governing Maxwell equations in terms of the x-component. The solution for the Helmholtz equation together with the boundary conditions leads to the dyadic Green's function, which relates the tangential currents and electric fields to the slot fields and the strip currents. The application of the Galerkin method yields a set of algebraic equations. Setting the determinant of the algebraic equations equal to zero results in solutions for the propagation constants at a given frequency. The power corresponding to the propagation constants is then calculated in terms of the electric and magnetic fields. The coupling power between the strip line and the slot line and the power propagating on each line need to be identified for the impedance calculation. The analysis can be readily extended to coupled slot line structures and coupled strip line structures.

Also presented in Chapter 2 is a quasi-TEM analysis of the coupled strip-slot structure by the spectral domain method. The Laplace equation is simplified to a homogeneous ordinary differential equation by using the Fourier transform. Again, the solution of the equation together with the boundary conditions leads to the Green's function, which relates potentials to the unknown charge distributions. The charge distributions are expanded in terms of known functions with unknown coefficients which are to be determined by using the Galerkin method. The computation of the capacitances of the strips in a coupled strip-slot structure is an easy task, once the charge distributions are found. The inductances, the characteristic impedances, and the propagation constants are computed with the knowledge of the capacitances.

In Chapter 3, different impedance definitions for coupled transmission lines are discussed in terms of their usefulness in microwave circuit design. The convergence of the modal analysis is checked in terms of the basis functions, which are used to expand the electric fields on slots, and the summation terms used in the analysis. The impedance characteristics of various unilateral as well as bilateral fin line structures are systematically studied by using the normal mode impedance definition for the first time. Design examples are given to illustrate the applications of the coupled fin lines in directional couplers.

The characteristics of the coupled strip-slot structure are detailed in Chapter 4. There are two fundamental normal modes in the structure: the strip (c) mode where the total power is dominated by the power from the strip line and the slot (π) mode where the total power is mainly contributed by the power from the slot line. An assumption has been made that the ratio of the coupling power contributed by the strip line to the total coupling power in the strip mode is equal to that of the coupling power contributed by the slot line to the total coupling power in the slot mode. The symmetry of the impedance matrix of the structure in a lossless, linear, and isotropic medium is guaranteed under this assumption.

The results for the propagation characteristics of the multiconductor quasi-TEM modes of various coupled strip-slot structures are given in Chapter 5. Again, the convergence of the quasi-TEM spectral domain analysis is checked in terms of the basis functions, which approximate the charge distributions on the strip lines and the ground plane conductors, and the summation terms used in the analysis. The results are used in a SPICE circuit simulator to study the crosstalk reduction in digital systems. The SPICE simulation and the experimental results show that ground plane slots can reduce the far-end crosstalk in coupled interconnects.

Conclusions are summarized in Chapter 6. In addition, suggestions for possible future work are briefly discussed.

2. ANALYSIS OF COUPLED STRIP-SLOT STRUCTURE

A general layered structure consisting of multiple strips and slots at various interfaces can support a number of hybrid as well as quasi-TEM like modes. Placed in the E-plane of a rectangular waveguide, slots can be referred as fin lines whereas the strips can represent interconnects in a multilevel printed circuit board (PCB) structure.

Due to its wide single-mode bandwidth, low loss, ease of fabrication, and high compatibility with other circuit elements [9], the fin line structure has been widely used in millimeter-wave integrated circuits at lower millimeter-wave frequencies since it was invented in the early 1970s [10]. The characteristics of single fin line structures have been well documented [6, 8, 9, 11-17]. Attempts have been made to characterize coupled fin line structures [6, 14, 18-21]. However, the availability of the useful design parameters such as propagation constants and characteristic impedances is basically limited to symmetric coupled fin line structures. Since asymmetric as well as symmetric structures are important ones in the design of couplers, filters, and other circuit components at millimeter-wave frequencies, a comprehensive study on them is deemed necessary.

A coupled strip-slot structure provides more freedom in the design of couplers and filters [20, 22-27] due to the fact that it consists of strip lines and fin lines at different interfaces of substrates. The combination of strip lines and fin lines brings many advantageous features to the coupled strip-slot structure. Useful frequency dependent design information is only seen in the literature for the symmetric coupled structure where the center of the strip line is aligned with that of the slot line. Although the propagation characteristics of asymmetric and multiple coupled strip-slot structures are readily obtainable, the impedance characteristics are either hardly available or not useful in the design of the circuits.

In order to find the characteristics of the coupled strip-slot structures, a rigorous modal analysis is introduced in this chapter. It can be readily extended to the coupled fin line and the coupled strip line structures. Due to the inherent difficulty of the multiple coupled strip-slot structures, the useful frequency dependent impedance characteristics are still not available to date. Therefore, it is valuable to find quasi-TEM propagation and impedance characteristics of the multiple coupled strip-slot structures for applications at lower microwave frequencies. The second part of this chapter is devoted to a quasi-TEM spectral domain analysis [2, 28, 29] of the multiple coupled strip-slot structures.

2.1 MODAL ANALYSIS

A coupled strip-slot structure is shown in Fig. 2.1. The substrate of thickness d and relative dielectric constant ε_r is assumed to be linear, isotropic, and lossless. In addition, all conductors are considered to be ideal conductors of zero thickness. The structure extends to infinity in the z-direction.

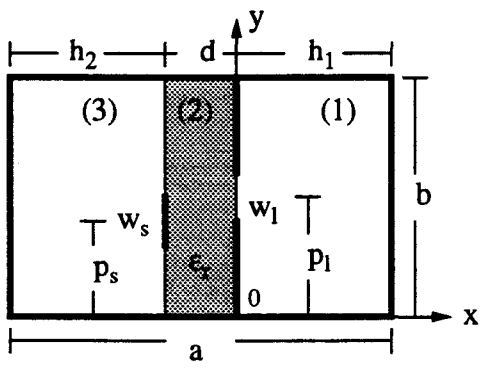

Fig. 2.1 Cross section of a coupled strip-slot structure.

Furthermore, it is assumed that the electromagnetic waves propagate in the positive z-direction with an unknown propagation constant $j\beta$ and have time

dependence with an angular frequency ω, i.e., the dependent factors of the electromagnetic fields on z and t can be expressed as $e^{-j\beta z}$ and $e^{j\omega t}$, respectively.

Since the cross-section of the coupled strip-slot structure is non-uniform in the x-direction, the electric and magnetic fields have discontinuities along the direction. The x-components of the electric and magnetic fields, E_x and H_x, must satisfy the Helmholtz wave equation:

$$\left[\frac{\partial^2}{\partial x^2}+\frac{\partial^2}{\partial y^2}+(k^2-\beta^2)\right]\begin{bmatrix}E_x\\H_x\end{bmatrix}=0 \tag{2.1}$$

where $k=\omega\sqrt{\mu_0\varepsilon_0\varepsilon_{ri}}$ is the wave number, μ_0 is the free-space permeability, ε_0 is the free-space permittivity, and ε_{ri} is the relative dielectric constant of region i (i = 1, 2, 3).

The tangential electric and magnetic fields on the surface of an ideal conductor must satisfy the Dirichlet and Neumann boundary conditions given by

$$E_x=0 \qquad \text{at } y=0,\ b \tag{2.2a}$$

$$\frac{\partial H_x}{\partial y}=0 \qquad \text{at } y=0,\ b. \tag{2.2b}$$

Applying the method of separation of variables to (2.1) leads to the solutions for the x-components of electric and magnetic fields in three regions:

$$E_{x1}=\sum_{n=1}^{\infty}A_{n1}\cos[\gamma_{n1}(x-h_1)]\sin(\alpha_n y) \tag{2.3a}$$

$$H_{x1}=\sum_{n=0}^{\infty}B_{n1}\sin[\gamma_{n1}(x-h_1)]\cos(\alpha_n y) \tag{2.3b}$$

$$E_{x2}=\sum_{n=1}^{\infty}[A_{n2}\sin(\gamma_{n2}x)+A'_{n2}\cos(\gamma_{n2}x)]\sin(\alpha_n y) \tag{2.3c}$$

$$H_{x2}=\sum_{n=0}^{\infty}[B_{n2}\cos(\gamma_{n2}x)+B'_{n2}\sin(\gamma_{n2}x)]\cos(\alpha_n y) \tag{2.3d}$$

$$E_{x3}=\sum_{n=1}^{\infty}A_{n3}\cos[\gamma_{n3}(x+d+h_2)]\sin(\alpha_n y) \tag{2.3e}$$

$$H_{x3} = \sum_{n=0}^{\infty} B_{n3}\sin[\gamma_{n3}(x + d + h_2)] \cos(\alpha_n y) \tag{2.3f}$$

where the indexes in the subscript stand for the corresponding regions and

$$\gamma_{n1} = \gamma_{n3} = k_{x1} = k_{x3} \tag{2.4a}$$

$$\gamma_{n2} = k_{x2} \tag{2.4b}$$

$$k_{y1} = k_{y2} = k_{y3} = \alpha_n = \frac{n\pi}{b} \tag{2.4c}$$

$$k_{xi}^2 + k_{yi}^2 + \beta^2 = k^2 \qquad (i = 1, 2, 3) \tag{2.4d}$$

here k_{xi} and k_{yi} are the separation constants. The y- and z-components of the electric and magnetic fields, which are derived from the Maxwell equations in terms of the x-components E_x and H_x, are given by

$$E_y = \frac{1}{(k^2 - k_{xi}^2)}\left[\frac{\partial^2 E_x}{\partial x \partial y} - j\omega\mu_0 \frac{\partial H_x}{\partial z}\right] \tag{2.5a}$$

$$H_y = \frac{1}{(k^2 - k_{xi}^2)}\left[\frac{\partial^2 H_x}{\partial x \partial y} + j\omega\varepsilon_0\varepsilon_{ri} \frac{\partial E_x}{\partial z}\right] \tag{2.5b}$$

$$E_z = \frac{1}{(k^2 - k_{xi}^2)}\left[\frac{\partial^2 E_x}{\partial x \partial z} + j\omega\mu_0 \frac{\partial H_x}{\partial y}\right] \tag{2.5c}$$

$$H_z = \frac{1}{(k^2 - k_{xi}^2)}\left[\frac{\partial^2 H_x}{\partial x \partial z} - j\omega\varepsilon_0\varepsilon_{ri} \frac{\partial E_x}{\partial y}\right]. \tag{2.5d}$$

Substituting (2.3) in (2.5) yields the expressions for y- and z-components of electric and magnetic fields:

$$E_{y1} = \sum_{n=0}^{\infty} S_{n1}\sin[\gamma_{n1}(x - h_1)] \cos(\alpha_n y) \tag{2.6a}$$

$$H_{y1} = \sum_{n=1}^{\infty} M_{n1}\cos[\gamma_{n1}(x - h_1)] \sin(\alpha_n y) \tag{2.6b}$$

$$E_{y2} = \sum_{n=0}^{\infty} [S_{n2}\cos(\gamma_{n2}x) + S'_{n2}\sin(\gamma_{n2}x)] \cos(\alpha_n y) \tag{2.6c}$$

$$H_{y2} = \sum_{n=1}^{\infty} [M_{n2}\sin(\gamma_{n2}x) + M'_{n2}\cos(\gamma_{n2}x)] \sin(\alpha_n y) \tag{2.6d}$$

$$E_{y3} = \sum_{n=0}^{\infty} S_{n3}\sin[\gamma_{n3}(x + d + h_2)]\cos(\alpha_n y) \tag{2.6e}$$

$$H_{y3} = \sum_{n=1}^{\infty} M_{n3}\cos[\gamma_{n3}(x + d + h_2)]\sin(\alpha_n y) \tag{2.6f}$$

where

$$S_{n1} = \frac{1}{(\alpha_n^2 + \beta^2)}(-\gamma_{n1}\alpha_n A_{n1} - \omega\mu_0\beta B_{n1}) \tag{2.7a}$$

$$S_{n2} = \frac{1}{(\alpha_n^2 + \beta^2)}(\gamma_{n2}\alpha_n A_{n2} - \omega\mu_0\beta B_{n2}) \tag{2.7b}$$

$$S'_{n2} = \frac{1}{(\alpha_n^2 + \beta^2)}(-\gamma_{n2}\alpha_n A'_{n2} - \omega\mu_0\beta B'_{n2}) \tag{2.7c}$$

$$S_{n3} = \frac{1}{(\alpha_n^2 + \beta^2)}(-\gamma_{n3}\alpha_n A_{n3} - \omega\mu_0\beta B_{n3}) \tag{2.7d}$$

$$M_{n1} = \frac{1}{(\alpha_n^2 + \beta^2)}(\omega\varepsilon_0\beta A_{n1} - \alpha_n\gamma_{n1}B_{n1}) \tag{2.7e}$$

$$M_{n2} = \frac{1}{(\alpha_n^2 + \beta^2)}(\omega\varepsilon_r\varepsilon_0\beta A_{n2} + \alpha_n\gamma_{n2}B_{n2}) \tag{2.7f}$$

$$M'_{n2} = \frac{1}{(\alpha_n^2 + \beta^2)}(\omega\varepsilon_r\varepsilon_0\beta A'_{n2} - \alpha_n\gamma_{n2}B'_{n2}) \tag{2.7g}$$

$$M_{n3} = \frac{1}{(\alpha_n^2 + \beta^2)}(\omega\varepsilon_0\beta A_{n3} - \alpha_n\gamma_{n3}B_{n3}) \tag{2.7h}$$

and

$$E_{z1} = \sum_{n=1}^{\infty} C_{n1}\sin[\gamma_{n1}(x - h_1)]\sin(\alpha_n y) \tag{2.8a}$$

$$H_{z1} = \sum_{n=0}^{\infty} D_{n1}\cos[\gamma_{n1}(x - h_1)]\cos(\alpha_n y) \tag{2.8b}$$

$$E_{z2} = \sum_{n=1}^{\infty} [C_{n2}\cos(\gamma_{n2}x) + C'_{n2}\sin(\gamma_{n2}x)]\sin(\alpha_n y) \tag{2.8c}$$

$$H_{z2} = \sum_{n=0}^{\infty} [D_{n2}\sin(\gamma_{n2}x) + D'_{n2}\cos(\gamma_{n2}x)]\cos(\alpha_n y) \tag{2.8d}$$

$$E_{z3} = \sum_{n=1}^{\infty} C_{n3}\sin[\gamma_{n3}(x + d + h_2)]\sin(\alpha_n y) \tag{2.8e}$$

$$H_{z3} = \sum_{n=0}^{\infty} D_{n3}\cos[\gamma_{n3}(x + d + h_2)]\cos(\alpha_n y) \tag{2.8f}$$

where

$$C_{n1} = \frac{1}{(\alpha_n^2 + \beta^2)} j(\beta\gamma_{n1}A_{n1} - \omega\mu_0\alpha_n B_{n1}) \quad (2.9a)$$

$$C_{n2} = \frac{1}{(\alpha_n^2 + \beta^2)} j(-\beta\gamma_{n2}A_{n2} - \omega\mu_0\alpha_n B_{n2}) \quad (2.9b)$$

$$C'_{n2} = \frac{1}{(\alpha_n^2 + \beta^2)} j(\beta\gamma_{n2}A'_{n2} - \omega\mu_0\alpha_n B'_{n2}) \quad (2.9c)$$

$$C_{n3} = \frac{1}{(\alpha_n^2 + \beta^2)} j(\beta\gamma_{n3}A_{n3} - \omega\mu_0\alpha_n B_{n3}) \quad (2.9d)$$

$$D_{n1} = \frac{1}{(\alpha_n^2 + \beta^2)} j(-\omega\varepsilon_0\alpha_n A_{n1} - \beta\gamma_{n1}B_{n1}) \quad (2.9e)$$

$$D_{n2} = \frac{1}{(\alpha_n^2 + \beta^2)} j(-\omega\varepsilon_0\varepsilon_r\alpha_n A_{n2} + \beta\gamma_{n2}B_{n2}) \quad (2.9f)$$

$$D'_{n2} = \frac{1}{(\alpha_n^2 + \beta^2)} j(-\omega\varepsilon_0\varepsilon_r\alpha_n A'_{n2} - \beta\gamma_{n2}B'_{n2}) \quad (2.9g)$$

$$D_{n3} = \frac{1}{(\alpha_n^2 + \beta^2)} j(-\omega\varepsilon_0\alpha_n A_{n3} - \beta\gamma_{n3}B_{n3}). \quad (2.9h)$$

The boundary conditions at x = 0 require:

$$H_{x1} = H_{x2} \quad (2.10a)$$

$$E_{y1} = E_{y2}. \quad (2.10b)$$

The replacement of the corresponding field expressions in (2.10) leads to:

$$A_{n2} = A_{n1}\frac{\gamma_{n1}}{\gamma_{n2}}\sin(\gamma_{n1}h_1) \quad (2.11a)$$

$$B_{n2} = -B_{n1}\sin(\gamma_{n1}h_1). \quad (2.11b)$$

The boundary conditions at x = -d are given by

$$E_{y2} = E_{y3} \quad (2.12a)$$

$$E_{z2} = E_{z3} \quad (2.12b)$$

$$H_{y2} - H_{y3} = J_{zst} \quad (2.12c)$$

$$-H_{z2} + H_{z3} = J_{yst} \quad (2.12d)$$

where J_{yst} and J_{zst} are the y- and z-components of the strip current density. Replacing the corresponding field expressions in (2.12) results in

$$A'_{n2} = F_{a1}A_{n2} + 2F_{a2}(\beta I_{nz} - j\alpha_n I'_{ny})/(\omega\varepsilon_0 b) \tag{2.13a}$$

$$B'_{n2} = F_{b1}B_{n2} - 2F_{b2}(\alpha_n I_{nz} + j\beta I'_{ny})/b \tag{2.13b}$$

where

$$F_{a1} = \frac{\varepsilon_{r2}\,\gamma_{n3}\tan(\gamma_{n2}d)\tan(\gamma_{n3}h_2) - \gamma_{n2}}{\varepsilon_{r2}\,\gamma_{n3}\tan(\gamma_{n3}h_2) + \gamma_{n2}\tan(\gamma_{n2}d)} \tag{2.14a}$$

$$F_{a2} = \frac{\gamma_{n3}\tan(\gamma_{n3}h_2)}{\varepsilon_{r2}\,\gamma_{n3}\cos(\gamma_{n2}d)\tan(\gamma_{n3}h_2) + \gamma_{n2}\sin(\gamma_{n2}d)} \tag{2.14b}$$

$$F_{b1} = \frac{\gamma_{n3} - \gamma_{n2}\tan(\gamma_{n2}d)\tan(\gamma_{n3}h_2)}{\gamma_{n3}\tan(\gamma_{n2}d) + \gamma_{n2}\tan(\gamma_{n3}h_2)} \tag{2.14c}$$

$$F_{b2} = \frac{\tan(\gamma_{n3}h_2)}{\gamma_{n3}\sin(\gamma_{n2}d) + \gamma_{n2}\cos(\gamma_{n2}d)\tan(\gamma_{n3}h_2)} \tag{2.14d}$$

$$I_{nz} = \int_0^b J_{zst}\sin(\alpha_n y)\,dy \tag{2.14e}$$

$$I'_{ny} = \frac{1}{\delta}\int_0^b J_{yst}\cos(\alpha_n y)\,dy \qquad \delta = \begin{cases} 2 & n = 0 \\ 1 & n \neq 0 \end{cases} \tag{2.14f}$$

and

$$A_{n3} = -\frac{\gamma_{n2}}{\gamma_{n3}\sin(\gamma_{n3}h_2)}[A_{n2}\cos(\gamma_{n2}d) + A'_{n2}\sin(\gamma_{n2}d)] \tag{2.15a}$$

$$B_{n3} = \frac{1}{\sin(\gamma_{n3}h_2)}[B_{n2}\cos(\gamma_{n2}d) - B'_{n2}\sin(\gamma_{n2}d)]. \tag{2.15b}$$

The y- and z-components of the electric field on the slot (x = 0) can be written as:

$$E_{y1}\big|_{x=0} = -\sum_{n=0}^{\infty} S_{n1}\sin(\gamma_{n1}h_1)\cos(\alpha_n y) \tag{2.16a}$$

$$E_{z1}\big|_{x=0} = -\sum_{n=1}^{\infty} C_{n1}\sin(\gamma_{n1}h_1)\sin(\alpha_n y). \tag{2.16b}$$

The use of the orthogonality of the sinusoidal functions yields

$$V'_{ny} = \frac{1}{\delta}\int_0^b E_{y1}\big|_{x=0}\cos(\alpha_n y)\,dy = -\frac{2}{b}S_{n1}\sin(\gamma_{n1}h_1) \tag{2.17a}$$

$$V_{nz} = \int_0^b E_{z1}\big|_{x=0}\sin(\alpha_n y)\,dy = -\frac{2}{b}C_{n1}\sin(\gamma_{n1}h_1). \tag{2.17b}$$

Substituting S_{n1} and C_{n1} in (2.17) leads to the expressions for A_{n1} and B_{n1} in terms of V'_{ny} and V_{nz}:

$$A_{n1} = \frac{2}{b} \frac{\alpha_n V'_{ny} + j\beta V_{nz}}{\gamma_{n1} \sin(\gamma_{n1} h_1)} \tag{2.18a}$$

$$B_{n1} = \frac{2}{b} \frac{\beta V'_{ny} - j\alpha_n V_{nz}}{\omega\mu_0 \sin(\gamma_{n1} h_1)}. \tag{2.18b}$$

On the other hand, the boundary conditions of the magnetic field at x = 0 require:

$$H_{y1} - H_{y2} = J_{zsl} \tag{2.19a}$$

$$- H_{z1} + H_{z2} = J_{ysl} \tag{2.19b}$$

where J_{ysl} and J_{zsl} are the y- and z-components of the current density on the fins at x = 0. The y- and z-components of the electric field at x = -d are

$$E_{y2} = \sum_{n=0}^{\infty} [S_{n2}\cos(\gamma_{n2} d) - S'_{n2}\sin(\gamma_{n2} d)]\cos(\alpha_n y) \tag{2.20a}$$

$$E_{z2} = \sum_{n=1}^{\infty} [C_{n2}\cos(\gamma_{n2} d) - C'_{n2}\sin(\gamma_{n2} d)]\sin(\alpha_n y). \tag{2.20b}$$

Substituting the corresponding field components of the magnetic field and the coefficients in (2.19) and (2.20) leads to the following expressions after some algebraic manipulations:

$$\sum_{n=0}^{\infty} [G_{11} V'_{ny} + G_{12} V_{nz} + G_{13} I_{nz} + G_{14} I'_{ny}] \cos(\alpha_n y) = \frac{b}{2} J_{ysl} \tag{2.21a}$$

$$\sum_{n=1}^{\infty} [G_{21} V'_{ny} + G_{22} V_{nz} + G_{23} I_{nz} + G_{24} I'_{ny}] \sin(\alpha_n y) = \frac{b}{2} J_{zsl} \tag{2.21b}$$

$$\sum_{n=1}^{\infty} [G_{31} V'_{ny} + G_{32} V_{nz} + G_{33} I_{nz} + G_{34} I'_{ny}] \sin(\alpha_n y) = E_{z2}\big|_{x=-d} \tag{2.21c}$$

$$\sum_{n=0}^{\infty} [G_{41} V'_{ny} + G_{42} V_{nz} + G_{43} I_{nz} + G_{44} I'_{ny}] \cos(\alpha_n y) = E_{y2}\big|_{x=-d} \tag{2.21d}$$

where G_{ij} (i,j = 1, 2, 3, 4) are Green's functions of the coupled strip-slot structure as given by

$$G_{11} = \frac{1}{(\alpha_n^2 + \beta^2)}\{j\omega\varepsilon_0\alpha_n^2\,[\frac{\cot(\gamma_{n1}h_1)}{\gamma_{n1}} - \frac{\varepsilon_r F_{a1}}{\gamma_{n2}}] + \frac{j\beta^2}{\omega\mu_0}\,[\gamma_{n1}\cot(\gamma_{n1}h_1) + \gamma_{n2}F_{b1}]\} \quad (2.22a)$$

$$G_{12} = \frac{1}{(\alpha_n^2 + \beta^2)}\{-\omega\varepsilon_0\alpha_n\beta\,[\frac{\cot(\gamma_{n1}h_1)}{\gamma_{n1}} - \frac{\varepsilon_r F_{b1}}{\gamma_{n2}}] + \frac{\alpha_n\beta}{\omega\mu_0}\,[\gamma_{n1}\cot(\gamma_{n1}h_1) + \gamma_{n2}F_{b1}]\} \quad (2.22b)$$

$$G_{13} = -G_{24} = G_{31} = -G_{42} = \frac{1}{(\alpha_n^2 + \beta^2)}\,j\alpha_n\beta(-\varepsilon_r F_{a2} + \gamma_{n2}F_{b2}) \quad (2.22c)$$

$$G_{14} = -G_{41} = \frac{1}{(\alpha_n^2 + \beta^2)}\,(-\varepsilon_r\,\alpha_n^2 F_{a2} - \gamma_{n2}\beta^2\,F_{b2}) \quad (2.22d)$$

$$G_{21} = -G_{12} \quad (2.22e)$$

$$G_{22} = \frac{1}{(\alpha_n^2 + \beta^2)}\{j\omega\varepsilon_0\beta^2\,[\frac{\cot(\gamma_{n1}h_1)}{\gamma_{n1}} - \frac{\varepsilon_{r2}F_{a1}}{\gamma_{n2}}] + \frac{j\alpha_n^2}{\omega\mu_0}\,[\gamma_{n1}\cot(\gamma_{n1}h_1) + \gamma_{n2}F_{b1}]\} \quad (2.22f)$$

$$G_{23} = -G_{32} = \frac{1}{(\alpha_n^2 + \beta^2)}\,(-\varepsilon_r\,\beta^2 F_{a2} - \gamma_{n2}\alpha_n^2\,F_{b2}) \quad (2.22g)$$

$$G_{33} = \frac{1}{(\alpha_n^2 + \beta^2)}\sin(\gamma_{n2}d)(-j\,\frac{\beta^2\gamma_{n2}}{\omega\varepsilon_0}\,F_{a2} - j\omega\mu_0\alpha_n^2 F_{b2}) \quad (2.22h)$$

$$G_{34} = -G_{43} = \frac{1}{(\alpha_n^2 + \beta^2)}\alpha_n\beta\,\sin(\gamma_{n2}d)(-\frac{\gamma_{n2}}{\omega\varepsilon_0}\,F_{a2} + \omega\mu_0 F_{b2}) \quad (2.22i)$$

$$G_{44} = \frac{1}{(\alpha_n^2 + \beta^2)}\sin(\gamma_{n2}d)(-j\,\frac{\alpha_n^2\gamma_{n2}}{\omega\varepsilon_0}\,F_{a2} - j\omega\mu_0\beta^2 F_{b2}). \quad (2.22j)$$

The unknown slot fields, i.e., the electric fields at x = 0 and the unknown strip current densities can, in general, be expressed in terms of known basis functions as follows:

$$E_{ysl} = \sum_{m=0}^{M} c_m\,e_{ym}(y) \qquad p_l - 0.5w_l \le y \le p_l + 0.5w_l \quad (2.23a)$$

$$E_{zsl} = \sum_{m=1}^{M} d_m\,e_{zm}(y) \qquad p_l - 0.5w_l \le y \le p_l + 0.5w_l \quad (2.23b)$$

$$J_{zst} = \sum_{l=0}^{L} f_l\,j_{zl}(y) \qquad p_t - 0.5w_t \le y \le p_t + 0.5w_t \quad (2.23c)$$

$$J_{yst} = \sum_{l=1}^{L} g_l\,j_{yl}(y) \qquad p_t - 0.5w_t \le y \le p_t + 0.5w_t \quad (2.23d)$$

where c_m, d_m, f_l, and g_l are unknown coefficients to be determined and $e_{ym}(y)$, $e_{zm}(y)$, $j_{zl}(y)$, and $j_{yl}(y)$ are known functions to be chosen to approximate the slot fields and the strip current densities.

Substituting (2.23) in (2.14) and (2.17) leads to

$$V'_{ny} = \sum_{m=0}^{M} c_m V_{ny}^m \tag{2.24a}$$

$$V_{nz} = \sum_{m=1}^{M} d_m V_{nz}^m \tag{2.24b}$$

$$I'_{nz} = \sum_{l=1}^{L} f_l I_{nz}^l \tag{2.24c}$$

$$I_{ny} = \sum_{l=0}^{L} g_l I_{ny}^l \tag{2.24d}$$

where

$$I_{nz}^l = \int_{p_t - 0.5w_t}^{p_t + 0.5w_t} j_{zl}(y) \sin(\alpha_n y)\, dy \tag{2.25a}$$

$$I_{ny}^l = \frac{1}{\delta} \int_{p_t - 0.5w_t}^{p_t + 0.5w_t} j_{yl}(y) \cos(\alpha_n y)\, dy \tag{2.25b}$$

$$V_{ny}^m = \int_{p_l - 0.5w_l}^{p_l + 0.5w_l} e_{ym}(y) \cos(\alpha_n y)\, dy \tag{2.25c}$$

$$V_{nz}^m = \frac{1}{\delta} \int_{p_l - 0.5w_l}^{p_l + 0.5w_l} e_{zm}(y) \sin(\alpha_n y)\, dy. \tag{2.25d}$$

Now, applying (2.24) to (2.21) results in

$$\sum_{n=0}^{\infty} \left[\sum_{j=0}^{M} c_j G_{11} V_{ny}^j + \sum_{j=1}^{M} d_j G_{12} V_{nz}^j + \sum_{k=0}^{L} f_k G_{13} I_{nz}^k + \sum_{k=1}^{L} g_k G_{14} I_{ny}^k \right] \cos(\alpha_n y) = \frac{b}{2} J_{ysl} \tag{2.26a}$$

$$\sum_{n=1}^{\infty} \left[\sum_{j=0}^{M} c_j G_{21} V_{ny}^j + \sum_{j=1}^{M} d_j G_{22} V_{nz}^j + \sum_{k=0}^{L} f_k G_{23} I_{nz}^k + \sum_{k=1}^{L} g_k G_{24} I_{ny}^k \right] \sin(\alpha_n y) = \frac{b}{2} J_{zsl} \tag{2.26b}$$

$$\sum_{n=1}^{\infty} \left[\sum_{j=0}^{M} c_j G_{31} V_{ny}^j + \sum_{j=1}^{M} d_j G_{32} V_{nz}^j + \sum_{k=0}^{L} f_k G_{33} I_{nz}^k + \sum_{k=1}^{L} g_k G_{34} I_{ny}^k \right] \sin(\alpha_n y) = \frac{b}{2} E_{z2} \Big|_{x=-d} \tag{2.26c}$$

$$\sum_{n=0}^{\infty} \left[\sum_{j=0}^{M} c_j G_{41} V_{ny}^j + \sum_{j=1}^{M} d_j G_{42} V_{nz}^j + \sum_{k=0}^{L} f_k G_{43} I_{nz}^k + \sum_{k=1}^{L} g_k G_{44} I_{ny}^k \right] \cos(\alpha_n y) = \frac{b}{2} E_{y2} \Big|_{x=-d}. \tag{2.26d}$$

Taking the inner products of (2.26a) to (2.26d) with $e_{ym}(y)$, $e_{zm}(y)$, $j_{zl}(y)$, and $j_{yl}(y)$ leads to the following equations due to the fact that $E_{y,z}$ and $J_{y,z}$ at x = 0 and -d are nonzero only in the complementary regions:

$$\sum_{n=0}^{\infty}\Big[\sum_{j=0}^{M} c_j G_{11} V_{ny}^{j} V_{ny}^{m} + \sum_{j=1}^{M} d_j G_{12} V_{nz}^{j} V_{ny}^{m} + \sum_{k=0}^{L} f_k G_{13} I_{nz}^{k} V_{ny}^{m} + \sum_{k=1}^{L} g_k G_{14} I_{ny}^{k} V_{ny}^{m}\Big] = 0 \quad (2.27a)$$

$$\sum_{n=1}^{\infty}\Big[\sum_{j=0}^{M} c_j G_{21} V_{ny}^{j} V_{nz}^{m} + \sum_{j=1}^{M} d_j G_{22} V_{nz}^{j} V_{nz}^{m} + \sum_{k=0}^{L} f_k G_{23} I_{nz}^{k} V_{nz}^{m} + \sum_{k=1}^{L} g_k G_{24} I_{ny}^{k} V_{nz}^{m}\Big] = 0 \quad (2.27b)$$

$$\sum_{n=1}^{\infty}\Big[\sum_{j=0}^{M} c_j G_{31} V_{ny}^{j} I_{nz}^{m} + \sum_{j=1}^{M} d_j G_{32} V_{nz}^{j} I_{nz}^{m} + \sum_{k=0}^{L} f_k G_{33} I_{nz}^{k} I_{nz}^{m} + \sum_{k=1}^{L} g_k G_{34} I_{ny}^{k} I_{nz}^{m}\Big] = 0 \quad (2.27c)$$

$$\sum_{n=0}^{\infty}\Big[\sum_{j=0}^{M} c_j G_{41} V_{ny}^{j} I_{ny}^{m} + \sum_{j=1}^{M} d_j G_{42} V_{nz}^{j} I_{ny}^{m} + \sum_{k=0}^{L} f_k G_{43} I_{nz}^{k} I_{ny}^{m} + \sum_{k=1}^{L} g_k G_{44} I_{ny}^{k} I_{ny}^{m}\Big] = 0. \quad (2.27d)$$

The propagation constant β is determined by setting the determinant of (2.27) equal to zero. Once β is obtained, the electromagnetic fields and the total power propagating in the structure can be readily calculated except for a constant factor, which will be canceled out in the impedance calculation.

2.2 QUASI-TEM SPECTRAL DOMAIN ANALYSIS

For the strip-slot structure with conductors of zero thickness shown in Fig. 2.2, the potential ϕ under the quasi-TEM approximation is the solution of Laplace's equation:

$$\nabla^2\phi = \frac{\partial^2\phi}{\partial x^2} + \frac{\partial^2\phi}{\partial y^2} = 0 \quad (2.28)$$

with the associated boundary conditions given by

$$\phi(x,h_{1+}) = \phi(x,h_{1-}) \quad (2.29a)$$

$$\varepsilon_r \frac{\partial\phi(x,h_{1+})}{\partial y} - \frac{\partial\phi(x,h_{1-})}{\partial y} = -\frac{\rho_g(x)}{\varepsilon_0} \quad (2.29b)$$

$$\phi(x,h_1) = \begin{cases} u_g(x) & \text{on slots} \\ v_g(x) & \text{otherwise} \end{cases} \quad (2.29c)$$

$$\phi(x,d+h_{1+}) = \phi(x,d+h_{1-}) \quad (2.29d)$$

$$\frac{\partial\phi(x,d+h_{1+})}{\partial y} - \varepsilon_r \frac{\partial\phi(x,d+h_{1-})}{\partial y} = - \frac{\rho_s(x)}{\varepsilon_0} \tag{2.29e}$$

$$\phi(x,d+h_1) = \left\{ \begin{array}{ll} v_s(x) & \text{on strips} \\ u_s(x) & \text{otherwise} \end{array} \right\} \tag{2.29f}$$

where $v_g(x)$ is the potential on the ground plane conductors, $u_g(x)$ the potential on the ground plane slots, $v_s(x)$ the potential on the strips, and $u_s(x)$ the potential on the dielectric surface complementary with the strips. $\rho_g(x)$ and $\rho_s(x)$ are the charge distribution functions on the ground plane conductors and the strips, respectively.

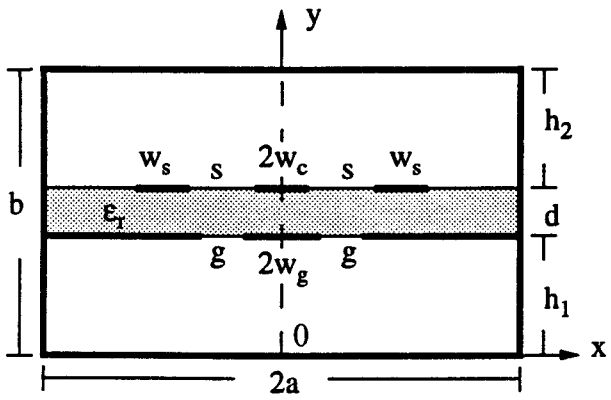

Fig. 2.2 Cross section of coupled strips with ground plane slots.

By introducing a proper Fourier transform, the partial differential equation of (2.28) in the space domain can be simplified to an ordinary differential equation in the spectral domain. The Fourier transform is, in general, defined as:

$$\Phi(\alpha_n) = \int_{-a}^{a} \phi(x)\, e^{j\alpha_n x}\, dx \qquad \alpha_n = \frac{\pi}{a}, \qquad n = 0, 1, 2, \ldots \tag{2.30}$$

However, different Fourier transforms can be introduced to simplify the analysis for a symmetric structure. Since there exist the even and odd modes in a symmetric structure, it is computationally more efficient to use the even- and odd-mode Fourier transforms as given by [28]

$$\Phi(\alpha_n) = \int_0^a \phi(x)\cos(\alpha_n x)\,dx \qquad \alpha_n = (n - \frac{1}{2})\frac{\pi}{a}, \quad n=1, 2, \ldots \tag{2.31a}$$

$$\Phi(\alpha_n) = \int_0^a \phi(x)\sin(\alpha_n x)\,dx \qquad \alpha_n = \frac{n\pi}{a}, \quad n=1, 2, \ldots \tag{2.31b}$$

The application of the Fourier transforms to (2.28) and (2.29) leads to

$$\frac{d^2\Phi(\alpha_n,y)}{dy^2} - \alpha_n^2\Phi(\alpha_n,y) = 0 \tag{2.32}$$

and

$$\Phi(\alpha_n,h_{1+}) = \Phi(\alpha_n,h_{1-}) \tag{2.33a}$$

$$\varepsilon_r \frac{d\Phi(\alpha_n,h_{1+})}{dy} - \frac{d\Phi(\alpha_n,h_{1-})}{dy} = - \frac{P_g(\alpha_n)}{\varepsilon_0} \tag{2.33b}$$

$$\Phi(\alpha_n,h_1) = V_g(\alpha_n) + U_g(\alpha_n) \tag{2.33c}$$

$$\Phi(\alpha_n,d+h_{1+}) = \Phi(\alpha_n,d+h_{1-}) \tag{2.33d}$$

$$\frac{d\Phi(\alpha_n,d+h_{1+})}{dy} - \varepsilon_r \frac{d\Phi(\alpha_n,d+h_{1-})}{dy} = - \frac{P_s(\alpha_n)}{\varepsilon_0} \tag{2.33e}$$

$$\Phi(\alpha_n, d+h_1) = V_s(\alpha_n) + U_s(\alpha_n) \tag{2.33f}$$

where

$$V_{g,s}(\alpha_n) = \int_0^a v_{g,s}(x) \begin{Bmatrix}\cos(\alpha_n)\\ \sin(\alpha_n)\end{Bmatrix} dx \tag{2.34a}$$

$$U_{g,s}(\alpha_n) = \int_0^a u_{g,s}(x) \begin{Bmatrix}\cos(\alpha_n)\\ \sin(\alpha_n)\end{Bmatrix} dx \tag{2.34b}$$

$$P_{g,s}(\alpha_n) = \int_0^a \rho_{g,s}(x) \begin{Bmatrix}\cos(\alpha_n)\\ \sin(\alpha_n)\end{Bmatrix} dx. \tag{2.34c}$$

The general solution of (2.32) which satisfies the boundary conditions at y = 0 and b has the following forms:

$$\Phi(\alpha_n, y) = A_n\sinh(\alpha_n y) \qquad 0 \le y \le h_1 \tag{2.35a}$$

$$\Phi(\alpha_n, y) = B_n\sinh[\alpha_n(y-h_1)] + B'_n\cosh[\alpha_n(y-h_1)] \qquad h_1 \le y \le h_1 + d \tag{2.35b}$$

$$\Phi(\alpha_n, y) = C_n\sinh[\alpha_n(b-y)] \qquad h_1 + d \le y \le b \tag{2.35c}$$

The unknown coefficients A_n, B_n, B'_n, and C_n in (2.35) are determined by using the spectral domain boundary conditions in (2.33). Eliminating the unknown coefficients yields:

$$G_{11}(\alpha_n)\, P_s(\alpha_n) + G_{12}(\alpha_n)\, P_g(\alpha_n) = V_s(\alpha_n) + U_s(\alpha_n) \tag{2.36a}$$

$$G_{21}(\alpha_n)\, P_s(\alpha_n) + G_{22}(\alpha_n)\, P_g(\alpha_n) = V_g(\alpha_n) + U_g(\alpha_n) \tag{2.36b}$$

where

$$G_{11}(\alpha_n) = \frac{1}{\Delta}\left[\coth(\alpha_n d) + \frac{1}{\varepsilon_r}\coth(\alpha_n h_1)\right] \tag{2.37a}$$

$$G_{12}(\alpha_n) = G_{21}(\alpha_n) = \frac{1}{\Delta \sinh(\alpha_n d)} \tag{2.37b}$$

$$G_{22}(\alpha_n) = \frac{1}{\Delta}\left[\coth(\alpha_n d) + \frac{1}{\varepsilon_r}\coth(\alpha_n h_2)\right] \tag{2.37c}$$

and

$$\Delta = \alpha_n \varepsilon_0\{\varepsilon_r + \coth(\alpha_n d)\coth(\alpha_n h_1) + \coth(\alpha_n h_2)[\coth(\alpha_n d) + \frac{1}{\varepsilon_r}\coth(\alpha_n h_1)]\}. \tag{2.37d}$$

To apply the Galerkin method to (2.36), one needs to expand the charge distributions on the conductors in terms of known basis functions. The total charge distributions in the spectral domain on the strips and the ground plane conductors are the summations of the corresponding charge distributions, which can be written as:

$$P_s(\alpha_n) = \sum_{u=1}^{U} P_{su}(\alpha_n) \tag{2.38a}$$

$$P_g(\alpha_n) = \sum_{v=1}^{V} P_{gv}(\alpha_n). \tag{2.38b}$$

where U and V are the numbers of the strips and the ground plane conductors and the charge distributions on individual conductors can be expanded in terms of known basis functions given by

$$P_{su}(\alpha_n) = \sum_{m=1}^{M} a_m^u\, P_{sm}^u(\alpha_n) \tag{2.39a}$$

$$P_{gv}(\alpha_n) = \sum_{j=1}^{J} b_j^v\, P_{gj}^v(\alpha_n) \tag{2.39b}$$

Substituting (2.38) and (2.39) in (2.36) and taking the inner products of (2.36) with $P^p_{sk}(\alpha_n)$ and $P^q_{gl}(\alpha_n)$ lead to

$$\sum_{n=1}^{N}\sum_{m=1}^{M} K11^{pn}_{km} a^n_m + \sum_{i=1}^{I}\sum_{j=1}^{J} K12^{pi}_{kj} b^i_j = R^p_k \quad k=1, 2, \ldots, M; \quad p=1, 2,\ldots, N \tag{2.40a}$$

$$\sum_{n=1}^{N}\sum_{m=1}^{M} K21^{qn}_{lm} a^n_m + \sum_{i=1}^{I}\sum_{j=1}^{J} K22^{qi}_{lj} b^i_j = S^q_l \quad l=1, 2, \ldots, J; \quad q=1, 2,\ldots, I \tag{2.40b}$$

where

$$K11^{pn}_{km} = \sum_{n=1}^{\infty} P^n_{sm}(\alpha_n) G_{11}(\alpha_n) P^p_{sk}(\alpha_n) \tag{2.41a}$$

$$K12^{pi}_{kj} = \sum_{n=1}^{\infty} P^i_{gj}(\alpha_n) G_{12}(\alpha_n) P^p_{sk}(\alpha_n) \tag{2.41b}$$

$$K21^{qn}_{lm} = \sum_{n=1}^{\infty} P^n_{sm}(\alpha_n) G_{21}(\alpha_n) P^q_{gl}(\alpha_n) \tag{2.41c}$$

$$K22^{pi}_{lj} = \sum_{n=1}^{\infty} P^i_{gj}(\alpha_n) G_{22}(\alpha_n) P^q_{gl}(\alpha_n) \tag{2.41d}$$

$$R^p_k = \sum_{n=1}^{\infty} [V_s(\alpha_n) + U_s(\alpha_n)]\, P^p_{sk}(\alpha_n) = \frac{a}{2} \int_0^a \rho^p_{sk}(x)\, v_s(x)\, dx \tag{2.41e}$$

$$S^q_l = \sum_{n=1}^{\infty} [V_g(\alpha_n) + U_g(\alpha_n)]\, P^q_{gl}(\alpha_n) = \frac{a}{2} \int_0^a \rho^q_{gl}(x)\, v_g(x)\, dx. \tag{2.41f}$$

Use of the Parseval relation has been made in the derivation of (2.41), where the product terms $U_s(\alpha_n)P^{\ p}_{sk}(\alpha_n)$ and $U_g(\alpha_n)P^{\ q}_{gl}(\alpha_n)$ vanish due to the fact that the corresponding charge distribution functions and the potential functions are non-zero only in the regions complementary to each other, i.e.,

$$\sum_{n=1}^{\infty} U_s(\alpha_n)\, P^p_{sk}(\alpha_n) = \frac{a}{2} \int_0^a \rho^p_{sk}(x)\, u_s(x)\, dx = 0 \tag{2.42a}$$

$$\sum_{n=1}^{\infty} U_g(\alpha_n)\, P^q_{gl}(\alpha_n) = \frac{a}{2} \int_0^a \rho^q_{gl}(x)\, u_g(x)\, dx = 0 \tag{2.42b}$$

It is clear from (2.40) and (2.41) that the coefficients of the charge distributions are related to the potentials on the strips and the ground plane conductors, which can be written in a concise matrix form given by

$$[Q] = [C]\,[V] \tag{2.43}$$

where [Q] is a column vector with N elements, each of which represents the total charge on a corresponding strip or ground plane conductor, [C] is an N×N capacitance matrix, which relates the charges to the potentials on the conductors, and [V] is a column vector of N elements consisting of the potentials on the conductors, N is the total number of the strips and the ground plane conductors in the structure. With the knowledge of $[C_0]$, the capacitance matrix of the structure with all the relative dielectric constants set to one, the inductance matrix can be readily obtained from the following relationship:

$$[L][C_0] = \frac{1}{\upsilon_0^2}[U] \tag{2.44}$$

where υ_0 is the speed of light in free space and [U] is an identity matrix. Under the quasi-TEM consideration, it is sufficient to use $[C_0]$, [C], and [L] to characterize a multiconductor transmission line system.

2.3 SUMMARY

The full-wave and quasi-TEM analyses of the coupled strip-slot structures are formulated by the modal analysis method and the spectral domain technique, respectively.

In the full-wave analysis, the electric and magnetic fields are constructed in terms of modal fields in different regions. The application of the boundary conditions at interfaces for the tangential components of the electric and magnetic fields results in the dyadic Green's function, which interrelates the tangential currents and fields at the boundaries. The use of the Galerkin method reduces the problem under consideration to a set of homogeneous equations associated with the unknown coefficients of the strip currents and the slot fields. The eigenvalues of the equations are the solutions of the propagation constants of the structure.

In the quasi-TEM analysis, the Fourier transform is introduced to simplify the Laplace equation to an ordinary differential equation in the spectral domain. The solution of the equation together with the boundary conditions results in the Green's function, which relates the charge distributions to the potentials. The application of the Galerkin method yields a set of algebraic equations associated with the unknown coefficients of the charge distributions on the strips and the ground plane conductors. The non-trivial solution of the algebraic equation leads to the capacitances.

3. CHARACTERISTICS OF MULTIPLE COUPLED FIN LINES

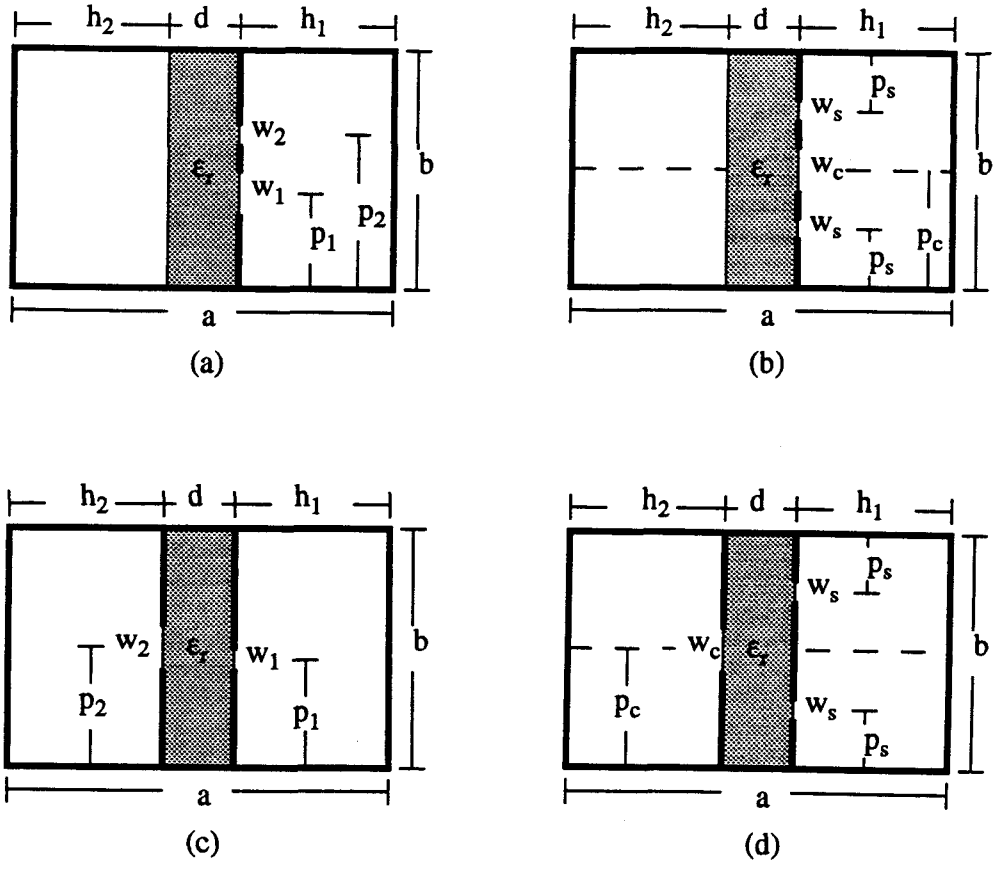

Fig. 3.1 Cross sections of some typical fin lines: (a) unilateral asymmetric coupled two-slot, (b) unilateral symmetric coupled three-slot, (c) bilateral asymmetric coupled two-slot, and (d) bilateral symmetric coupled three-slot structures.

The propagation constant and the characteristic impedance are the two most important parameters for a transmission line structure. Efforts [6, 30] have been made to characterize single as well as coupled fin lines. Some of typical fin line structures are shown in Fig. 3.1. Unlike a TEM transmission line, a fin line does not have a unique impedance definition due to its non-TEM mode nature. Among the various

impedance definitions for the fin line [11], the most commonly used one is the one based on the power-voltage definition, i.e.,

$$Z = \frac{V^2}{2P} \tag{3.1}$$

where P is the time averaged power propagating on the fin line and V is the voltage across the slot. The total average power is calculated by

$$P = \frac{1}{2} \mathrm{Re}[\iint (\mathbf{E} \times \mathbf{H}^*) \bullet \, ds] \tag{3.2}$$

where the integration is over the entire cross-section of the propagation structure. The voltage across the slot line is defined as

$$V = \int_{slot} E_y(y) \, dy \tag{3.3}$$

where $E_y(y)$ is the y-components of the electric field on the slot. However, the impedance definition of (3.1) is only directly applicable to single slot and symmetrically coupled two-slot fin lines.

For the asymmetrical or multiple coupled fin lines, the partial powers associated with the individual slots have to be used in the impedance calculation. One of the preconditions in the impedance calculation is that the summation of the partial powers equals to the total power. Based on this precondition, Jansen [31] proposed the following admittance definition for *m*th slot in a multiple coupled fin (slot) line structure and the impedance definition for the *m*th strip in a multiple coupled strip line structure:

$$Y_m = \frac{2P_m}{V_m^2} = \frac{1}{V_m^2} \mathrm{Re}[\iint (\mathbf{e}_m \times \mathbf{h}^*) \bullet \, ds] \qquad \mathbf{h} = \sum_m \mathbf{h}_m \tag{3.4a}$$

$$Z_m = \frac{2P_m}{I_m^2} = \frac{1}{I_m^2} \mathrm{Re}[\iint (\mathbf{e} \times \mathbf{h}_m^*) \bullet \, ds] \qquad \mathbf{e} = \sum_m \mathbf{e}_m \tag{3.4b}$$

where V_m is the voltage across the *m*th slot, I_m is the *m*th strip current flowing in the propagation direction, $\mathbf{e}_m$ and $\mathbf{h}_m$ are the partial fields associated only with the *m*th

portion of the expansion functions of the total fields. Although the total power is conservative by using Jansen's impedance definitions, the resultant impedance matrix violates the reciprocity for a linear, isotropic, passive transmission line structure. Therefore, they are not applicable to the multiple coupled line structures except the single and symmetric coupled two line structures. An impedance definition proposed by Tripathi and Lee [32] for a multiple coupled strip line structure satisfies both the reciprocity and the conservation of the total power. It has been used to characterize the asymmetric coupled two fin line and symmetric coupled three fin line structures [21, 33]. However, the comprehensive design information on the multiple coupled fin (slot) lines is still not made available to date.

In the full-wave analysis of a multiple coupled slot (strip) line structure, the slot voltages (strip currents) and total power can be readily computed for all normal modes. The voltage and current vectors are biorthogonal [32]:

$$\mathbf{V}_m^T \mathbf{I}_j = \sum_{l=1}^{N} V_{lm} I_{lj} = \begin{cases} 0 & j \neq m \\ P_m & j = m \end{cases} \qquad j, m = 1, 2, \ldots, N \tag{3.5}$$

where subscript l refers to the *l*th line, m and j the *m*th and *j*th modes, N the total number of the transmission lines or the normal modes of the structure, and P_m the total power associated with the *m*th mode. Once the slot voltages (strip currents) and the modal powers are known, the equivalent slot currents (strip voltages) of the *l*th line can be derived from the partial modal power of the line:

$$P_{lm} = V_{lm} I_{lm}. \tag{3.6}$$

Then, the modal impedance of the *l*th line can be unambiguously defined as

$$Z_{lm} = \frac{P_{lm}}{I_{lm}^2} = \frac{V_{lm}^2}{P_{lm}} = \frac{V_{lm}}{I_{lm}} \tag{3.7}$$

which guarantees that the resultant 2N port impedance, admittance, and scattering matrices are symmetric for a transmission line structure in a lossless, linear, and isotropic medium.

In an asymmetric coupled two line structure, there exist two normal modes: c- and π-modes [34]. The c- and π–modes correspond to the even- and odd-modes in a symmetric coupled two line structure. The biorthogonality of the voltage and current vectors yields:

$$\begin{bmatrix} V_{1c} & V_{2c} \\ V_{1\pi} & V_{2\pi} \end{bmatrix} \begin{bmatrix} I_{1c} & I_{1\pi} \\ I_{2c} & I_{2\pi} \end{bmatrix} = \begin{bmatrix} P_c & 0 \\ 0 & P_\pi \end{bmatrix}. \tag{3.8}$$

where P_c and P_π are the modal powers associated with the c- and π-modes. The voltage or current ratios for c- and π-modes are defined as:

$$R_{vc} = \frac{V_{2c}}{V_{1c}} = -\frac{I_{1\pi}}{I_{2\pi}} = -\frac{1}{R_{I\pi}} \tag{3.9a}$$

$$R_{v\pi} = \frac{V_{2\pi}}{V_{1\pi}} = -\frac{I_{1c}}{I_{2c}} = -\frac{1}{R_{Ic}}. \tag{3.9b}$$

The modal impedances are derived in terms of the modal powers, voltages, and voltage ratios as given by:

$$Z_{1c} = \left(1 - \frac{R_{vc}}{R_{v\pi}}\right) \frac{V_{1c}^2}{P_c} \tag{3.10a}$$

$$Z_{1\pi} = \left(1 - \frac{R_{v\pi}}{R_{vc}}\right) \frac{V_{1\pi}^2}{P_\pi} \tag{3.10b}$$

and

$$\frac{Z_{2c}}{Z_{1c}} = \frac{Z_{2\pi}}{Z_{1\pi}} = -R_{vc}R_{v\pi}. \tag{3.10c}$$

Likewise, there are three normal modes: the odd mode (a), the even-even mode (b), and the even-odd mode (c) in a symmetric three line structure [35]. The use of the biorthogonality of the voltage current vectors leads to

$$\begin{bmatrix} V_{1a} & 0 & -V_{1a} \\ V_{1b} & V_{2b} & V_{1b} \\ V_{1c} & V_{2c} & V_{1c} \end{bmatrix} \begin{bmatrix} I_{1a} & I_{1b} & I_{1c} \\ 0 & I_{2b} & I_{2c} \\ -I_{1a} & I_{1b} & I_{1c} \end{bmatrix} = \begin{bmatrix} P_a & 0 & 0 \\ 0 & P_b & 0 \\ 0 & 0 & P_c \end{bmatrix}. \tag{3.11}$$

The voltage and current ratios are defined as

$$R_{vm} = \frac{V_{2m}}{V_{1m}} \tag{3.12a}$$

$$R_{Im} = \frac{I_{2m}}{I_{1m}} \tag{3.12b}$$

where m = b or c and

$$R_{vb}R_{Ic} = R_{vc}R_{Ib} = -2. \tag{3.13}$$

Again, the modal impedances are expressed in terms of modal powers, voltages, voltage ratios as given by

$$Z_{1a} = \frac{2V_{1a}^2}{P_a} \tag{3.14a}$$

$$Z_{1b} = (1 - \frac{R_{vb}}{R_{vc}})\frac{2V_{1b}^2}{P_b} \tag{3.14b}$$

$$Z_{1c} = (1 - \frac{R_{vc}}{R_{vb}})\frac{2V_{1c}^2}{P_c} \tag{3.14c}$$

and

$$\frac{Z_{2b}}{Z_{1b}} = \frac{Z_{2c}}{Z_{1c}} = -\frac{R_{vb}R_{vc}}{2}. \tag{3.14d}$$

Similarly, the modal impedance can also be expressed in terms of the modal powers, currents, and current ratios.

In this chapter, the normalized guide wavelengths and the characteristic impedances of various asymmetric coupled two-slot and symmetric coupled three-slot fin line structures are calculated by using the modal analysis method and the above impedance definition. First, the effect of the basis functions representing the slot fields on the accuracy of the computational results is discussed. Second, the convergence of the modal analysis is checked in terms of the summation terms in the field expansion. Then, the characteristics of various fin line structures are illustrated

with numerical results. Finally, design examples of the fin line couplers are given to indicate the applications of the fin line structures.

3.1 BASIS FUNCTIONS AND SUMMATION TERMS

Electric and magnetic fields are singular in the vicinity of sharp edges which exist in most commonly used strip or slot line structures [2, 36]. In the modal analysis, the numerical solution is obtained by expanding the strip current or the slot field in terms of a set of known basis functions, which closely approximate the true strip current or slot field. Therefore, the accuracy of the final solution depends on how accurately the basis functions can represent the exact strip current or slot field.

Many different basis functions have been used in practice [6]. The most important criteria in choosing the basis functions lie in the singularity or edge condition, the completeness, and the ease of the Fourier transform of the basis functions. Detailed discussions about the basis functions can be found in [3]. Here, the sinusoidal functions corrected with the edge condition terms, which have been demonstrated to be efficient due to the fact that they have the closed forms of the Fourier transform [37], are chosen as the basis functions used in the field expansion:

$$e_{ym}(y) = \frac{\cos[m\pi(\frac{1}{2} + \frac{y - p_i}{w_i})]}{\sqrt{1 - [\frac{2(y - p_i)}{w_i}]^2}} \qquad p_i - 0.5w_i \le y \le p_i + 0.5w_i \qquad (3.15a)$$

$$e_{zm}(y) = \frac{\sin[m\pi(\frac{1}{2} + \frac{y - p_i}{w_i})]}{\sqrt{1 - [\frac{2(y - p_i)}{w_i}]^2}} \qquad p_i - 0.5w_i \le y \le p_i + 0.5w_i \qquad (3.15b)$$

where w_i is the width of the ith slot, p_i is the center of the ith slot, m (≥ 0) is an integer, $e_{ym}(y)$ and $e_{zm}(y)$ are zero in the undefined regions.

The even-mode normalized wavelength and characteristic impedance of a symmetric coupled unilateral fin line structure as a function of the number of the basis

function are shown in Fig. 3.2, where the odd-mode normalized wavelength and characteristic impedance are not shown due to their relatively smaller variations. The even- and odd-modes are defined by placing magnetic and electric walls in the center of the E-plane of the waveguide, respectively. It is seen that the errors between the results obtained with one basis function and those obtained with two basis functions for each component of the slot field are about 0.2% and -1.4% for the normalized wavelength and the characteristic impedance. The use of more basis functions reduces the errors, but the improvement in the accuracy is trivial by using three or more basis functions. On the other hand, it significantly increases the computation time. As the number of the basis functions used is increased from two to four, the characteristic impedance converges asymptotically whereas the normalized wavelength varies slightly. In the above calculations, 500 summation terms have been used in the modal field expansion.

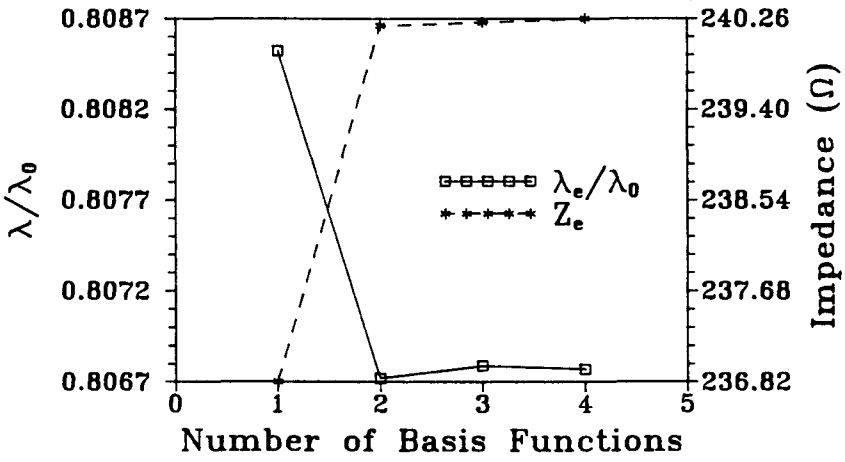

Fig. 3.2 The normalized wavelength λ_e/λ_0 and the characteristic impedance Z_e of the even mode vs. the number of basis functions (ε_r=2.22, d=0.254, h_1=3.556, w_1=w_2=0.2, p_1=1.578, p_2=1.978, f=33GHz, waveguide=WR-28, length unit: mm).

The convergence of the results obtained with two basis function for each component of the slot field for a centered unilateral fin line as a function of the summation terms is illustrated in Fig. 3.3. The normalized wavelength and the characteristic impedance converge initially very fast and then slowly as the summation terms are increased. Since the difference between the results of using 400 summation terms and 500 summation terms is negligibly small, it is trivial to reduce the errors by a further increase in the summation terms. Therefore, a modal analysis solution with 500 summation terms is adequate to yield accurate results. Of course, the number of the summation terms used also depends on the slot width. More summation terms should be used for the fin line with a wide slot.

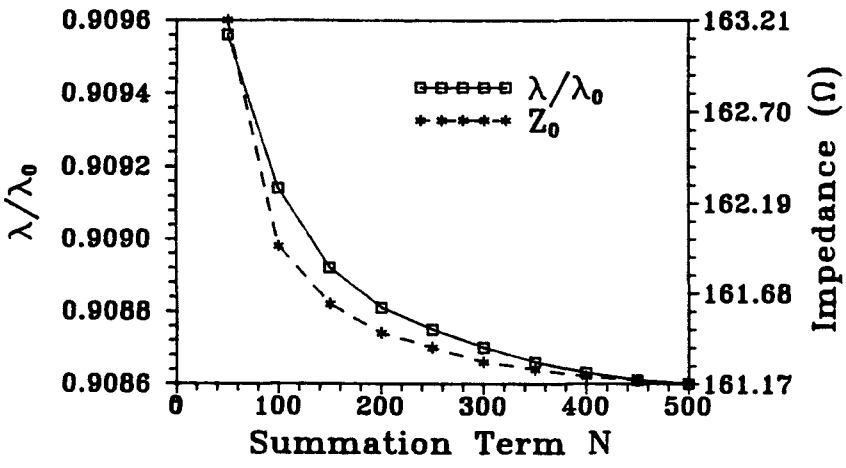

Fig. 3.3 The normalized wavelength λ/λ_0 and the characteristic impedance Z of a fin line with a centered slot vs. the number of summation terms (ε_r=2.22, d=0.254, h_1=3.556, w=0.2, f=33GHz, waveguide=WR-28, length unit: mm).

The numerical results obtained from the modal analysis were compared in [6] with those from the spectral domain method for a centered, unilateral fin line. It was found that they are in fairly good agreement for both the normalized wavelength and the characteristic impedance. In addition, it was reported in [18] that for a slot with

reasonably wide width, a 5% accuracy for both the propagation constant and the impedance can be achieved by using only two basis functions for each component of the slot field in the spectral domain analysis.

In the following calculations, two basis functions for each component of the slot field and 500 summation terms are used to evaluate the normalized wavelengths and the characteristic impedances of various fin line structures. In all cases, the fin lines are confined in a WR-28 waveguide, the frequency range of which covers the Ka band ranging from 26.5 to 40 GHz.

3.2 UNILATERAL COUPLED FIN LINE STRUCTURES

Coupled fin line structures have been used in circuit components such as couplers, filters, and mixers. To secure a designed circuit with high performance, one needs to know the accurate characteristics of the structures. Since the characteristics of symmetric coupled two-slot fin line structures have been detailed in [6], a further discussion of them is more or less redundant and not within the scope of this section. Instead, the characteristics of the asymmetric coupled two-slot and the symmetric coupled three-slot fin line structures will be examined.

3.2.1 Asymmetric Coupled Two-Slot Fin Line Structures

As seen in Fig. 3.4, the effects of the relative dielectric constant ε_r of the substrate on the normalized wavelength λ/λ_0, the characteristic impedance Z_1, and the modal voltage ratio R are different for c- and π-modes. As frequency is increased, both λ_c/λ_0 and λ_π/λ_0 decrease monotonically. However, the change in λ_c/λ_0 is relatively small. R_π rises slightly, whereas $|R_c|$ falls insignificantly. While $Z_{1\pi}$ decreases for $\varepsilon_r = 2.22$ and increases for $\varepsilon_r = 9.8$, Z_{1c} only increases a little for both $\varepsilon_r = 2.22$ and 9.8. When the slot width w_1 is increased from 0.2 to 0.8 mm with the w_2 =

$1.5w_1$, λ/λ_0 and Z_1 increase. The change in the modal voltage ratio is different. On one hand, R_π increases and $|R_c|$ decreases for $\varepsilon_r = 9.8$. On the other hand, R_π increases approximately at $f \geq 33$ GHz and decreases approximately at $f \leq 33$ GHz and $|R_c|$ decreases for $\varepsilon_r = 2.22$. As ε_r is increased from 2.22 to 9.8, λ/λ_0 decreases substantially. R_π increases, whereas $|R_c|$ decreases. While Z_{1c} decreases, the change in $Z_{1\pi}$ depends on the frequency as well as the slot width. $Z_{1\pi}$ decreases in the case of a narrower slot ($w_1 = 0.2$ mm). However, it decreases at approximately $f \leq 32.5$ GHz and increases at approximately $f \geq 32.5$ in the case of a broader slot ($w_1 = 0.8$ mm).

Fig. 3.5 shows that the variations of λ/λ_0, R and Z_1 for an asymmetric coupled two-slot fin line structure as a function of frequency with the substrate thickness d as a parameter. When d is increased, λ/λ_0 decreases due to the fact that a thicker substrate results in a higher effective dielectric constant. R_π decreases, whereas $|R_c|$ increases. Z_1 decreases with an increase in the substrate thickness..

Changes in λ/λ_0, R, and Z_1 with respect to the lateral position of the substrate h_1 for different slot separations are plotted in Fig. 3.6. As h_1 is increased, λ_π/λ_0 has a nearly symmetric change with a minimum value for the substrate placed close to the center of the broad wall, while λ_c/λ_0 shows only a slight change. The variations in R_π and $|R_c|$ are almost symmetric but bent in different directions. At the symmetric point, R_π and $|R_c|$ reach the maximum and minimum values, respectively. The change in R is more pronounced for a larger separation between the slots. Z_1 weakly depends on the lateral position of the substrate. The overall change in Z_1 is insignificant due to the high concentration of the electric field in the slot region for a narrow slot. As long as the slots are not too close to the side wall, the influence of the wall on the electric field in the slot region can be neglected [6].

The dependence of the dynamic characteristics of the asymmetric coupled two-slot fin line structure on the separation between two slot centers is shown in Fig. 3.7. As frequency is increased, λ_π/λ_0 decreases gradually and λ_c/λ_0 shows almost no change. Z_{1c} and R_π increase, whereas $Z_{1\pi}$ and $|R_c|$ decrease. As the separation is increased, λ/λ_0 also increases. However, its effect on λ_π/λ_0 is negligible when the coupling between the slots becomes weak, say, $s \geq 1.0$ mm. The decrease in $|R_c|$ at high frequencies is faster than that at low frequencies. R_π decreases at frequencies approximately below 36 GHz and it first decreases and then increases for frequencies approximately above 36 GHz. Z_{1c} decreases, while $Z_{1\pi}$ increases. $Z_{1c} > Z_{1\pi}$ for a small separation and $Z_{1c} < Z_{1\pi}$ for a large separation.

Fig. 3.8 illustrates λ/λ_0, R, and Z_1 as a function of the slot width w_1 with $w_2 = 1.5w_1$. As w_1 is increased, λ/λ_0 and Z_1 increase. It is observed that R_π initially increases and then decreases, whereas $|R_c|$ decreases monotonically.

The influence of the slot displacement in the symmetric E-plane on λ/λ_0, R, and Z_1 for a fixed separation between two slots with $w_2 = 1.5w_1$ is shown in Fig. 3.9. The change in λ_π/λ_0 depends not only on the slot displacement but also on the slot width. In the narrow slot ($w_1 = 0.2$ mm) case, λ_π/λ_0 decreases slightly when one of the slots is close to the broad wall, otherwise it is nearly a constant. In the broad slot case ($w_1 = 0.8$ mm), λ_π/λ_0 changes symmetrically and reaches its maximum at $p_1 \approx 1.1$ mm. On the other hand, λ_c/λ_0 shows almost no dependence on the slot displacement and the slot width. As the slot displacement is increased, both R_π and $|R_c|$ decrease, but there exists a region where R_π is almost a constant in the narrow slot case. Z_{1c} increases for both cases, whereas $Z_{1\pi}$ increases for a broad slot and it first increases and then decreases for a narrow slot.

In general, the π-mode parameters in the asymmetric coupled two-slot fin line structure are more sensitive to a change in the structural parameters than the c-mode parameters.

3.2.2 Symmetric Coupled Three-Slot Fin Line Structures

There are three normal modes in a symmetric coupled three line structure: odd mode (a), even-even mode (b), and even-odd mode (c). The frequency dependent characteristics of the symmetric coupled three-slot fin line structure with the relative dielectric constant ε_r of the substrate as a parameter are shown in Fig. 3.10. It is seen that as frequency is increased, λ_a/λ_0 and λ_c/λ_0 stay nearly unchanged, while λ_b/λ_0 decreases. R_b increases, whereas $|R_c|$ decreases. Z_{1a} increases and Z_{1c} decreases slightly, but Z_{1b} decreases for $\varepsilon_r = 2.22$ and increases for $\varepsilon_r = 9.8$. As ε_r is increased from 2.22 to 9.8, both λ/λ_0 and Z_1 decrease. R_b increases and $|R_c|$ decreases.

Fig. 3.11 indicates the influence of the substrate thickness on the characteristics of the structures. It is observed that the effect of increasing the substrate thickness d is equivalent to that of increasing the dielectric constant of the substrate while having the thickness fixed. This is clearly reflected by the fact that λ/λ_0 decreases with an increase in d. However, the change in Z_1 and R are different from those shown in Fig. 3.10. As d is increased, R_b increases and $|R_c|$ decreases. While Z_{1a} decreases, Z_{1b} decreases for frequencies approximately below 35 GHz and increases slightly for frequencies approximately above 35 GHz. In addition, Z_{1c} decreases for frequencies approximately below 27 GHz and increases for frequencies above 27 GHz.

The effect of the separation between the slots on λ/λ_0, R, and Z_1 is illustrated in Fig. 3.12. As the separation s is increased, λ_a/λ_0, λ_c/λ_0, and R_b increase while Z_{1a}

and Z_{1c} decrease. λ_b/λ_0 and Z_{1b} first increase and then decrease slightly. On the contrary, $|R_c|$ first decreases slightly and then increases.

The dependence of λ/λ_0, R, and Z_1 on the center slot width is plotted in Fig. 3.13. When the center slot width w_c is increased, λ/λ_0 also increases. Whereas the changes in λ_a/λ_0 and λ_c/λ_0 are very small, the change in λ_b/λ_0 is relatively large and almost linear. While $|R_c|$ remains nearly unchanged, R_b increases with w_c. In contrast to the change in λ/λ_0, Z_1 decreases with an increase in w_c. The decrease in Z_{1c}, which covers a wide range of values, is much faster than those in Z_{1a} and Z_{1b}.

As seen in Fig. 3.14, increasing the side slot width w_s with all other parameters fixed has a similar effect on λ/λ_0 as in the case of increasing the center slot width. However, the variations in R are different from those with a change in the center slot width. $|R_c|$ increases, while R_b decreases. As expected, Z_1 increases with w_s.

The variations of the characteristics of the structure with a lateral displacement h_1 of the substrate is shown in Fig. 3.15. It is clearly seen that all the characteristic parameters except λ_b/λ_0 change insignificantly as long as the fins are not located very close to either of the side walls. λ_b/λ_0 first decreases and then increases as h_1 is increased.

3.3 BILATERAL COUPLED FIN LINE STRUCTURES

Bilateral fin line structures are also important transmission line structures used in millimeter-wave integrated circuits. To date, most of studies on the bilateral fin line structures have been centered around the bilateral symmetric coupled two-slot fin line structures. The characteristics of the structures presented in [6] are predominated by λ/λ_0 and Z of the even mode. However, the characteristics of the odd mode play an

important role in designing the circuits using the bilateral symmetric fin line structures. The study on bilateral asymmetric coupled two-slot and symmetric coupled three-slot fin line structures is very limited, if not rear. In addition, they were incorrectly treated as one- and two-line structures, respectively, coupled with high order modes [37]. Therefore, a detailed study on them is necessary to provide the useful and important information on the characteristics which include the propagation constant and the characteristic impedance.

In this section, the characteristics of bilateral symmetric and asymmetric two-slot as well as symmetric three-slot fin line structures will be presented through various numerical results obtained from the modal analysis.

3.3.1 Coupled Two-Slot Fin Line Structures

The frequency dependent characteristics of a symmetric coupled two-slot fin line structure are shown in Fig. 3.16. As frequency is increased, the normalized even-mode wavelength λ_e/λ_0 decreases slightly. A rapid decrease in the normalized odd-mode wavelength λ_o/λ_0 for $\varepsilon_r = 2.22$ indicates that the associated cutoff frequency for the substrate with a small ε_r is higher than that with a large ε_r. In the case of $\varepsilon_r = 2.22$, the even-mode impedance Z_e initially decreases and then increases slightly, while the odd-mode impedance Z_o decreases first drastically and then smoothly. In the case of $\varepsilon_r = 9.8$, Z_e increases and Z_o decreases. When the substrate thickness is increased, both λ_e/λ_0 and λ_o/λ_0 decrease in the case of $\varepsilon_r = 2.22$. However, λ_e/λ_0 decreases and λ_o/λ_0 slightly increases in the case of $\varepsilon_r = 9.8$. The bilateral fin line structures have two features different from those of the unilateral fin line structures. One is that λ_o/λ_0 increases sharply in the case of $\varepsilon_r = 2.22$ as frequency is decreased. This indicates the odd-mode cutoff frequency of the bilateral fin line structure is higher than that of the unilateral fin line structure, as shown in [6], with the same physical dimensions. The

other is that $\lambda_o/\lambda_0 > \lambda_e/\lambda_0$ for the substrate with $\varepsilon_r = 2.22$, whereas $\lambda_o/\lambda_0 < \lambda_e/\lambda_0$ for the substrate with $\varepsilon_r = 9.8$. Furthermore, in the case of $\varepsilon_r = 9.8$, an increase in the substrate thickness results in a small increase in λ_o/λ_0 and a decrease in λ_e/λ_0. Therefore, it is possible to equalize λ_o/λ_0 and λ_e/λ_0 at certain frequencies by properly choosing the substrate material and thickness, which could be useful in the directional coupler design.

Since the odd-mode or π-mode cutoff frequency of a coupled bilateral two-slot fin line structure with a lower ε_r, as seen in Fig. 3.16, is higher, the application of the fin line structure in filters and couplers will be limited to a higher frequency range for a given waveguide. A substrate with a higher ε_r is needed to ensure that both modes propagate in the lower frequency range. In the following calculations, a substrate of $\varepsilon_r = 9.8$ is used in the fin line structures.

The effect of the center location of two equal slots in a symmetric structure on λ/λ_0 and Z is plotted in Fig 3.17. It is seen that as the slot center deviates from the E-plane center, λ_e/λ_0 only increases slightly. In contrast to the change in λ_e/λ_0, λ_o/λ_0 increases significantly. When the slot is located in the E-plane center, λ/λ_0 reaches its minimum. While Z_e slowly increases, Z_o initially decreases and then increases. The change in impedance is relatively small. The effect of the common center location of two unequal slots is illustrated in Fig. 3.18. The changes in λ/λ_0 are similar to those in the equal slot case. However, the change in Z_c is significantly different from that in Z_e. Z_c decreases drastically as the slot center deviates from the E-plane center.

Fig. 3.19 shows the influence of the slot width on λ/λ_0 and Z of the symmetric structure. As the slot width is increased from 0.2 to 1.0 mm, both λ/λ_0 and Z increase. The increase in the even mode is more significant than that in the odd mode.

The dependence of λ/λ_0 and Z of the structure with two equal slots on the lateral displacement of the substrate is plotted in Fig. 3.20. When the substrate is

located in a position other than the center of the broad wall, the structure is no longer symmetric. The two basic modes existing in the structure are the c- and π-modes instead of the even- and odd-modes. The overall effect of the displacement on the characteristics is insignificant. As the displacement from the center of the broad wall is increased, λ_c/λ_0 increases slowly and λ_π/λ_0 shows almost no change. While $Z_{1\pi}$ overlaps with $Z_{2\pi}$, Z_{1c} and Z_{2c} start to split when the substrate is moved close to the side wall. After the splitting, Z_{1c} decreases and Z_{2c} increases slightly. In other words, the difference between Z_{1c} and Z_{2c} is then distinguishable. In addition, the same dependence for the structure with unequal slots is shown in Fig. 3.21. λ/λ_0 behaves in a similar way as that discussed in the equal slot case. The change in Z_π is insignificant as the location of the substrate changes. When the substrate is moved close to the side wall, both Z_{1c} and Z_{2c} start to decrease. This is different from the case with two equal slots.

Fig. 3.22 illustrates the case where the centers of two slots shift from the E-plane center with an equal distance but in the opposite directions. As the slots shift from the E-plane center, λ_π/λ_0 and Z_π monotonically increase, whereas λ_c/λ_0 and Z_c initially decrease and then increase. As the distance between two slots increases, the coupling between them decreases. This is reflected by the fact that c- and π-mode parameters approach to each other for a large separation between the slots. For the same structure with unequal slots, a similar effect is seen in Fig. 3.23 when the slot centers deviate from the E-plane center with the equal distance but in the opposite directions. $Z_1 < Z_2$ for a small or medium separation between the slots. There exists a distance with which $Z_1 = Z_2$. A further increase in the distance makes $Z_1 > Z_2$.

The effect of changing the slot width w_2 on the characteristics of the structure is demonstrated in Fig. 3.24. As w_2 is increased, λ_π/λ_0, $Z_{1\pi}$, and $Z_{2\pi}$ slowly increase, whereas λ_c/λ_0, Z_{1c}, and Z_{2c} first increase and then decrease.

3.3.2 Symmetric Coupled Three-Slot Fin Line Structures

The influence of the dielectric constant of the substrate on the frequency dependent characteristics of the fin line structures is shown in Fig. 3.25. As frequency is increased, λ/λ_0 decreases. At lower frequencies, the even-odd mode corresponding to $\varepsilon_r = 2.22$ is in its cutoff region. At higher frequencies, λ_c/λ_0 decreases drastically. As the frequency is increased, R_b increases and $|R_c|$ decreases. Z_{1a} decreases for both $\varepsilon_r = 2.22$ and 9.8. Z_{1b} increases and Z_{1c} decreases slightly in the case of $\varepsilon_r = 9.8$. However, Z_{1b} decreases and Z_{1c} increases in the case of $\varepsilon_r = 2.22$. As expected, λ/λ_0 corresponding to a higher ε_r is smaller. The fact that the even-odd mode for the substrate with a lower ε_r has a much higher cutoff frequency than other two modes could mistakenly leads one to consider the structure as a two-line structure [37]. This suggests that a substrate with a higher ε_r be chosen to ensure that all three modes propagate in a desired frequency band. It is worthwhile to note that $\lambda_b/\lambda_0 > \lambda_c/\lambda_0$ in the case of $\varepsilon_r = 9.8$, whereas $\lambda_b/\lambda_0 < \lambda_c/\lambda_0$ in the case of $\varepsilon_r = 2.22$. On the other hand, as ε_r is increased from 2.22 to 9.8, R_b decreases while $|R_c|$ increases. Z_{1a} and Z_{1c} both decrease, whereas Z_{1b} increases.

The dependence of the characteristics on the center slot width w_c is plotted in Fig. 3. 26. As w_c is increased, λ/λ_0 also increases. R_b increases, whereas $|R_c|$ initially increases and then decreases. Z_{1a} first decreases and then increases, while Z_{1b} and Z_{1c} both increase. It is seen that $\lambda_b/\lambda_0 > \lambda_c/\lambda_0 > \lambda_a/\lambda_0$. When w_c is small, the increase in λ_b/λ_0 and the difference between λ_a/λ_0 and λ_c/λ_0 are relatively large. There is a region where the difference between λ_a/λ_0 and λ_c/λ_0 is very small and λ_b/λ_0 is almost a

constant. When w_c becomes large, the difference starts to increase. For small and medium size center slots ($w_c < 1.3$ mm), $Z_{1b} > Z_{1c} > Z_{1a}$. In addition, Z_{1a} remains small and Z_{1c} shows a slight variation. For a large w_c, Z_{1a} and Z_{1b} increase sharply.

The variations of λ/λ_0, R, and Z_1 as a function of the side slot width w_s are illustrated in Fig. 3.27. Again, it is seen that $\lambda_b/\lambda_0 > \lambda_c/\lambda_0 > \lambda_a/\lambda_0$. As w_s is increased, the overall change in λ_a/λ_0 is relatively small. λ_b/λ_0 changes slightly when w_s is small. However, it increases sharply when w_s becomes large. λ_c/λ_0 increases smoothly. While R_b slowly decreases, R_c undergoes a drastic change. It is seen that there is a divergent point in R_c where the voltage across the side slot in the c mode approaches to zero. Z_{1a} increases nonlinearly, whereas Z_{1c} initially increases slightly and then rapidly decreases to a negative value. On the other hand, Z_{1b} undergoes three different stages with one peak and one valley.

The dependence of the characteristics on the center position of the side slot, i.e., the separation between two side slot centers, is shown in Fig. 3. 28. As the separation is decreased, λ_a/λ_0 rises monotonically. λ_b/λ_0 first decreases and then increases, whereas λ_c/λ_0 first increases and then decreases. The change in λ_b/λ_0 is relatively large. While R_b increases slowly, R_c goes through a drastic change due to the existence of the divergent point. Z_{1a} decreases slowly and Z_{1c} increases from a negative value to a positive value. Z_{1b} first decreases and then increases.

The effect of the substrate thickness on the characteristics is plotted in Fig. 3.29. Increasing the thickness results in decreases in both λ_a/λ_0 and λ_b/λ_0, but an increase in λ_c/λ_0. The change in λ_b/λ_0 is relatively large. As the thickness is increased, R_b decreases while $|R_c|$ increases. Whereas both Z_{1a} and Z_{1c} increase, Z_{1b} decreases.

As seen in Fig. 3. 30, the lateral displacement of the substrate has a relatively small influence on the characteristics. All of the characteristic parameters are almost

unchanged as long as the substrate is located far from the side wall. When the substrate is placed close to the side wall, λ_b/λ_0, R_b, and Z_{1b} increase. $|R_c|$ increases when the two side slots are closer to the side wall and decreases when the center slot is closer to the side wall.

3.4 APPLICATIONS OF THE COUPLED FIN LINE STRUCTURES

Applications of the coupled fin line structures in directional couplers have been reported in the literature [6, 21, 23, 38, 39]. Design examples of the couplers using asymmetric coupled two-slot fin lines and symmetric coupled three-slot fin lines terminated in non-mode converting impedances [40], which result in closed-form expressions of the scattering parameters for the couplers, are given in [21, 33]. However, due to the fact that the characteristic impedances of the coupled lines are frequency dependent, the use of the derived scattering parameters for the couplers terminated in the non-mode converting impedances is confined to a single frequency point, such as the center frequency of the coupler, where the non-mode converting conditions are satisfied. The scattering parameters of the coupled two-line structure terminated with arbitrary impedances were derived in [41]. In general, the normalized scattering parameter matrix [S] of a multiport network can be written as [42]

$$[S] = [R_0]^{-0.5}\{[Z_{oc}] - [R_0]\}\{[Z_{oc}] + [R_0]\}^{-1}[R_0]^{0.5} \tag{3.16}$$

where $[R_0]$ is the characteristic reference impedance matrix and $[Z_{oc}]$ is the open-circuit impedance matrix. $[Z_{oc}]$ can be calculated in terms of the normal mode parameters [32, 34, 35] of the coupled line structure. For simplicity, the following analysis of the directional coupler design will be focused on the asymmetric coupled two-line four-port couplers.

A matched two-line four-port directional couplers, as shown in Fig. 3. 31, using coupled lines can be realized when the c- and π-mode impedances are

equalized, i.e., $Z_{1,2c} = Z_{1,2\pi}$. Terminating such coupler with $Z_{1,2} = Z_{1,2c}$, which are non-mode converting impedances, yields the scattering parameters as given by [41]

$$S_{11} = S_{22} = S_{33} = S_{44} = 0 \tag{3.17a}$$

$$S_{12} = S_{21} = S_{34} = S_{43} = 0 \tag{3.17b}$$

$$S_{13} = S_{31} = S_{24} = S_{42} = \frac{1}{R_c - R_\pi}\sqrt{-R_cR_\pi}\,(e^{-j\theta_c} - e^{-j\theta_\pi}) \tag{3.17c}$$

$$S_{14} = S_{41} = \frac{1}{R_c - R_\pi}(R_ce^{-j\theta_\pi} - R_\pi e^{-j\theta_c}) \tag{3.17d}$$

$$S_{23} = S_{32} = \frac{1}{R_c - R_\pi}(R_ce^{-j\theta_c} - R_\pi e^{-j\theta_\pi}) \tag{3.17e}$$

where $\theta_{c,\pi} = 2\pi L/\lambda_{c,\pi}$ and L is the length of the coupled line.

For a given coupled line structure, the maximum achievable coupling $|S_{31}|^2_{max}$ for the matched coupler is found from (3.17) to be

$$|S_{31}|^2_{max} = \left|\frac{4R_cR_\pi}{(R_c - R_\pi)^2}\right| \tag{3.18}$$

at the frequency where

$$\cos(\theta_c - \theta_\pi) = -1. \tag{3.19}$$

The four port coupler can be realized for a desired coupling by designing the physical structure to yield the required ratio of R_π/R_c or R_c/R_π at the center frequency [33].

Directional couplers with desired coupling coefficients less than the maximum value of $|S_{31}|^2$ as given by (3.18) can also be realized by an appropriate selection of a coupler length. For example, 3-dB couplers can be realized either by choosing the desired R_c/R_π at the center frequency or by choosing the coupler length such that

$$\cos(\theta_c - \theta_\pi) = \frac{(R_c + R_\pi)^2}{4R_cR_\pi}. \tag{3.20}$$

It is seen from Fig. 3.7 that Z_{1c} and $Z_{1\pi}$ can be equalized for a given two-slot fin line structure by changing the separation between two slots. The effect of the slot separation on the characteristic impedances of the asymmetric and symmetric coupled two-slot unilateral finlines is shown in Fig. 3.32. As the separation is increased, Z_e

and Z_{1c} decrease while Z_o and $Z_{1\pi}$ increase. It is obvious that there is an intersection point where $Z_{1c} = Z_{1\pi}$. That is, ideal codirectional couplers can indeed be physically realized by choosing the desired separation. In theory, an accurate result of the separation, which equalizes Z_{1c} and $Z_{1\pi}$, can be found numerically. However, a practically realizable separation is limited by the MIC processing technology. For the curves shown in Fig. 3.32, Z_{1c} = 151.31 Ω and $Z_{1\pi}$ = 151.29 Ω when the slot separation S = 1.304 mm, which is considered as acceptable for the design purpose. Therefore, the matched terminations for the ideal coupler are determined by $Z_1 = \sqrt{Z_{1c}Z_{1\pi}}$ and $Z_2 = \sqrt{Z_{2c}Z_{2\pi}}$ in the calculation. It should be noted that the difference between the impedances will decreases again with the slot separation as the two slots are decoupled.

Fig. 3.33 shows the coupling and isolation of an asymmetric coupler designed for maximum coupling at the center frequency f = 33 GHz. The coupler can be terminated with the matched terminations or the line impedances corresponding to the centered single-slot fin line impedances at the center frequency. The difference in the coupling between the two couplers is relatively small. However, the isolation of the coupler with the matched terminations corresponding to the characteristic values of $Z_1 = \sqrt{Z_{1c}Z_{1\pi}}$ and $Z_2 = \sqrt{Z_{2c}Z_{2\pi}}$ is much better than that of the coupler terminated with the line impedances. In the latter case, the isolation is still better than 50 dB.

Fig. 3.34 shows the coupling and the isolation of a 3-dB coupler terminated with the matched impedances and the line impedances at the center frequency f = 33 GHz. Again, the difference in coupling is insignificant. The isolation of the coupler with the matched terminations is about 90 dB whereas that of the coupler terminated with the line impedances is only about 28 dB at the center frequency.

3.5 SUMMARY

A useful normal mode impedance definition for the coupled strip lines or slot lines, which guarantees that the resultant impedance matrix is symmetric for a linear, isotropic, and passive transmission line structure, is introduced to characterize the coupled fin line structures. The propagation and impedance characteristics of the various uni- and bi-lateral, asymmetric coupled two-slot and symmetric coupled three-slot fin line structures are calculated by using the normal mode impedance definition. The application of the coupled fin lines in the directional couplers is illustrated through the design examples.

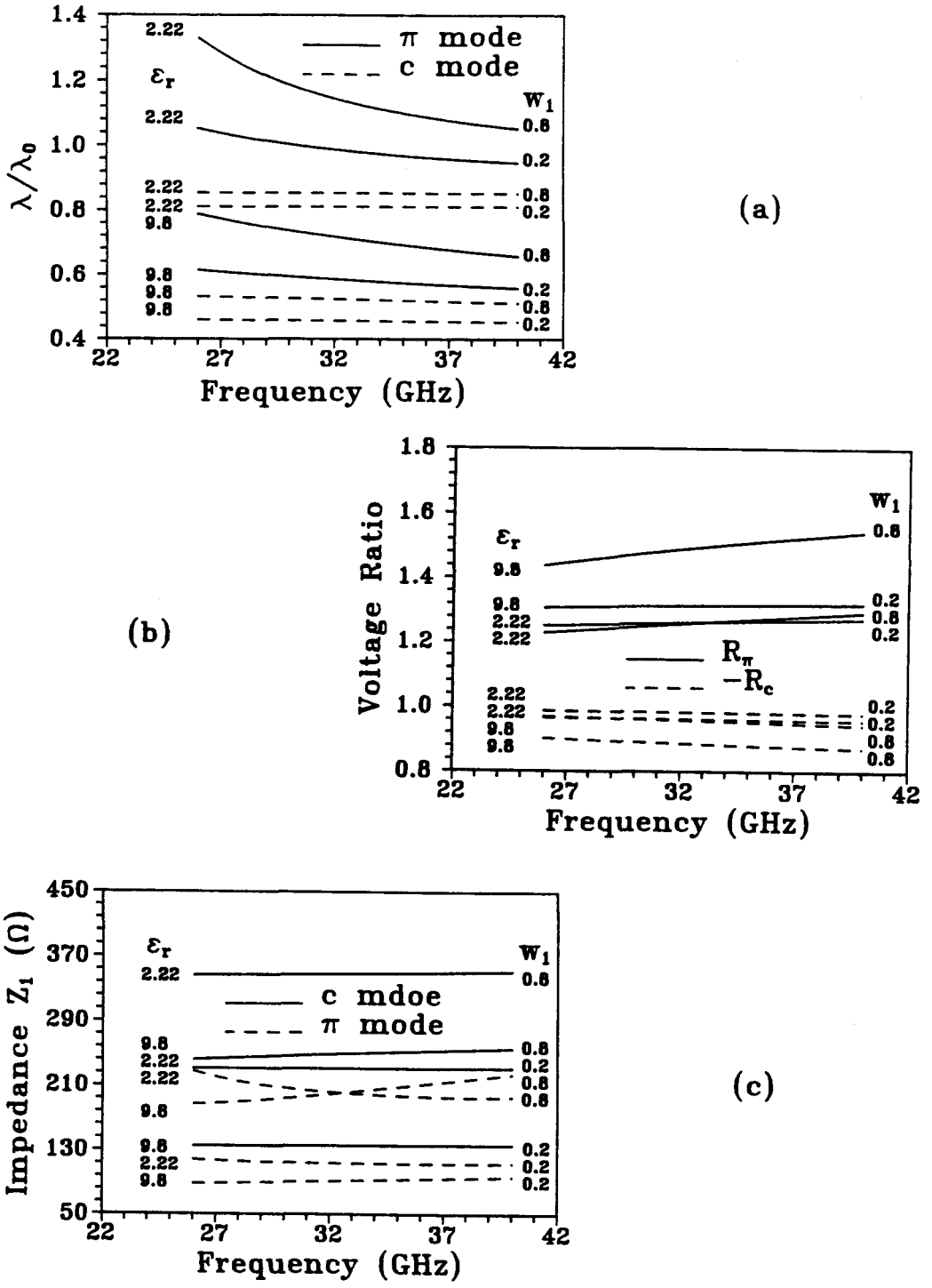

Fig. 3.4 (a) λ/λ_0, (b) voltage ratio, and (c) impedance Z_1 of a unilateral asymmetric coupled two-slot fin line as a function of frequency with ε_r and w_1 as parameters (h_1=3.556, d=0.254, w_2=1.5w_1, p_1=1.678-0.5w_1, p_2=1.878+0.5w_2, length unit: mm).

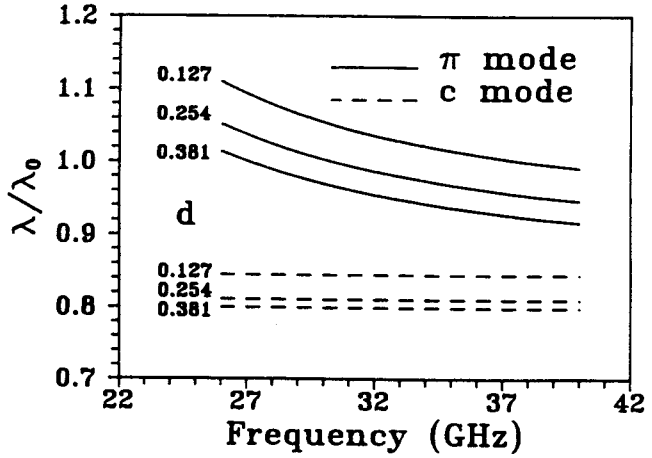

(a)

(b)

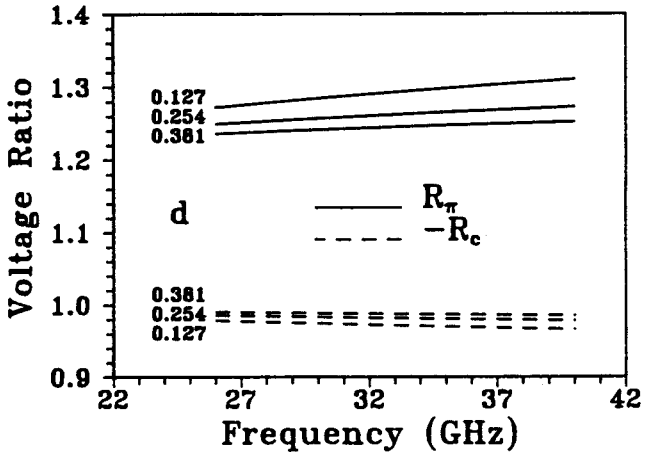

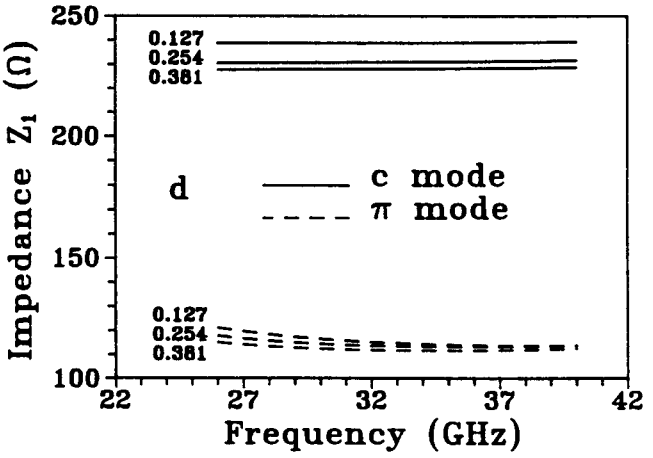

(c)

Fig. 3.5 (a) λ/λ_0, (b) voltage ratio, and (c) impedance Z_1 of a unilateral asymmetric coupled two-slot fin line as a function of frequency with d as a parameter (ε_r=2.22, h_1=3.556, w_1=0.2, w_2=0.3, p_1=1.578, p_2=2.028, length unit: mm).

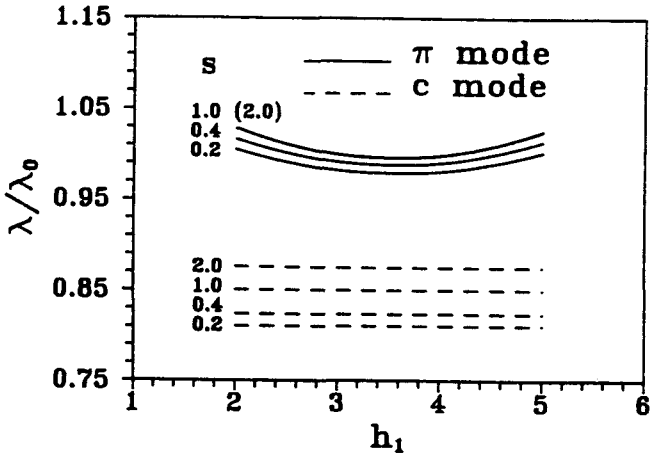

(a)

(b)

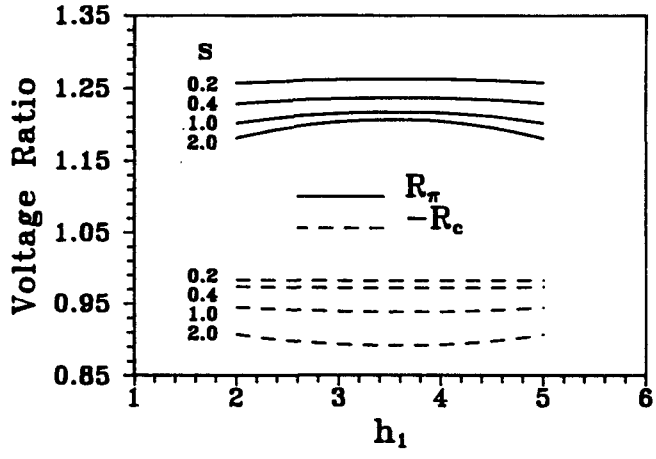

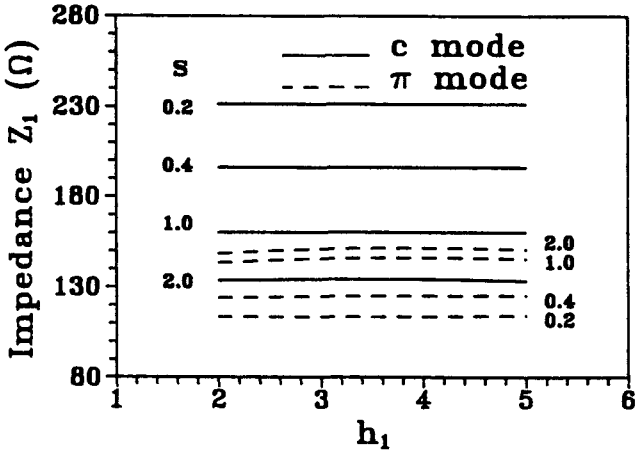

(c)

Fig. 3.6 (a) λ/λ_0, (b) voltage ratio, and (c) impedance Z_1 of a unilateral asymmetric coupled two-slot fin line as a function of the lateral displacement of the substrate with the slot separation s as a parameter (ε_r=2.22, d=0.254, w_1=0.2, w_2=0.3, p_1=1.778-0.5(s+w_1), p_2=1.778+0.5(s+w_2), f=33GHz, length unit: mm).

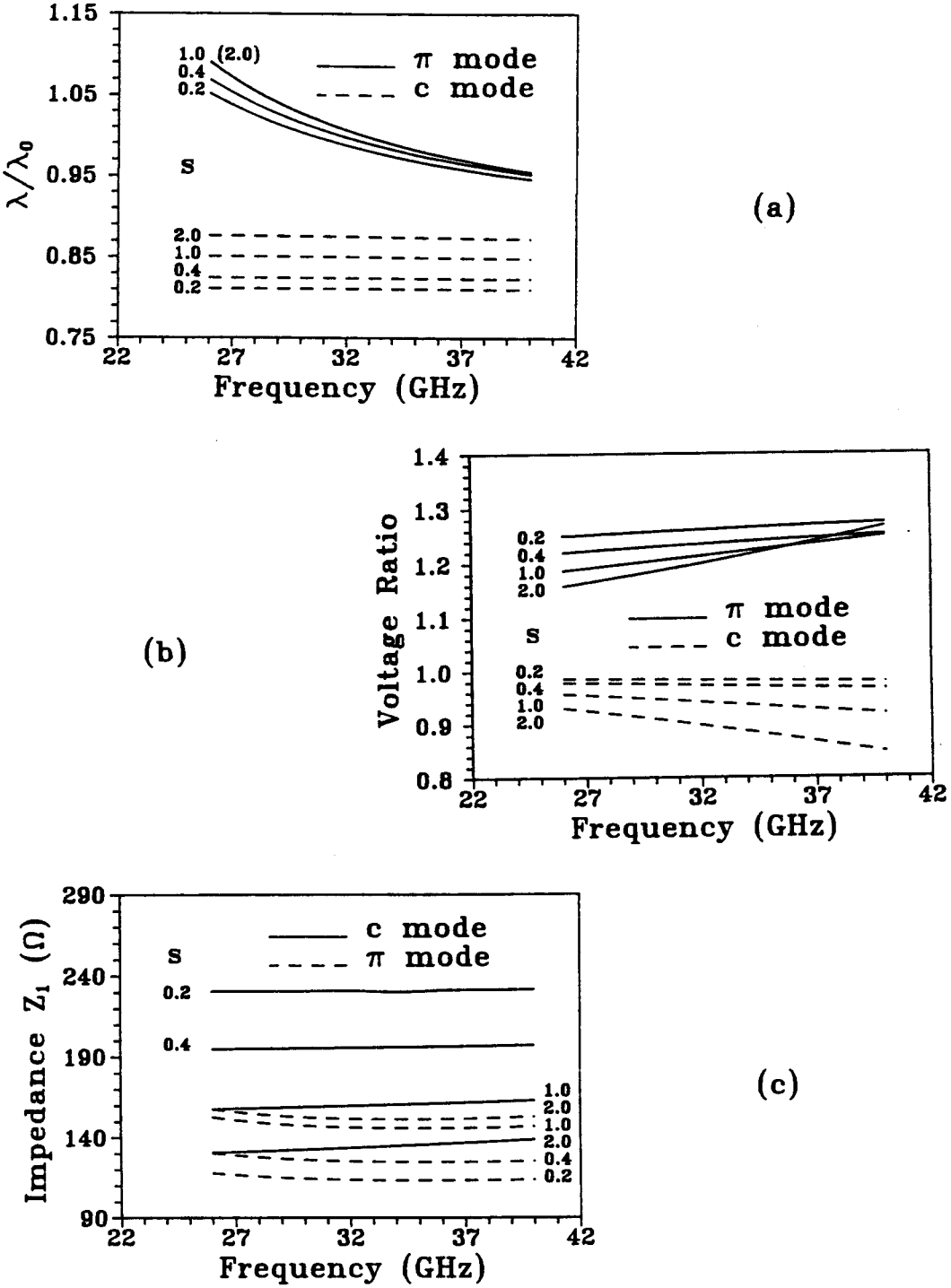

Fig. 3.7 (a) λ/λ_0, (b) voltage ratio, and (c) impedance Z_1 of a unilateral asymmetric coupled two-slot fin line as a function of frequency with the slot separation s as a parameter (ε_r=2.22, d=0.254, h_1=3.556, w_1=0.2, w_2=0.3, p_1=1.778-0.5(s+w_1), p_2=1.778+0.5(s+w_2), length unit: mm).

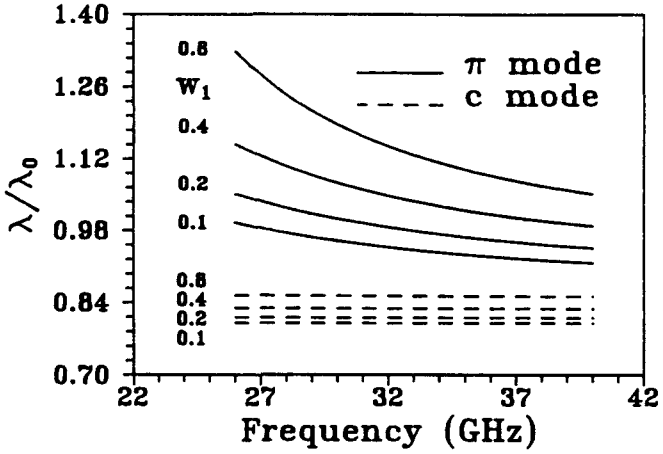

(a)

(b)

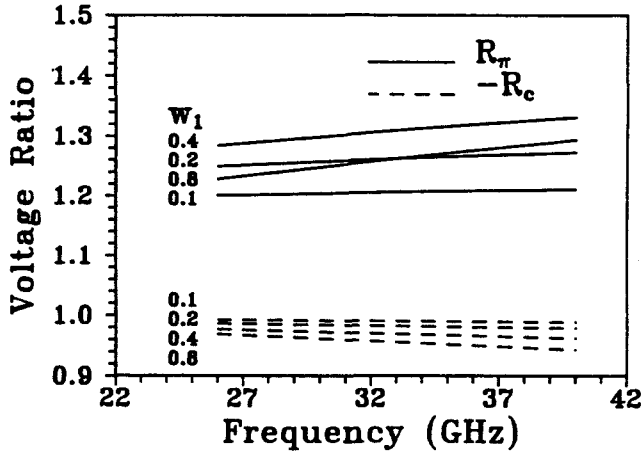

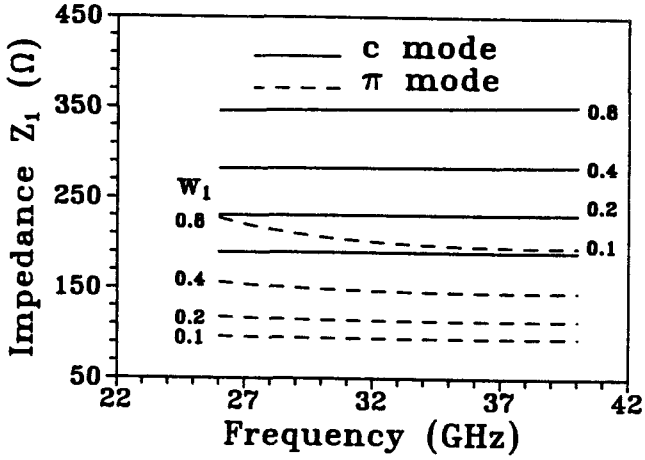

(c)

Fig. 3.8 (a) λ/λ_0, (b) voltage ratio, and (c) impedance Z_1 of a unilateral asymmetric coupled two-slot fin line as a function of frequency with w_1 as a parameter (ε_r=2.22, h_1=3.556, d=0.254, w_2=1.5w_1, p_1=1.678-0.5w_1, p_2=1.878+0.5w_2, length unit: mm).

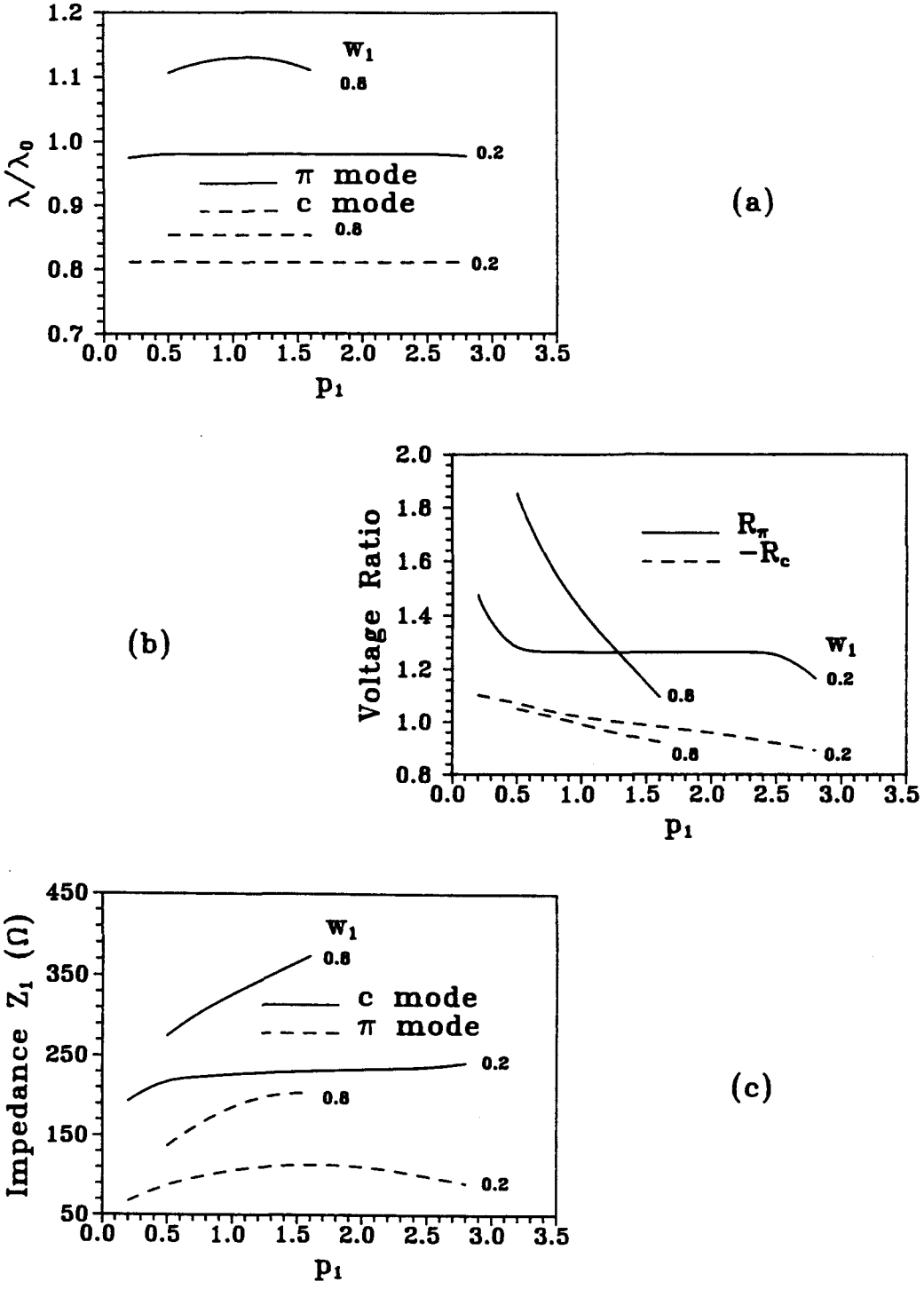

Fig. 3.9 (a) λ/λ_0, (b) voltage ratio, and (c) impedance Z_1 of a unilateral asymmetric coupled two-slot fin line as a function of the slot displacement p_1 (ε_r=2.22, h_1=3.556, d=0.254, w_1=0.2, w_2=0.3, $p_2=p_1+0.2+0.5(w_1+w_2)$, f=33GHz, length unit: mm).

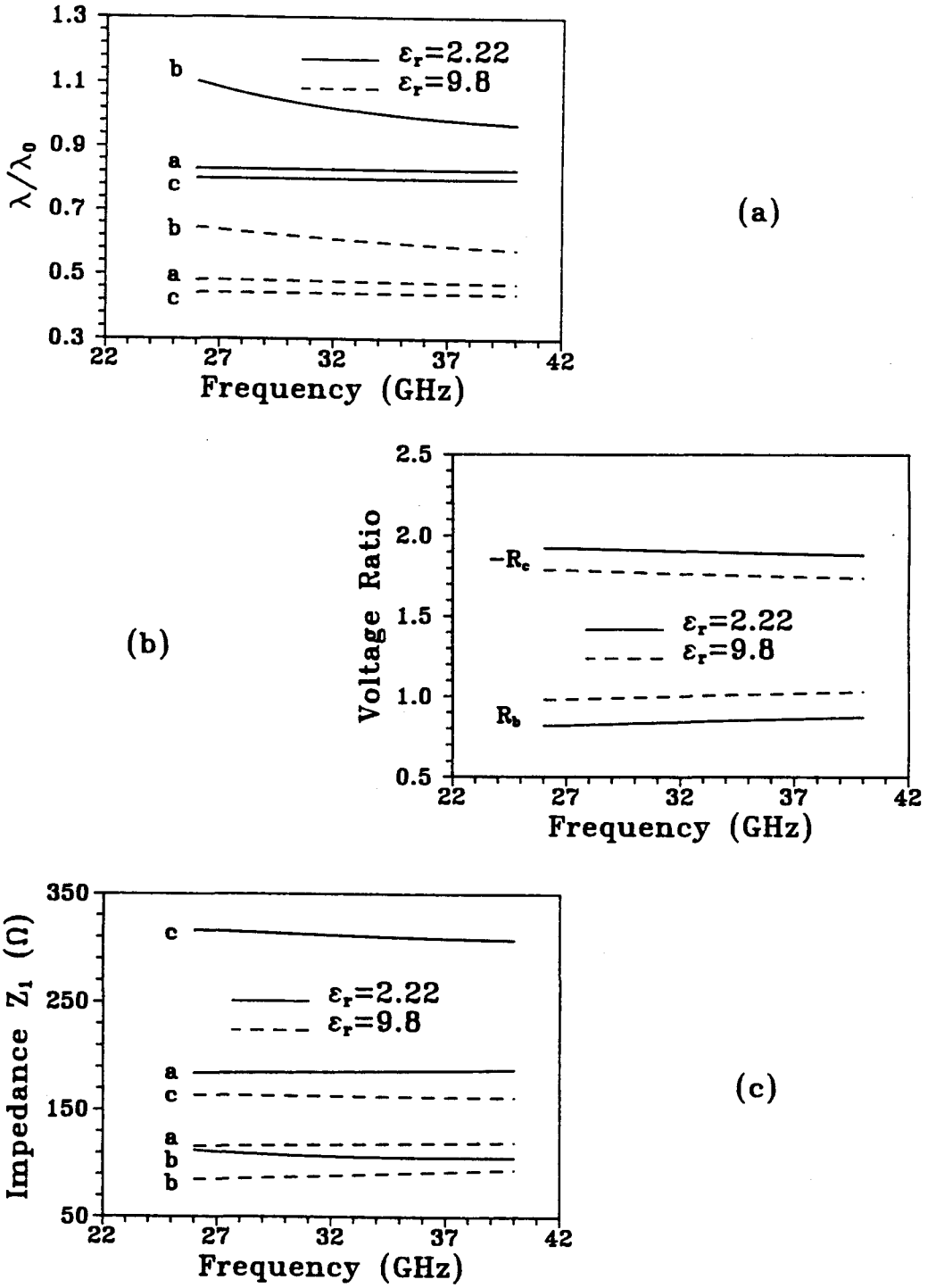

Fig. 3.10 (a) λ/λ_0, (b) voltage ratio, and (c) impedance Z_1 of a unilateral symmetric coupled three-slot fin line as a function of frequency with ε_r as a parameter (h_1=3.556, d=0.254, w_s=w_c=0.2, p_s=1.378, p_c=1.778, length unit: mm).

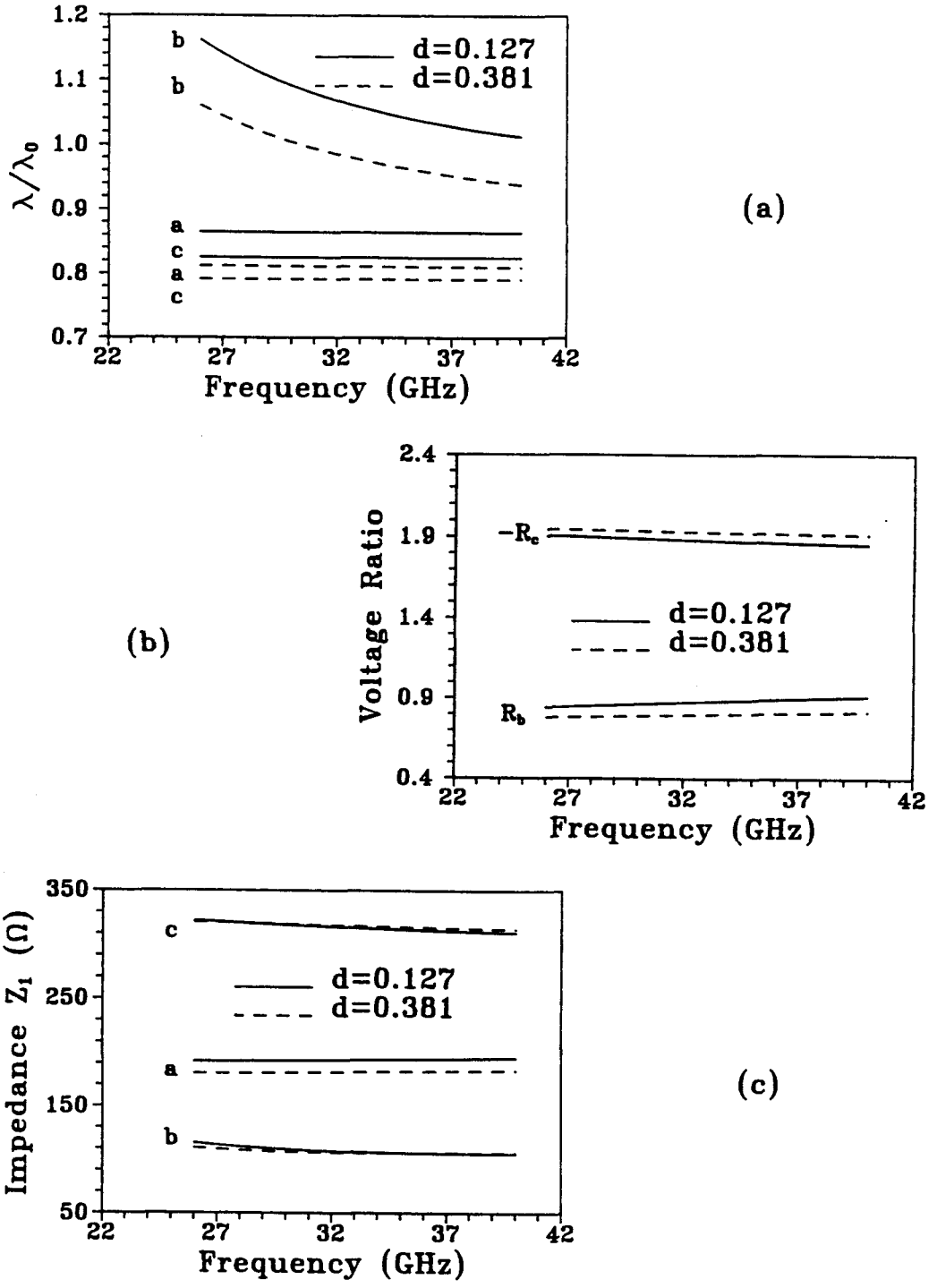

Fig. 3.11 (a) λ/λ_0, (b) voltage ratio, and (c) impedance Z_1 of a unilateral symmetric coupled three-slot fin line as a function of frequency with d as a parameter (ε_r=2.22, h_1=3.556, w_s=w_c=0.2, p_s=1.378, p_c=1.778, length unit: mm).

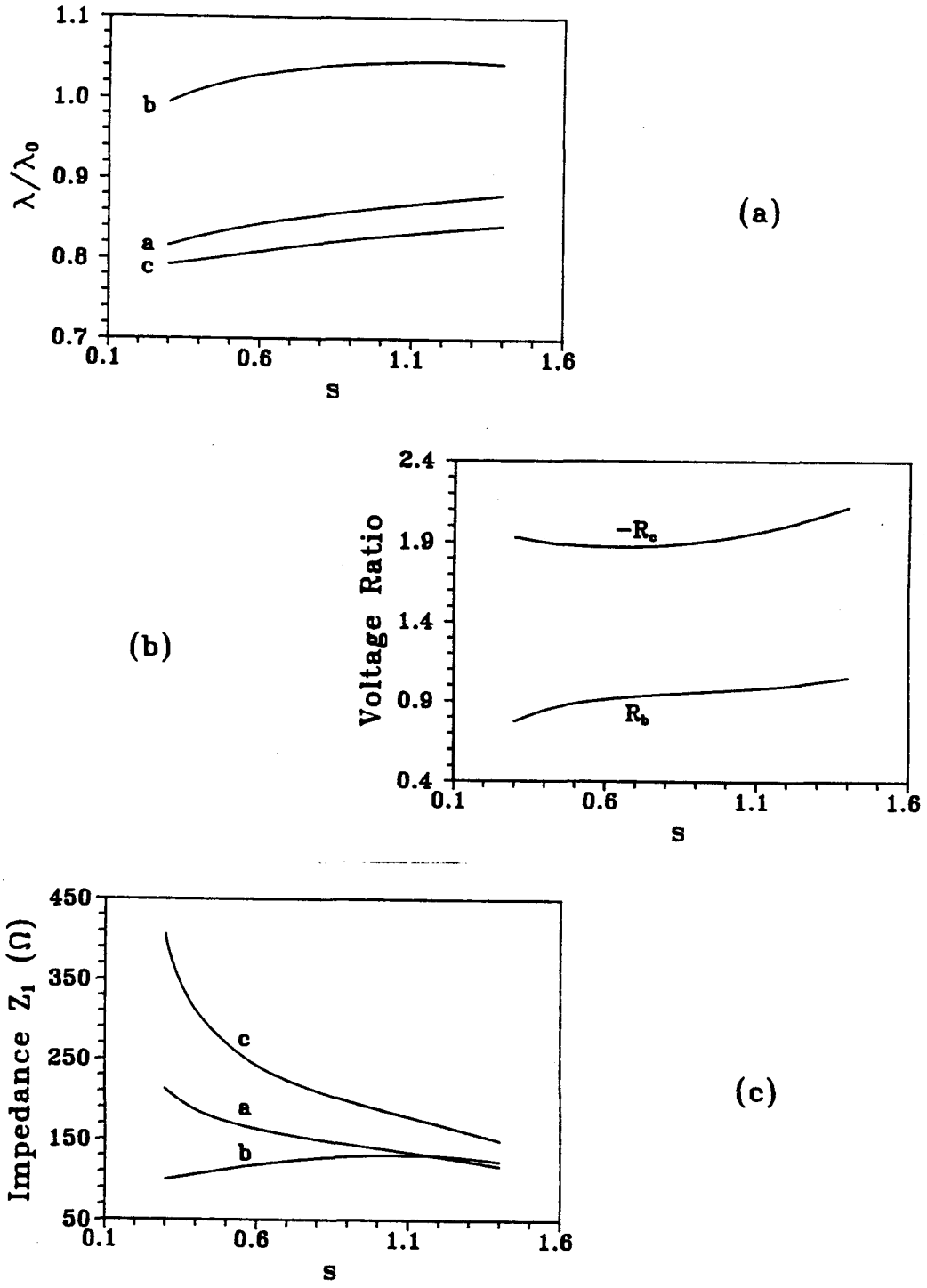

Fig. 3.12 (a) λ/λ_0, (b) voltage ratio, and (c) impedance Z_1 of a unilateral symmetric coupled three-slot fin line as a function of the separation between the centers of the side and the center slots (ε_r=2.22, h_1=3.556, d=0.254, w_s=w_c=0.2, p_s=1.778-s, p_c=1.778, f= 33GHz, length unit: mm).

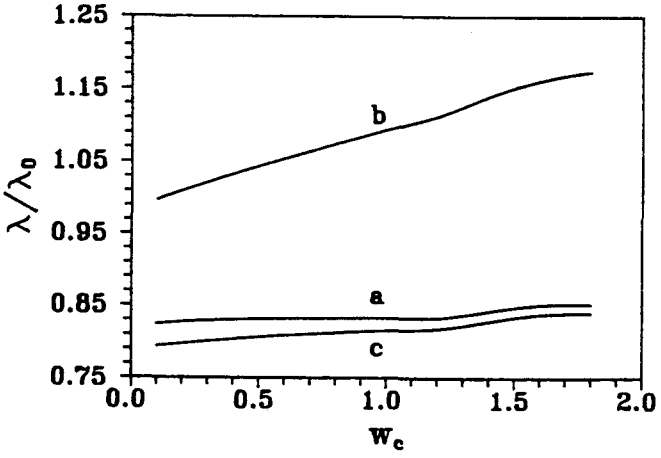

(a)

(b)

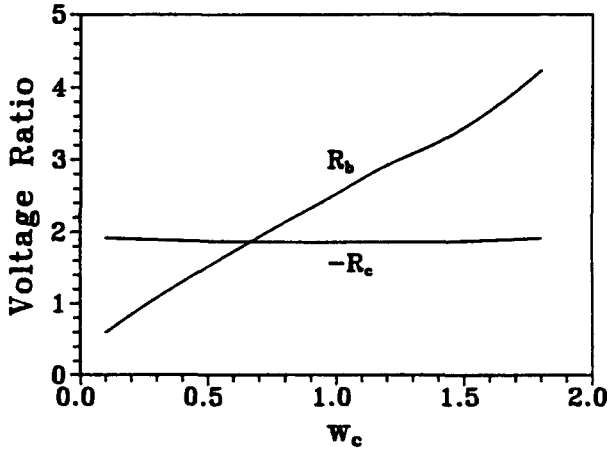

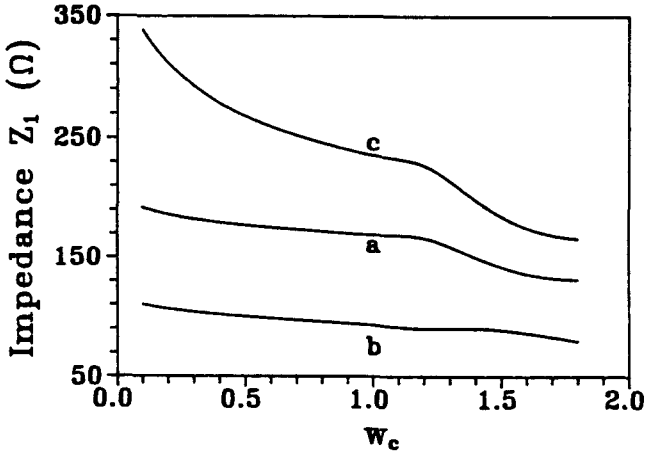

(c)

Fig. 3.13 (a) λ/λ_0, (b) voltage ratio, and (c) impedance Z_1 of a unilateral symmetric coupled three-slot fin line as a function of the center slot width (ε_r=2.22, h_1=3.556, d=0.254, w_s=0.2, p_s=1.578-0.5(w_c+w_s), p_c=1.778, f=33GHz, length unit: mm).

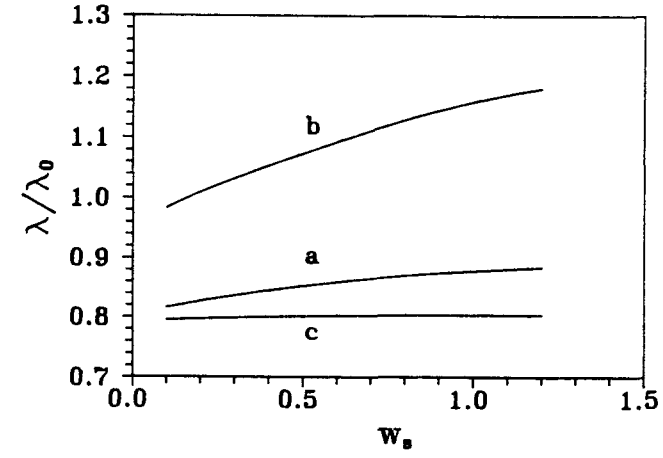

(a)

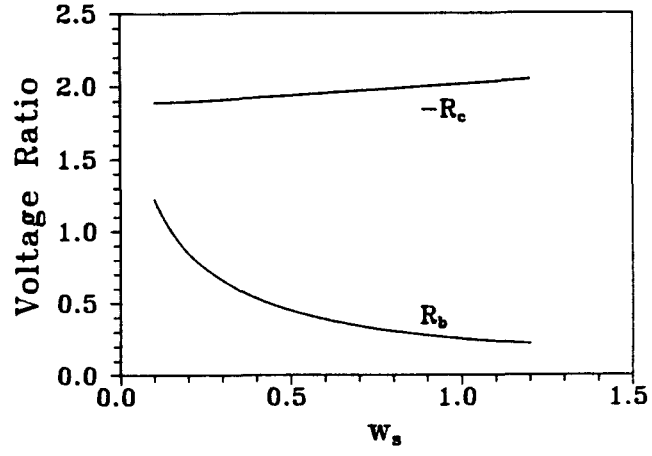

(b)

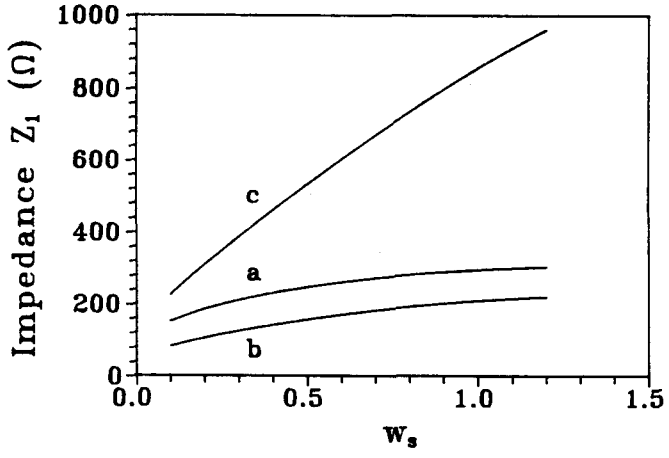

(c)

Fig. 3.14 (a) λ/λ_0, (b) voltage ratio, and (c) impedance Z_1 of a unilateral symmetric coupled three-slot fin line as a function of the side slot width (ε_r=2.22, h_1=3.556, d=0.254, w_c=0.2, p_s=1.578-0.5(w_c+w_s), p_c=1.778, f=33GHz, length unit: mm).

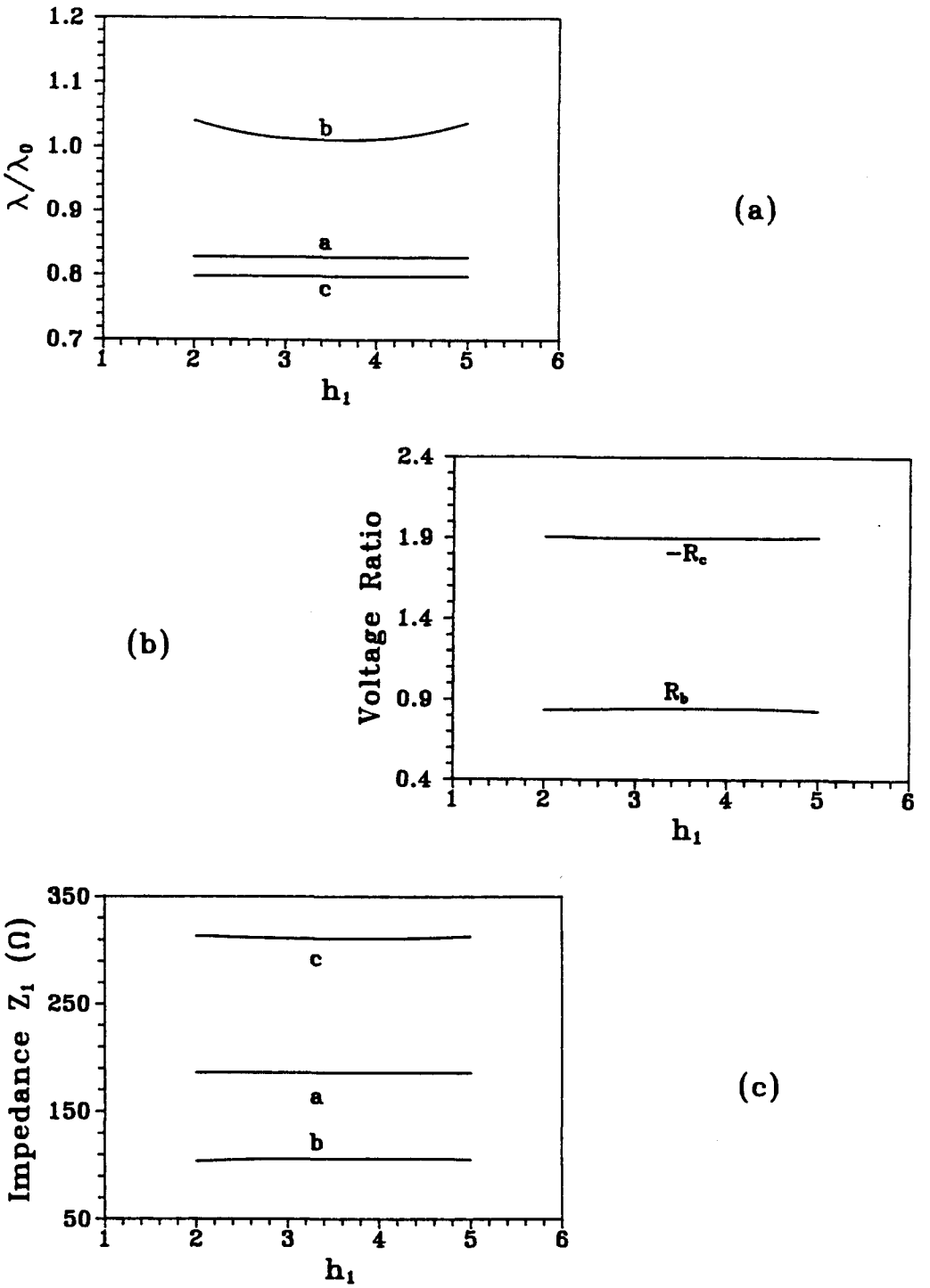

Fig. 3.15 (a) λ/λ_0, (b) voltage ratio, and (c) impedance Z_1 of a unilateral symmetric coupled three-slot fin line as a function of the lateral displacement of the substrate (ε_r=2.22, d=0.254, w_s=w_c=0.2, p_s=1.378, p_c=1.778, f=33GHz, length unit: mm).

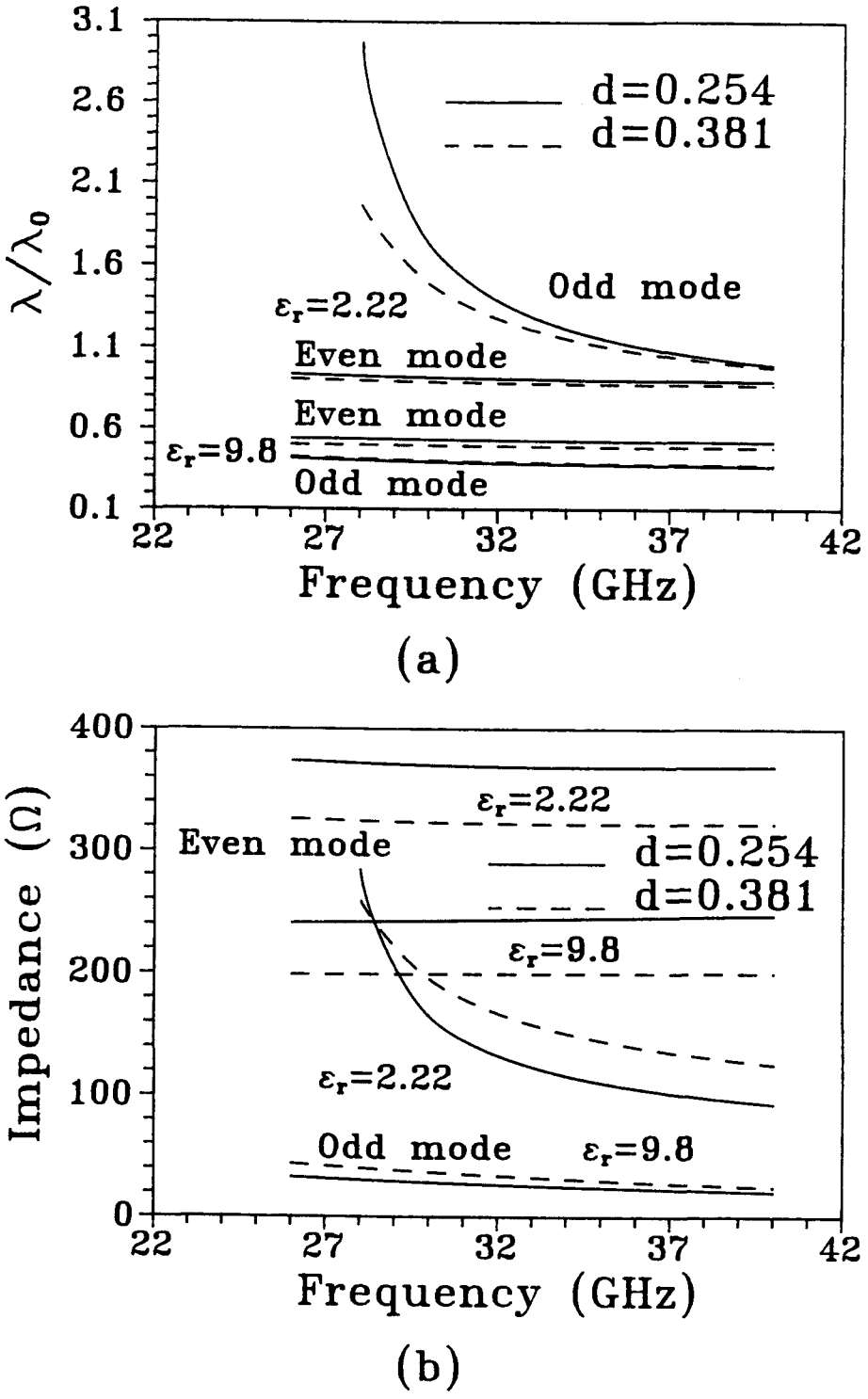

Fig. 3.16 (a) λ/λ_0 and (b) impedance of a bilateral symmetric coupled two-slot fin line as a function of frequency with ε_r and d as parameters (h_1=3.429, w_1=w_2=0.2, p_1=p_2=1.778, length unit: mm).

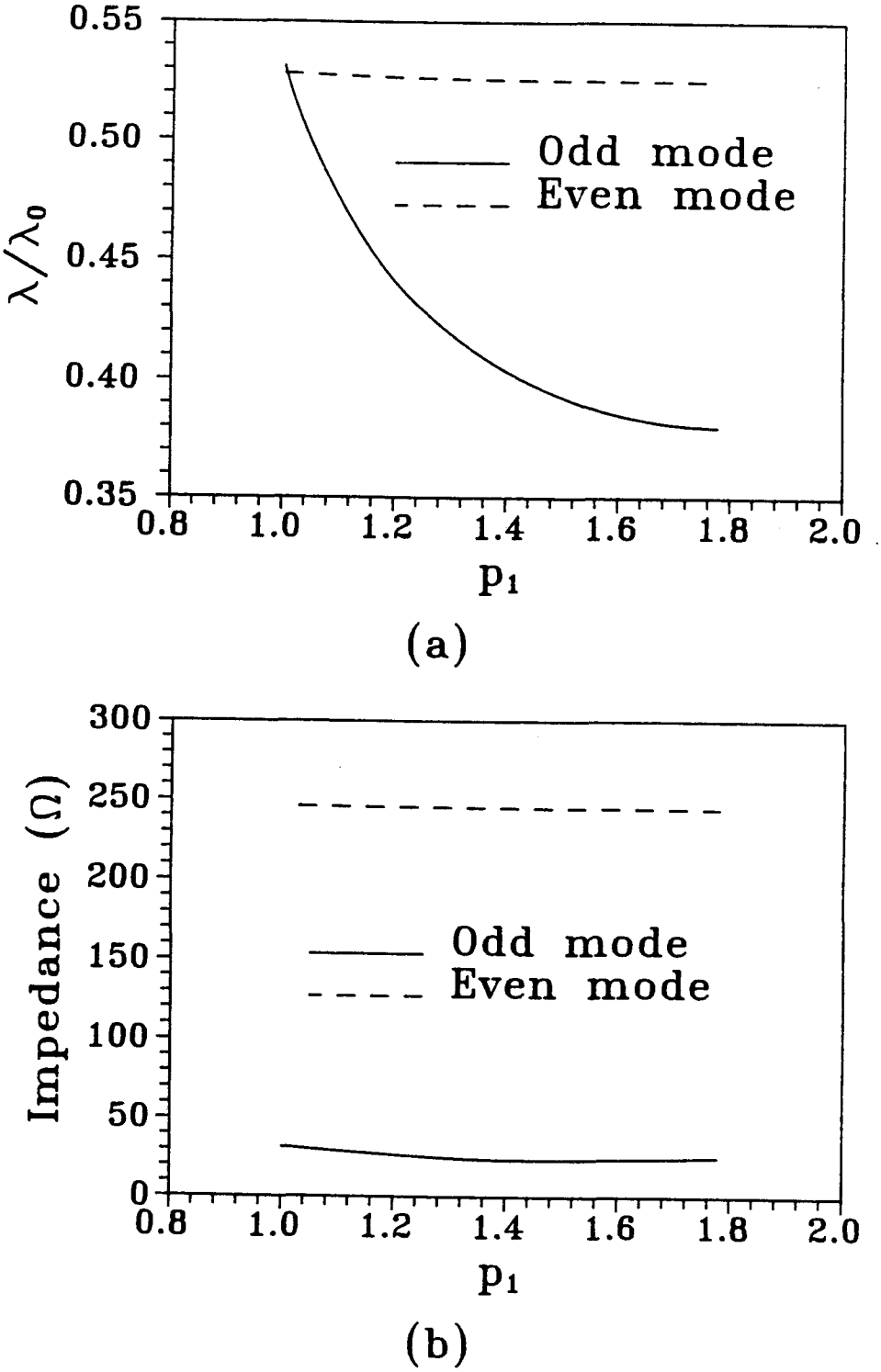

Fig. 3.17 (a) λ/λ_0 and (b) impedance of a bilateral symmetric coupled two-slot fin line as a function of the slot center p_1 (ε_r=9.8, h_1=3.429, d=0.254, w_1=w_2=0.2, p_2=p_1, f=33GHz, length unit: mm).

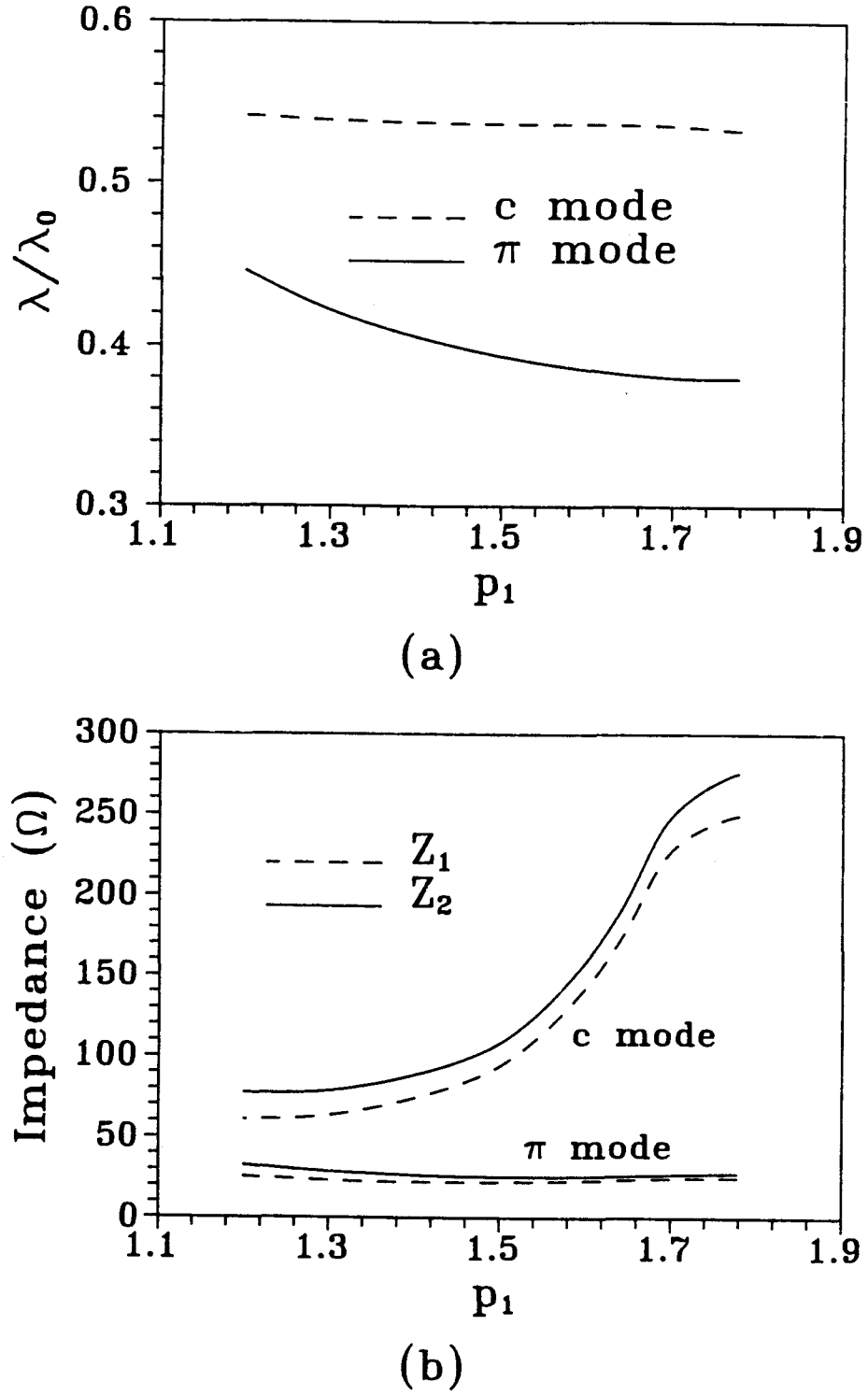

Fig. 3.18 (a) λ/λ_0 and (b) impedance of a bilateral asymmetric coupled two-slot fin line as a function of the slot center p_1 (ε_r=9.8, h_1=3.429, d=0.254, w_1=0.2, w_2=0.3, p_2=p_1, f=33GHz, length unit: mm).

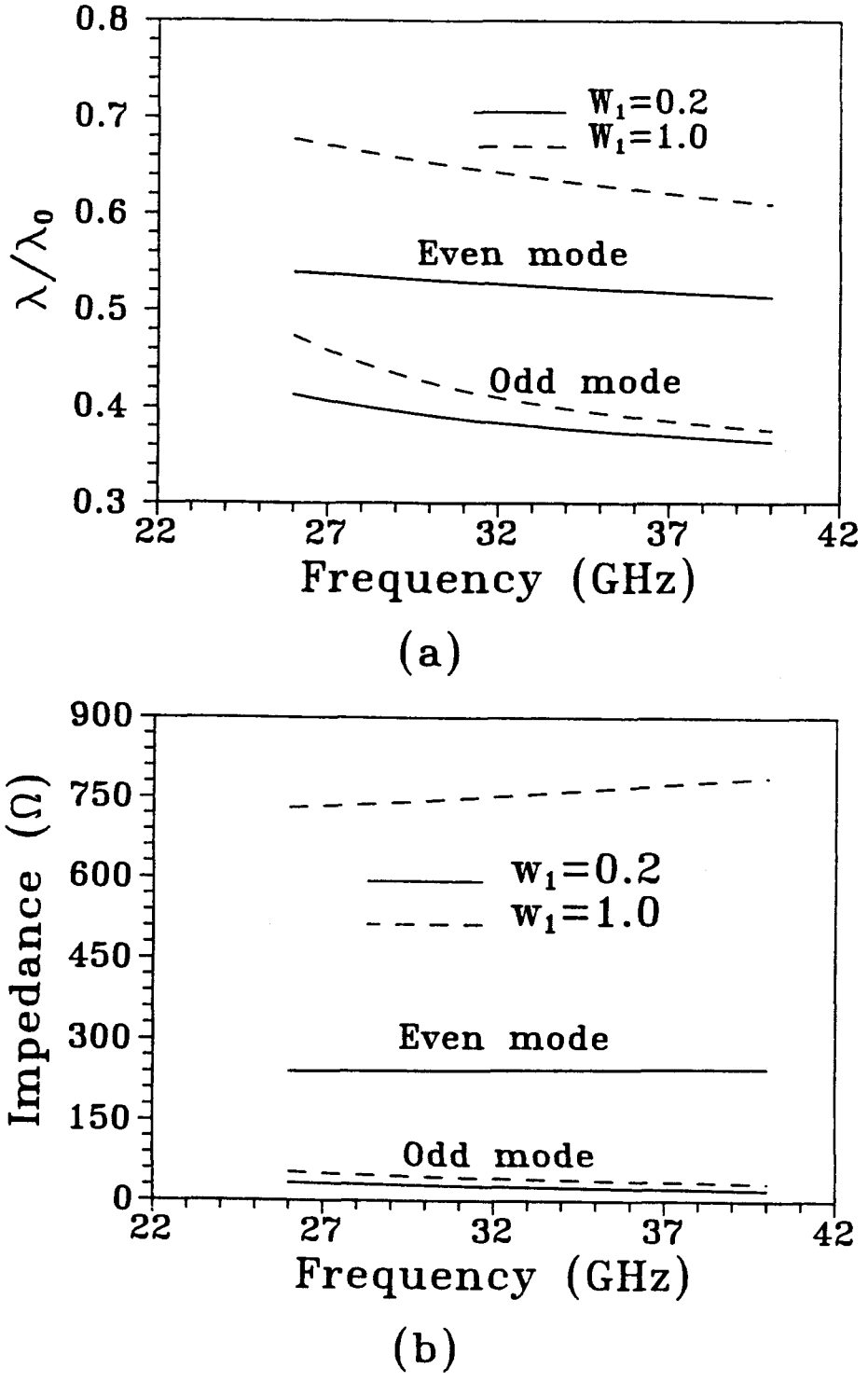

Fig. 3.19 (a) λ/λ_0 and (b) impedance of a bilateral symmetric coupled two-slot fin line as a function of frequency with the slot width as a parameter (ε_r=9.8, h_1=3.429, d=0.254, w_1=w_2, p_1=p_2=1.778, length unit: mm).

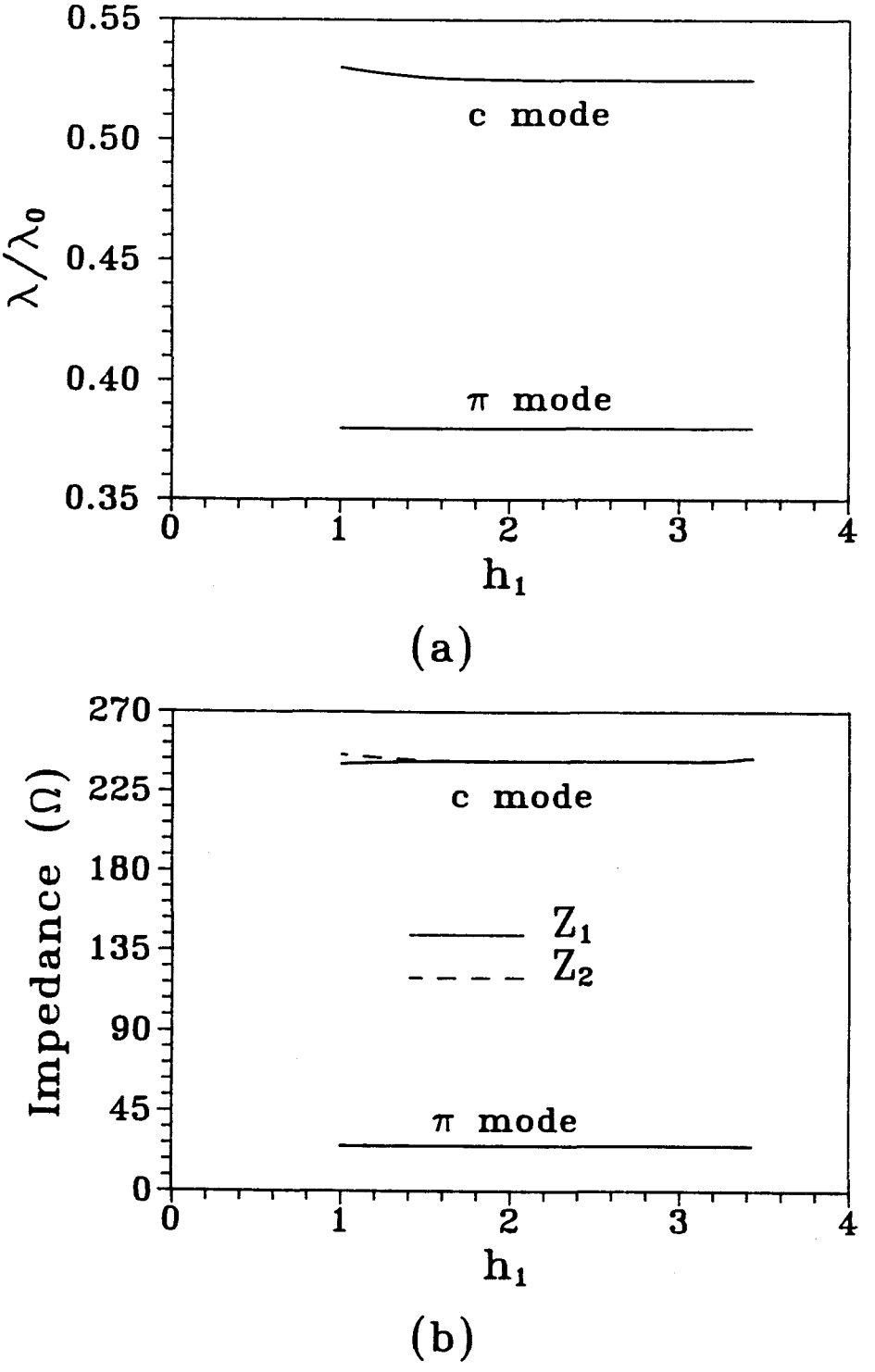

Fig. 3.20 (a) λ/λ_0 and (b) impedance of a bilateral coupled two-slot fin line with an equal slot width as a function of the lateral displacement of the substrate (ε_r=9.8, d=0.254, w_1=w_2=0.2, p_1=p_2=1.778, f=33GHz, length unit: mm).

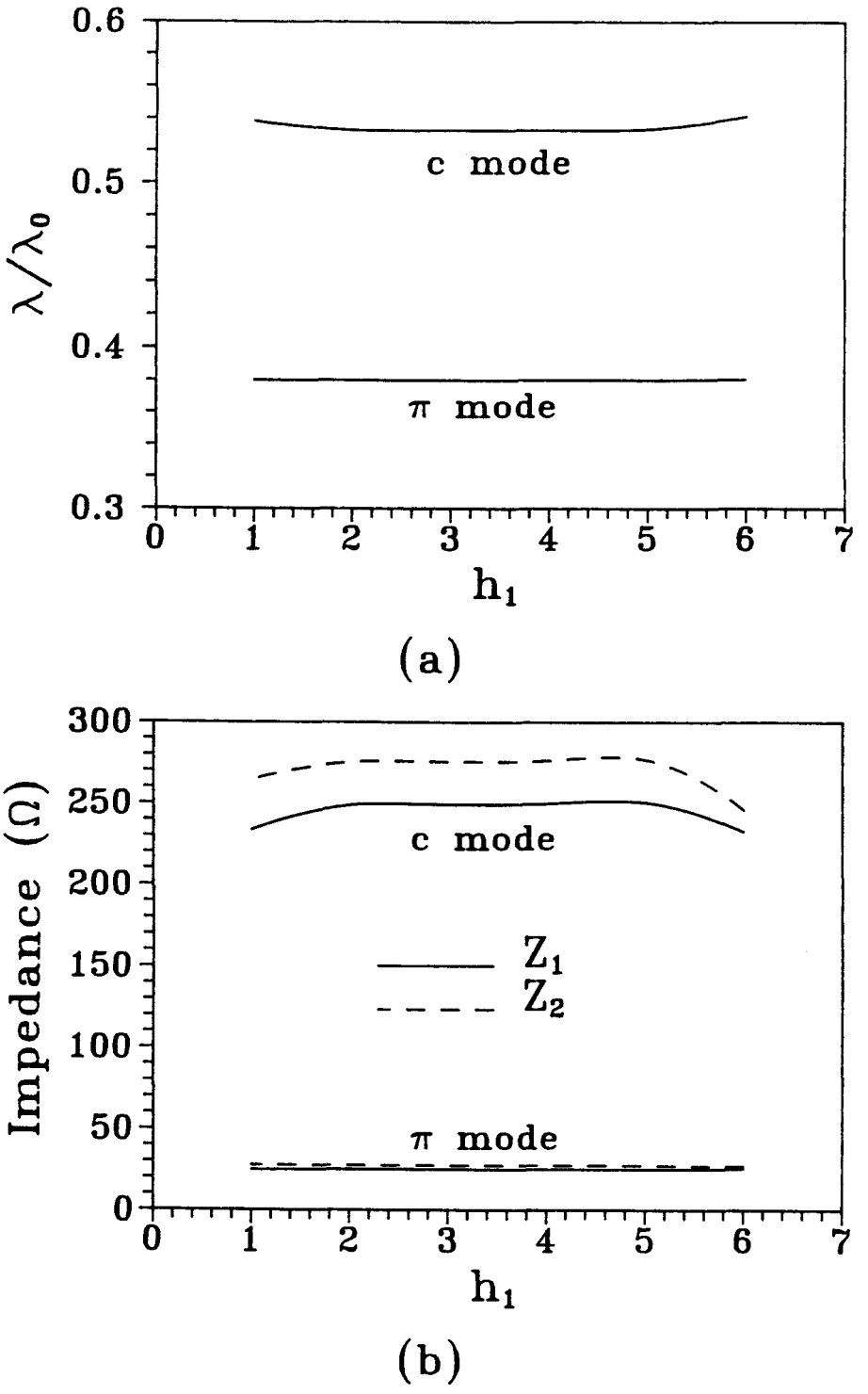

Fig. 3.21 (a) λ/λ_0 and (b) impedance of a bilateral coupled two-slot fin line with unequal slot widths as a function of the lateral displacement of the substrate (ε_r=9.8, d=0.254, w_1=0.2, w_2=0.3, p_1=p_2=1.778, f=33GHz, length unit: mm).

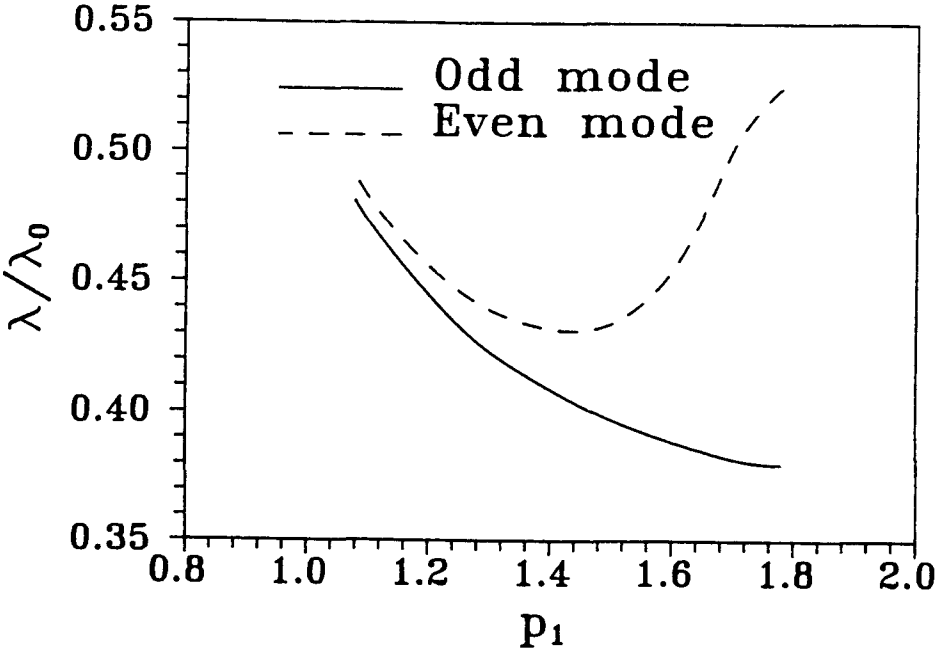

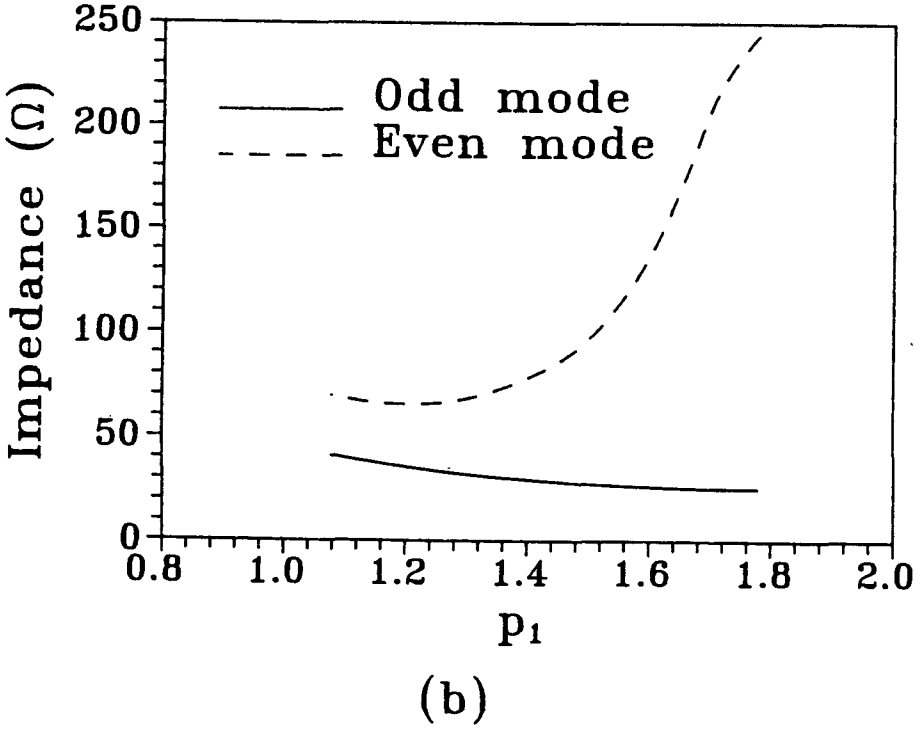

Fig. 3.22 (a) λ/λ_0 and (b) impedance of a bilateral coupled two-slot fin line with two equal slots symmetric to the structure center as a function of the slot center p_1 (ε_r=9.8, h_1=3.429, d=0.254, w_1=w_2=0.2, p_2=3.556-p_1, f=33GHz, length unit: mm).

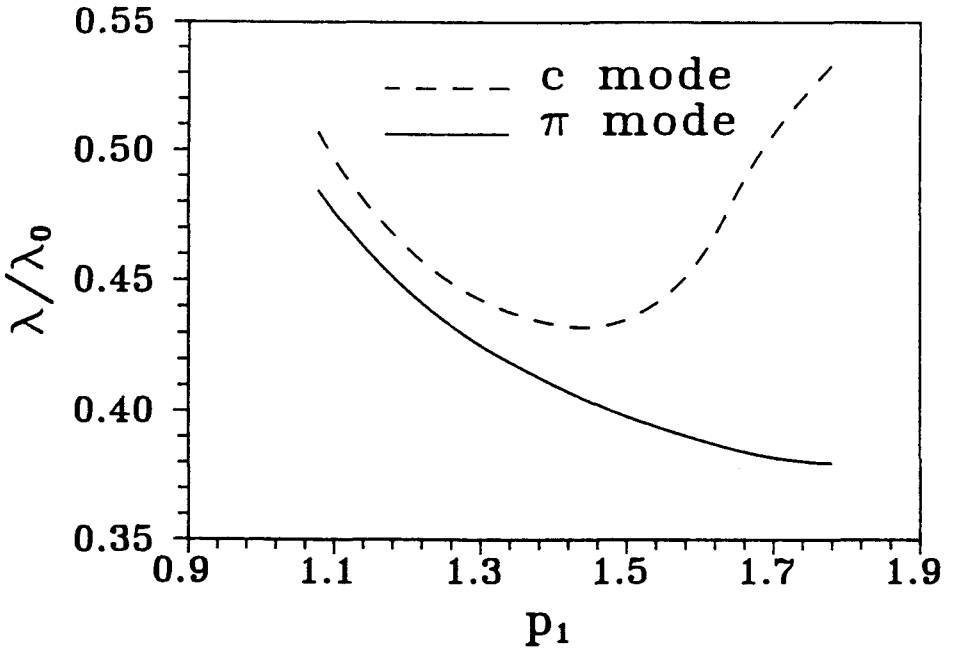

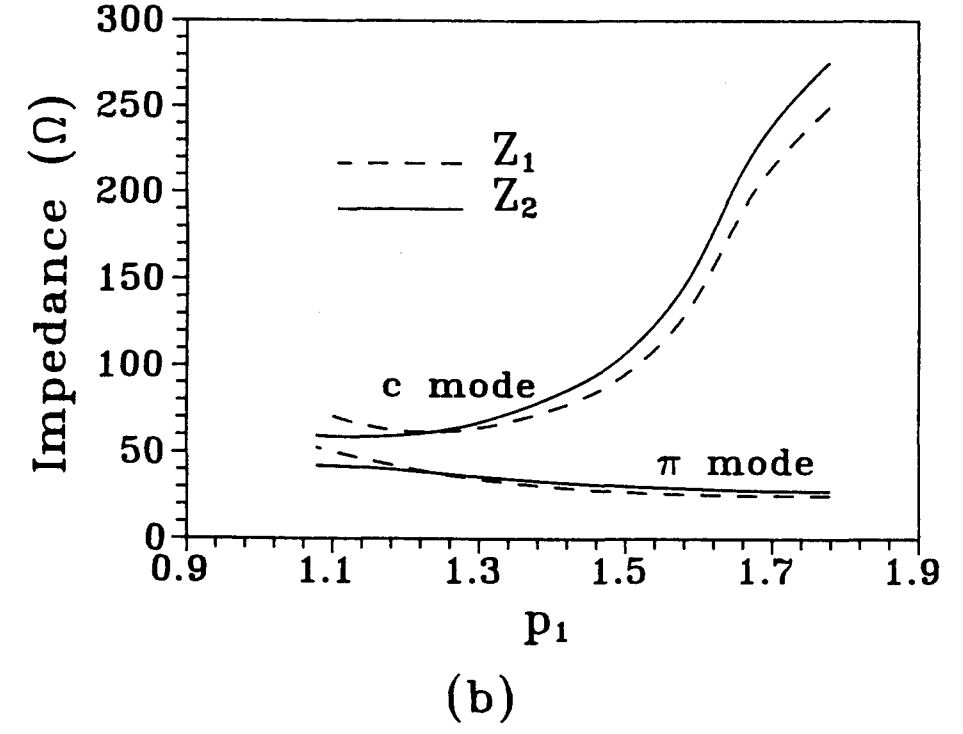

Fig. 3.23 (a) λ/λ_0 and (b) impedance of a bilateral coupled two-slot fin line with the centers of two unequal slots symmetric to the structure center as a function of the slot center p_1 (ε_r=9.8, h_1=3.429, d=0.254, w_1=0.2, w_2=0.3, p_2=3.556-p_1, f=33GHz, length unit: mm).

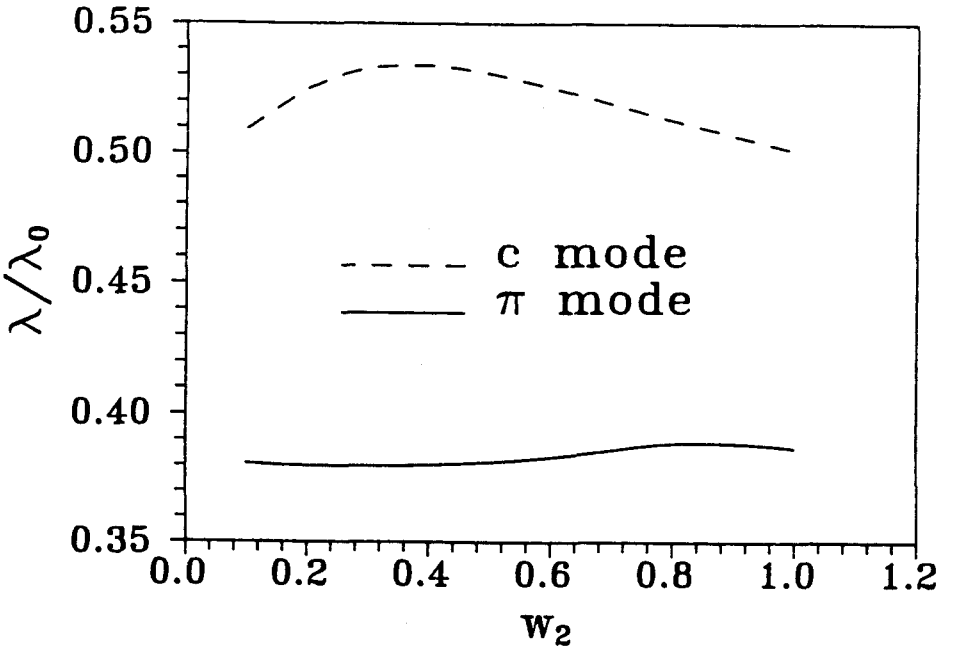

(a)

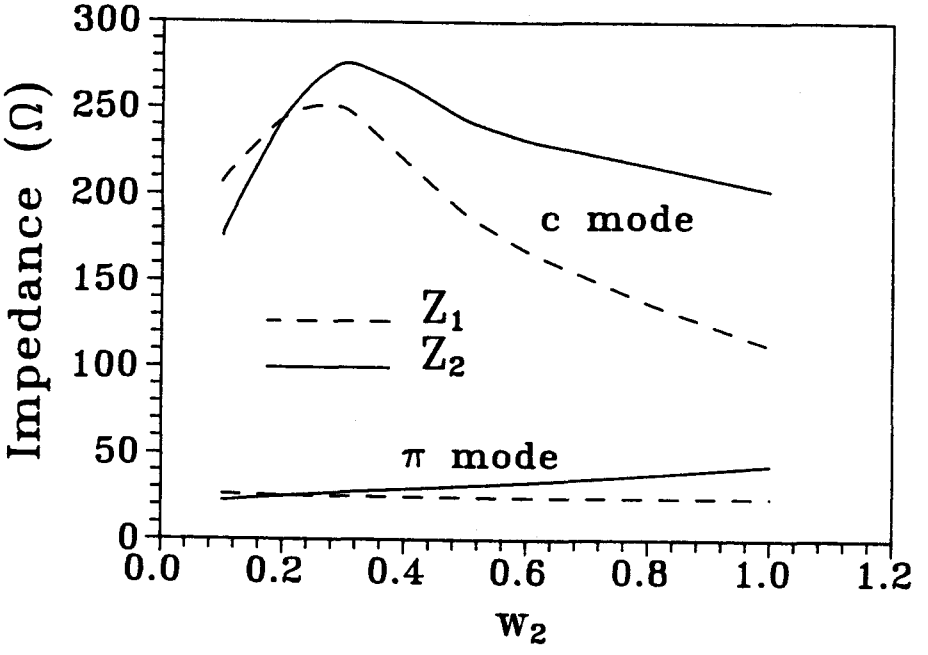

(b)

Fig. 3.24 (a) λ/λ_0 and (b) impedance of a bilateral asymmetric coupled two-slot fin line with two unequal slots as a function of the slot width w_2 (ε_r=9.8, h_1=3.429, d=0.254, w_1=0.2, p_1=p_2=1.778, f=33GHz, length unit: mm).

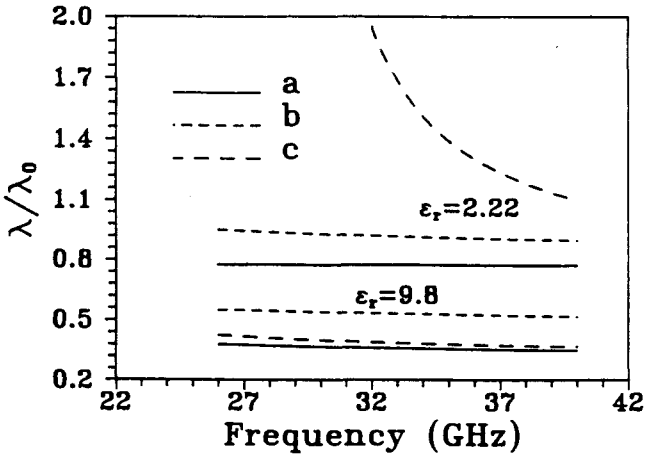

(a)

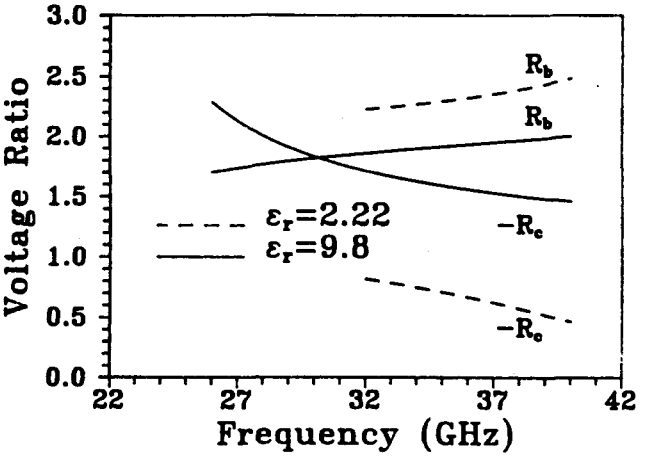

(b)

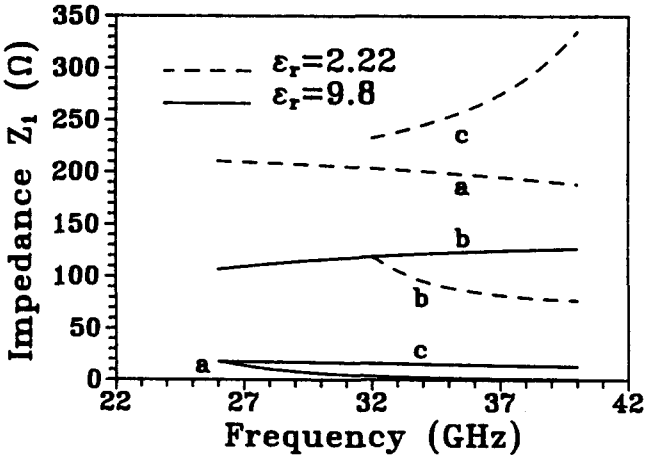

(c)

Fig. 3.25 (a) λ/λ_0, (b) voltage ratio, and (c) impedance Z_1 of a bilateral symmetric coupled three-slot fin line as a function of frequency with ε_r as a parameter (h_1=3.429, d=0.254, w_s=w_c=0.2, p_s=1.578, p_c=1.778, length unit: mm).

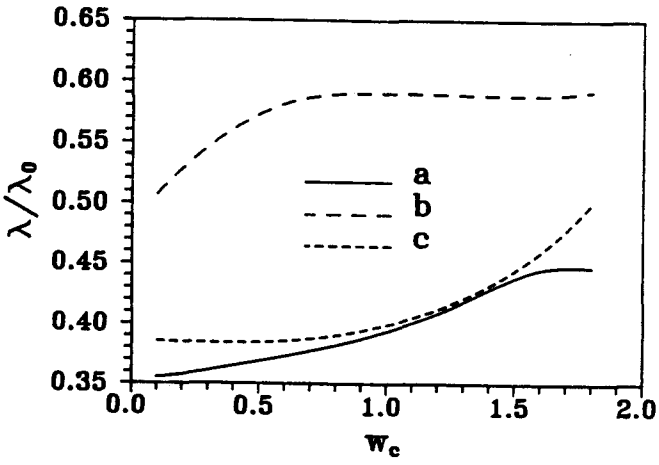

(a)

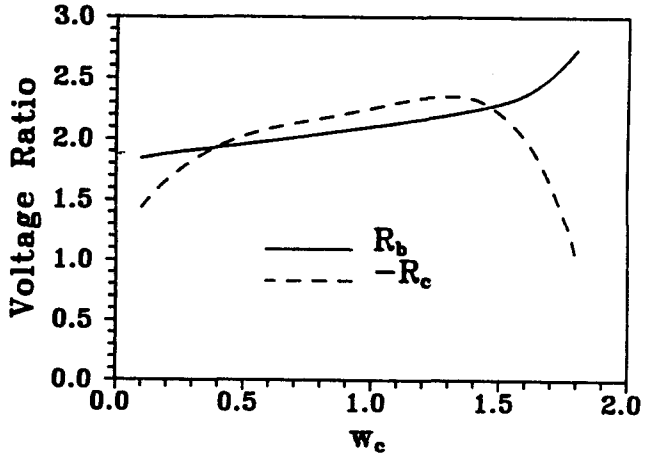

(b)

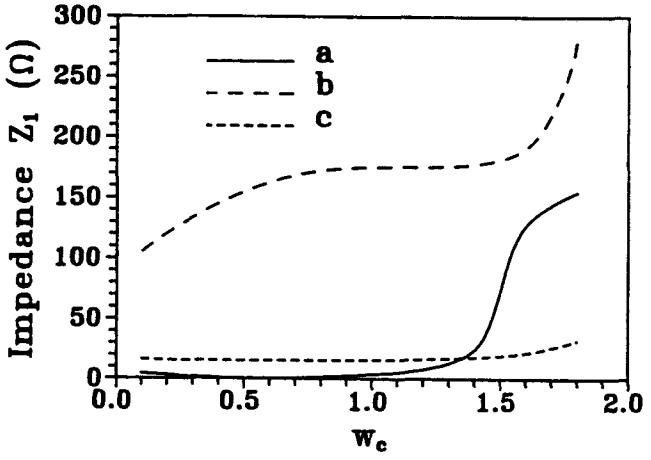

(c)

Fig. 3.26 (a) λ/λ_0, (b) voltage ratio, and (c) impedance Z_1 of a bilateral symmetric coupled three-slot fin line as a function of the center slot width (ε_r=9.8, h_1=3.429, d=0.254, w_s=0.2, p_s=1.578, p_c=1.778, f=33GHz, length unit: mm).

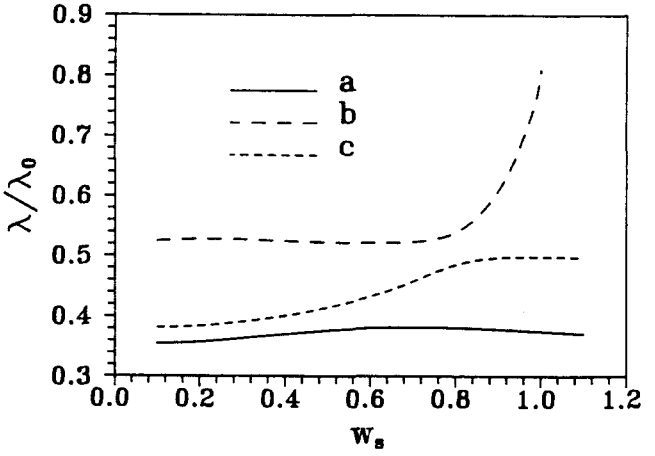

(a)

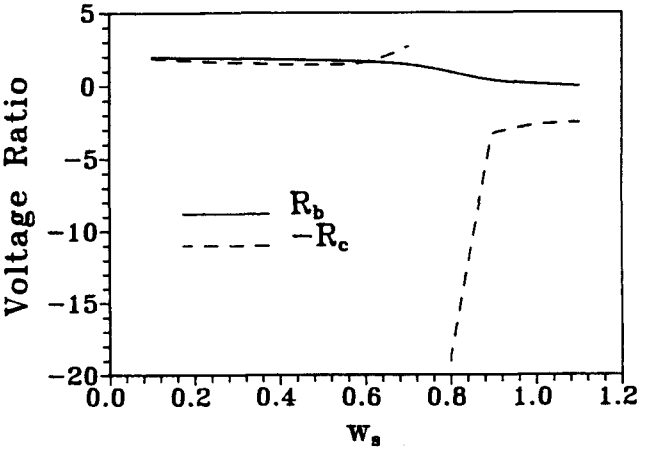

(b)

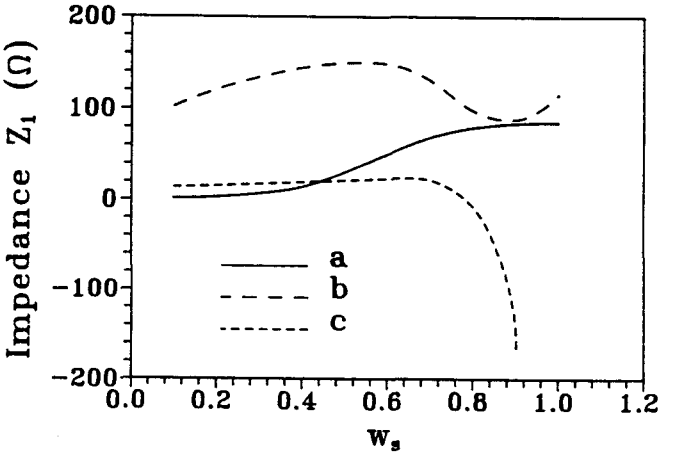

(c)

Fig. 3.27 (a) λ/λ_0, (b) voltage ratio, and (c) impedance Z_1 of a bilateral symmetric coupled three-slot fin line as a function of the side slot width (ε_r=9.8, h_1=3.429, d=0.254, w_c=0.2, p_s=1.678-0.5w_s, p_c=1.778, f=33GHz, length unit: mm).

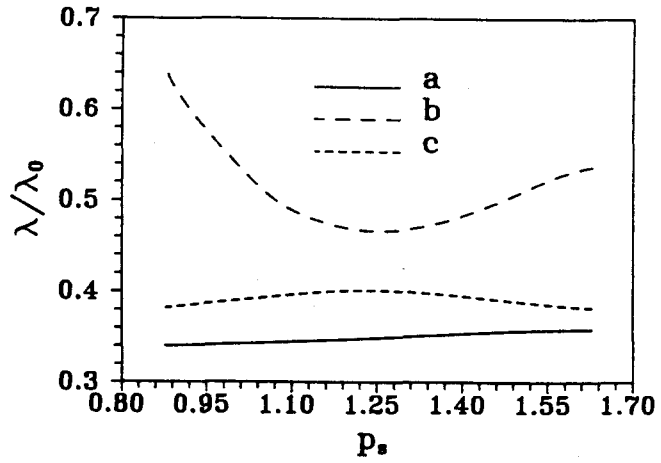

(a)

(b)

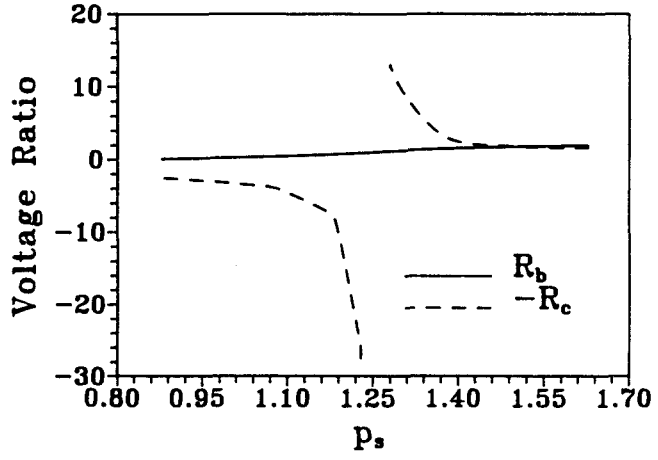

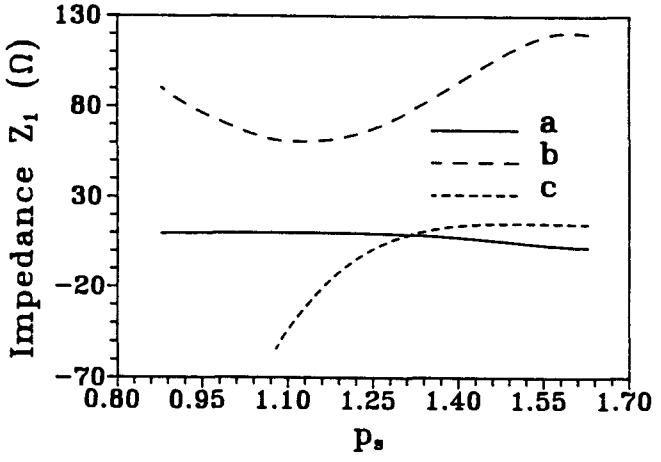

(c)

Fig. 3.28 (a) λ/λ_0, (b) voltage ratio, and (c) impedance Z_1 of a bilateral symmetric coupled three-slot fin line as a function of the side slot center p_s (ε_r=9.8, h_1=3.429, d=0.254, w_s=w_c=0.2, p_c=1.778, f=33GHz, length unit: mm).

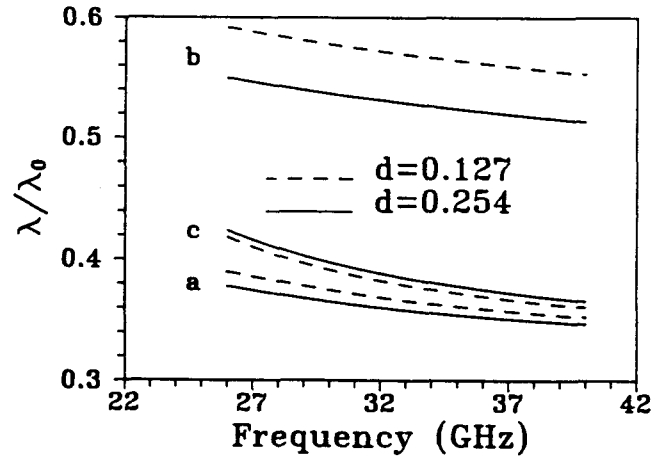

(a)

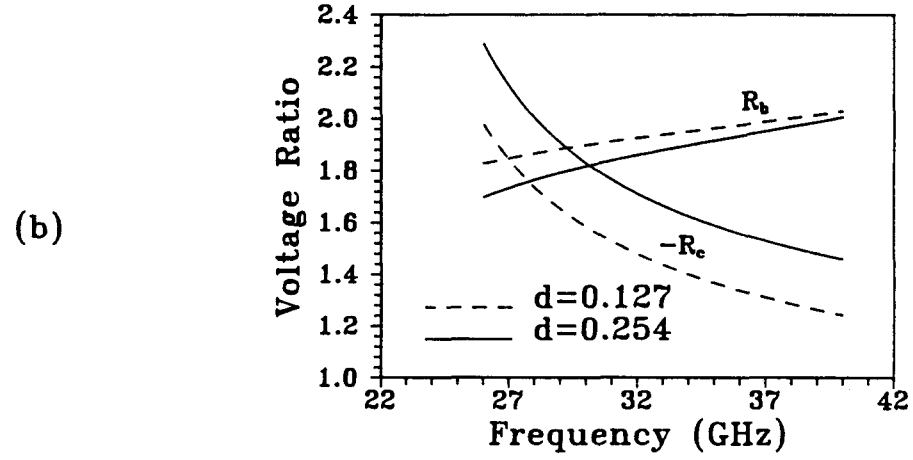

(b)

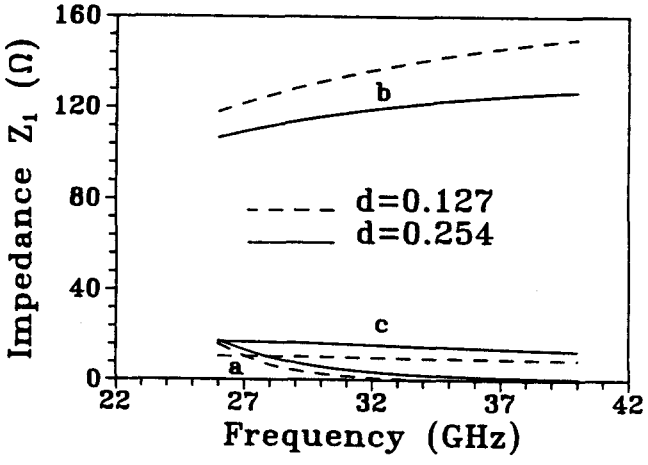

(c)

Fig. 3.29 (a) λ/λ_0, (b) voltage ratio, and (c) impedance Z_1 of a bilateral symmetric coupled three-slot fin line as a function of frequency with d as a parameter (ε_r=9.8, h_1=3.556-0.5d, w_s=w_c=0.2, p_s=1.578, p_c=1.778, length unit: mm).

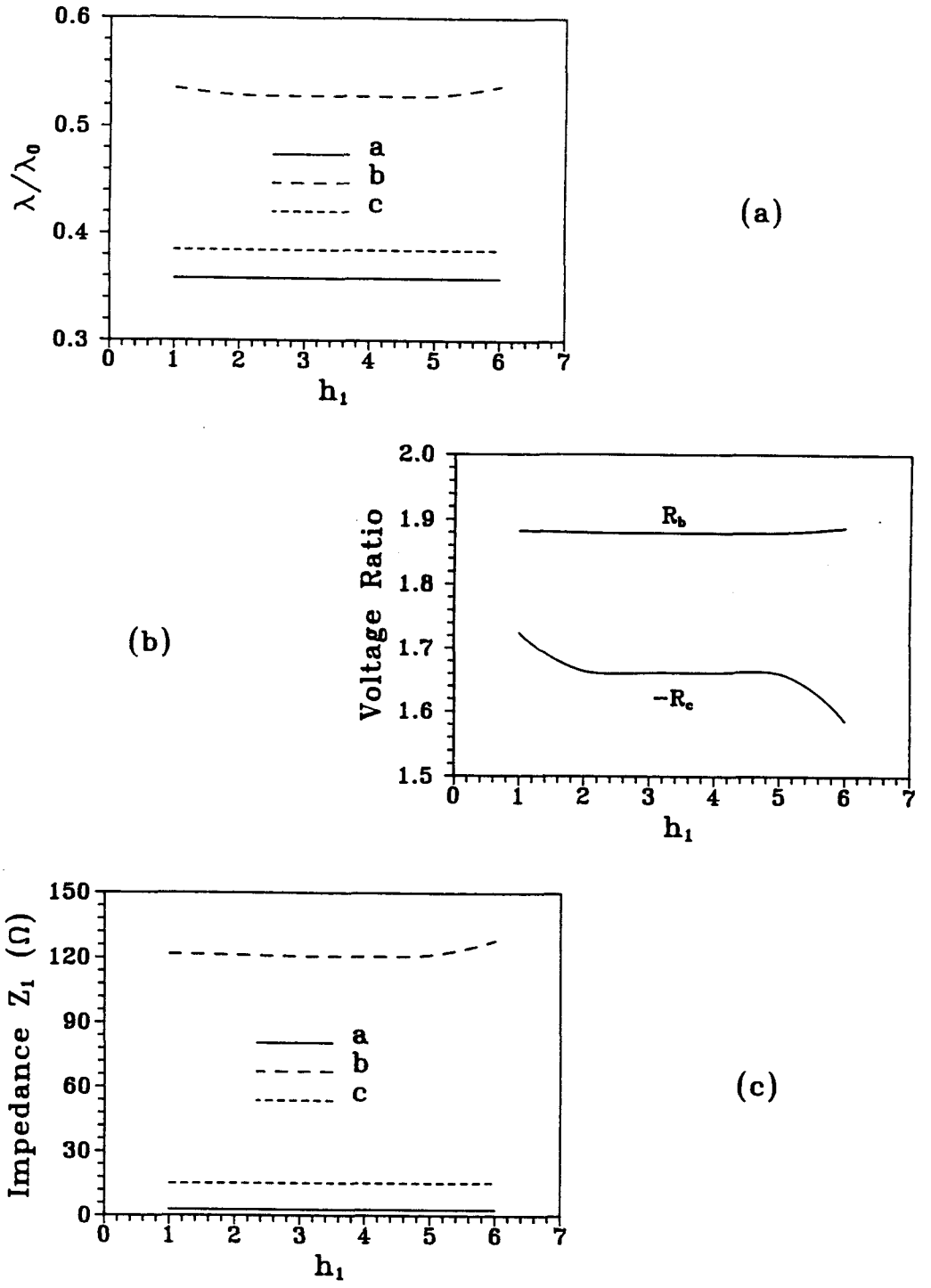

Fig. 3.30 (a) λ/λ_0, (b) voltage ratio, and (c) impedance Z_1 of a bilateral symmetric coupled three-slot fin line as a function of the lateral displacement of the substrate (ε_r=9.8, d=0.254, w_s=w_c=0.2, p_s=1.578, p_c=1.778, f=33GHz, length unit: mm).

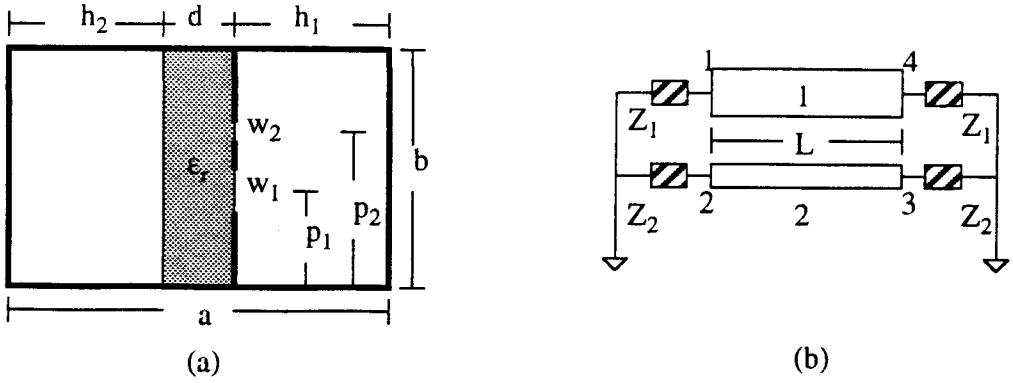

Fig. 3.31 Four-port directional coupler: (a) cross section and (b) circuit schematic.

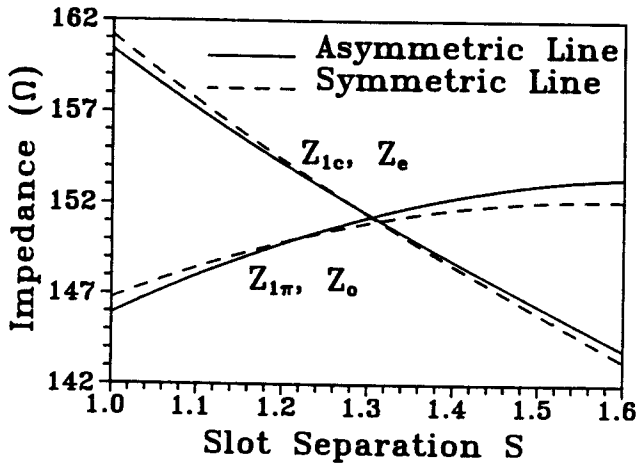

Fig. 3.32 Characteristic impedances of asymmetric and symmetric unilateral coupled fin lines as a function of the slot separation S (f=33GHz, ε_r=2.22, d=0.254, h_1=3.556, p_1=1.778-0.5(S+w_1), p_2=1.778+0.5(S+w_2), symmetric case: w_1=w_2=0.2, asymmetric case: w_1=0.2, w_2 = 0.3, length unit: mm).

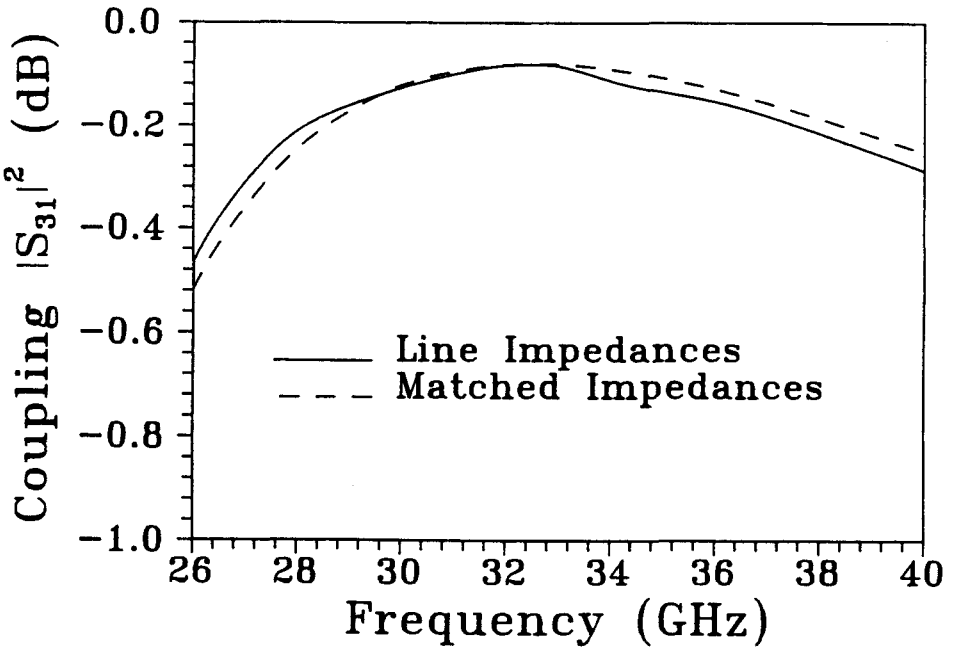

(a)

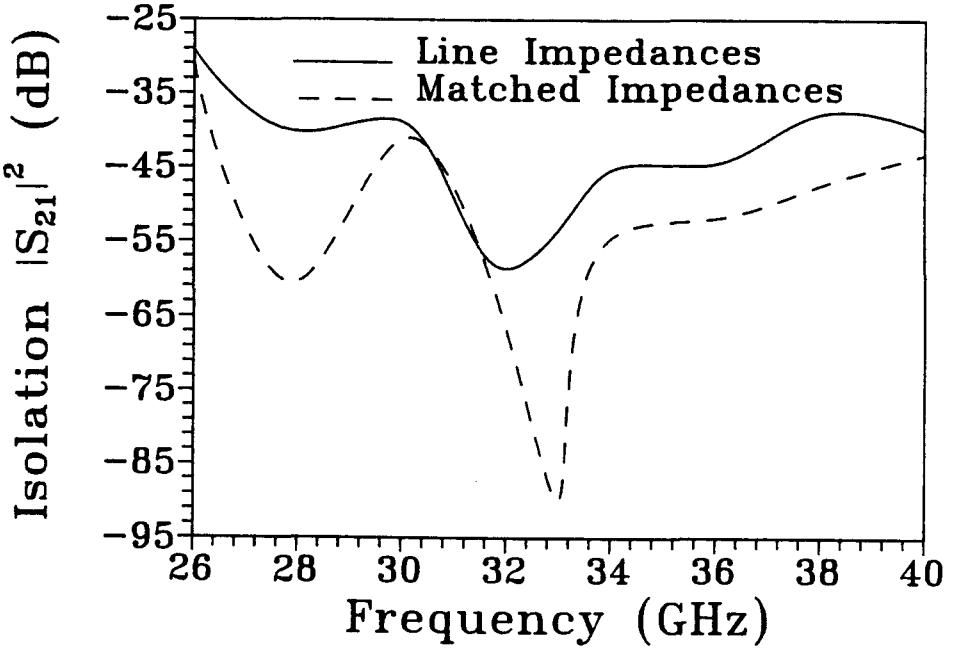

(b)

Fig. 3.33 (a) Coupling and (b) isolation of maximum coupling couplers terminated with the matched (L=27.946mm) and the line (L=27.615mm) impedances.

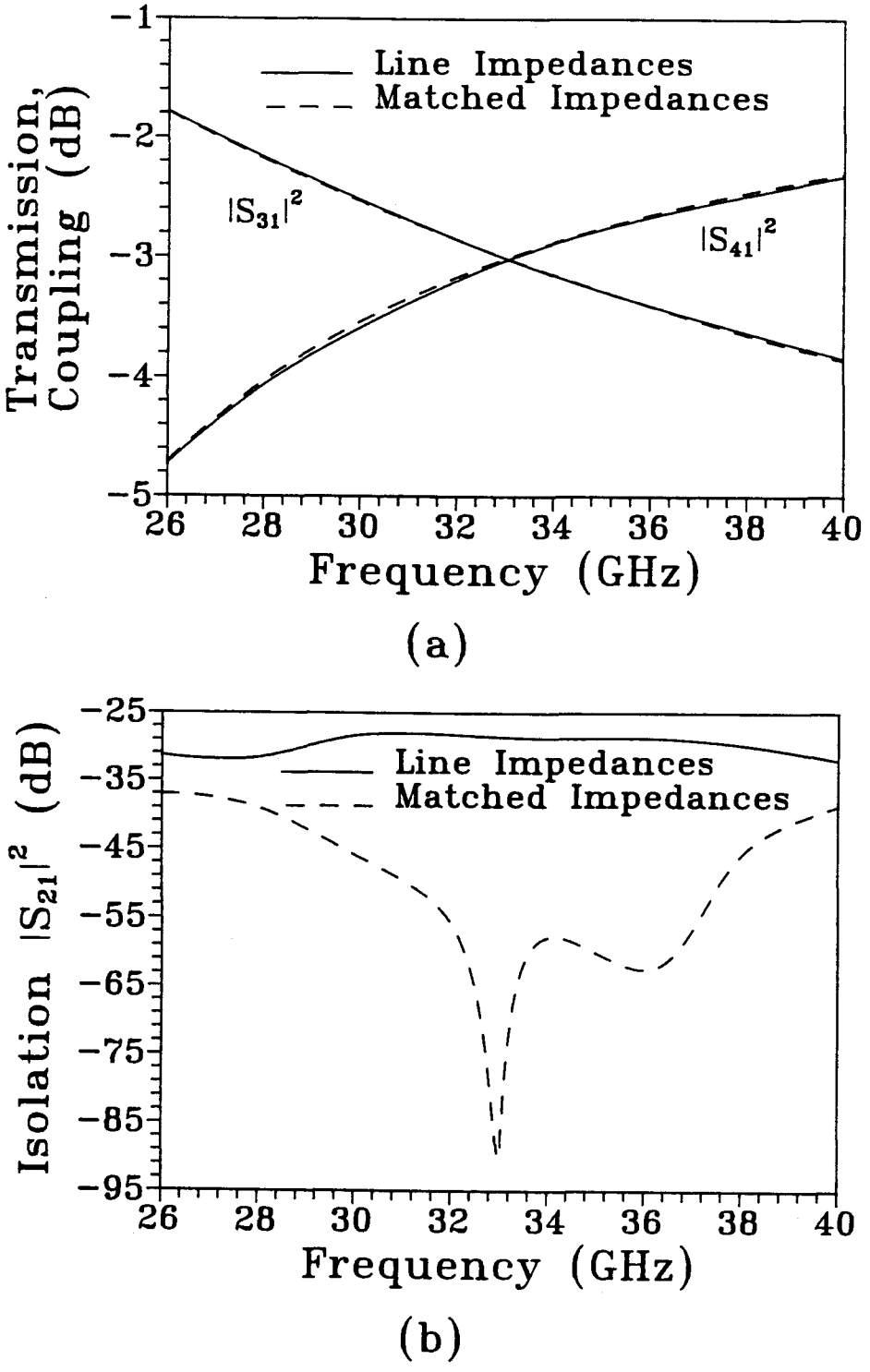

Fig. 3.34 (a) Coupling and (b) isolation of 3-dB couplers terminated with the matched (L=14.142mm) and the line (L=14.176mm) impedances.

4. CHARACTERISTICS OF COUPLED STRIP-SLOT STRUCTURES

The coupler design using coupled strip-slot structures has been reported in [7, 22-27, 43]. However, it has been limited to the use of the symmetric coupled strip-slot structures. For the general case, the coupled strip-slot structures have not been accurately characterized. An effort [44] was made to characterize the general coupled strip-slot structure by using the impedance definition proposed by Jansen [31]. As pointed in Chapter 3, the definition will leads to an impedance matrix which is non-symmetric for the strip-slot structure in a lossless, linear, and isotropic medium. Therefore, it is not suitable for microwave circuit design.

In this chapter, an assumption is proposed to resolve the problem which exists in characterizing the coupled strip-slot structures. In general, there are two basic normal modes in the structures: the strip mode where the total power is dominated by the power propagating on the strip line and the slot mode where the total power is mainly contributed by the power propagating along the slot line. It is assumed that the ratio of the coupling power contributed by the strip line to the total coupling power in the strip mode is equal to that of the coupling power contributed by the slot line to the total coupling power in the slot mode. With this assumption, a symmetric impedance matrix for the coupled strip-slot structure is ensured.

4.1 THE FORMULATION OF THE SOLUTION

Since the slot voltage and the strip current are well defined in the modal analysis of the coupled strip-slot structure and solutions for the equivalent slot current and strip voltage can, in general, be expressed in terms of two forward propagating waves and two backward propagating waves as given by

$$V_{sl} = A_1 e^{-\gamma_c z} + A_2 e^{\gamma_c z} + A_3 e^{-\gamma_\pi z} + A_4 e^{\gamma_\pi z} \qquad (4.1a)$$

$$I_{st} = m_c A_1 e^{-\gamma_c z} - m_c A_2 e^{\gamma_c z} + m_\pi A_3 e^{-\gamma_\pi z} - m_\pi A_4 e^{\gamma_\pi z} \quad (4.1b)$$

$$I_{sl} = Y_{slc} A_1 e^{-\gamma_c z} - Y_{slc} A_2 e^{\gamma_c z} + Y_{sl\pi} A_3 e^{-\gamma_\pi z} - Y_{sl\pi} A_4 e^{\gamma_\pi z} \quad (4.1c)$$

$$V_{st} = m_c Z_{stc} A_1 e^{-\gamma_c z} + m_c Z_{stc} A_2 e^{\gamma_c z} + m_\pi Z_{st\pi} A_3 e^{-\gamma_\pi z} + m_\pi Z_{st\pi} A_4 e^{\gamma_\pi z} \quad (4.1d)$$

where the subscripts c and π stand for the strip and slot modes, Y_{sl} and Z_{st} are the characteristic admittance of the slot line and the characteristic impedance of the strip line, and the transadmittance m is defined as:

$$m = \frac{I_{st}}{V_{sl}}. \quad (4.2)$$

The admittance matrix for an equivalent four-port network of the coupled strip-slot structure can be obtained by solving for the port current-voltage relationships in (4.1). The symmetry of an admittance matrix in a lossless, isotropic, and linear system requires

$$Y_{12} = Y_{21} = Y_{34} = Y_{43} \quad (4.3a)$$

$$Y_{13} = Y_{31} = Y_{24} = Y_{42} \quad (4.3b)$$

which lead to

$$Y_{slc,\pi} = - m_c m_\pi Z_{st\pi,c} \quad (4.4)$$

Since the characteristic admittance of the slot line and the characteristic impedance of the strip line are defined as:

$$Y_{sl} = \frac{P_{sl}}{V_{sl}^2} \quad (4.5a)$$

$$Z_{st} = \frac{P_{st}}{I_{st}^2} \quad (4.5b)$$

where P_{sl} and P_{st} are the powers propagating on the slot line and the strip line, respectively. The following power ratios can be derived from (4.4) and (4.5):

$$\frac{P_{stc}}{P_{sl\pi}} = \frac{P_{slc}}{P_{st\pi}} = \frac{P_c}{P_\pi} \quad (4.6)$$

where P_c and P_π are the total c- and π-mode powers, which are the sum of the power on the strip line and the power on the slot line as given by

$$P_c = P_{stc} + P_{slc} \tag{4.7a}$$

$$P_\pi = P_{st\pi} + P_{sl\pi}. \tag{4.7b}$$

Re-examining the expressions for the electric and magnetic fields, one finds that the total fields can be separated into two parts: the fields solely due to the existence of the strip line and those solely due to the existence of the slot line in the coupled structure, that is,

$$\mathbf{E} = \mathbf{E}_{st} + \mathbf{E}_{sl} \tag{4.8a}$$

$$\mathbf{H} = \mathbf{H}_{st} + \mathbf{H}_{sl}. \tag{4.8b}$$

The total power propagating in the structure is given by

$$P = \mathrm{Re}[\iint(\mathbf{E}\times\mathbf{H})\bullet d\mathbf{s}] = P_{st0} + P_{sl0} + P_{cp} \tag{4.9}$$

where

$$P_{st0} = \mathrm{Re}[\iint(\mathbf{E}_{st}\times\mathbf{H}_{st})\bullet d\mathbf{s}] \tag{4.10a}$$

$$P_{sl0} = \mathrm{Re}[\iint(\mathbf{E}_{sl}\times\mathbf{H}_{sl})\bullet d\mathbf{s}] \tag{4.10b}$$

$$P_{cp} = \mathrm{Re}[\iint(\mathbf{E}_{st}\times\mathbf{H}_{sl} + \mathbf{E}_{sl}\times\mathbf{H}_{st})\bullet d\mathbf{s}]. \tag{4.10c}$$

It is clear that P_{st0} and P_{sl0} are attributed to the fields of the strip line and the slot line and P_{cp} is due to the coupling between the strip line and the slot line.

Rearranging (4.6) leads to

$$\frac{P_{stc}}{P_{slc}} = \frac{P_{sl\pi}}{P_{st\pi}} \tag{4.11}$$

which indicates that if there is an x portion of the total c-mode power propagating on the strip line, there is also the same portion of the total π-mode power propagating on the slot line. One more equation is needed to find the solution for decoupled powers in (4.11), which cannot be derived from the previous equations. Similar to the power relationship in (4.11), it is assumed that an x portion of the c-mode coupling power in

the c-mode is contributed by the strip line and the same portion of the coupling power in the π-mode is contributed by the slot line, i.e.,

$$P_{stc} = P_{st0c} + xP_{cpc} \tag{4.12a}$$

$$P_{slc} = P_{sl0c} + (1 - x)P_{cpc} \tag{4.12b}$$

$$P_{sl\pi} = P_{sl0\pi} + xP_{cp\pi} \tag{4.12c}$$

$$P_{st\pi} = P_{st0\pi} + (1 - x)P_{cp\pi} \tag{4.12d}$$

Replacing (4.6) with (4.12) yields

$$\frac{P_{st0c} + xP_{cpc}}{P_{st0\pi} + xP_{cp\pi}} = \frac{P_{sl0c} + (1 - x)P_{cpc}}{P_{st0\pi} + (1 - x)P_{cp\pi}} = \frac{P_c}{P_\pi} \tag{4.13}$$

which together with (4.12) results in

$$Z_{stc} = \frac{P_c}{I_{stc}^2} \frac{P_{cp\pi}P_{st0c} - P_{cpc}P_{sl0\pi}}{P_cP_{cp\pi} - P_\pi P_{cpc}} \tag{4.14a}$$

$$Z_{st\pi} = \frac{P_\pi}{I_{st\pi}^2} \frac{P_{cp\pi}P_{sl0c} - P_{cpc}P_{st0\pi}}{P_cP_{cp\pi} - P_\pi P_{cpc}}. \tag{4.14b}$$

The corresponding slot impedances can be found from (4.4).

4.2 NUMERICAL RESULTS

The frequency dependent characteristics of the coupled strip-slot structure are shown in Fig. 4.1. As frequency is increased, the effective dielectric constant also increases. A higher ε_r leads to a higher effective dielectric constant. The c-mode transadmittance m_c decreases and the π-mode transadmittance m_π changes slightly for the substrate with $\varepsilon_r = 2.2$, while m_c first decreases and then increases slightly and $|m_\pi|$ increases insignificantly for the substrate with $\varepsilon_r = 9.8$. Both m_c and $|m_\pi|$ for the case of $\varepsilon_r = 9.8$ are larger than those for the case of $\varepsilon_r = 2.2$. The π-mode strip impedance $Z_{st\pi}$ decreases, whereas the c-mode strip impedance Z_{stc} increases. There exists a point where $Z_{stc} = Z_{st\pi}$ for the substrate with $\varepsilon_r = 2.2$.

The effect of the substrate thickness on the effective dielectric constant, the transadmittance, and the strip impedance is illustrated in Fig. 4.2. A thicker substrate results in a higher π-mode and a lower c-mode effective dielectric constants. As the substrate thickness is increased, m_c decreases and $|m_\pi|$ has no significant change. The strip impedance increases. This is consistent with the impedance variation of a single strip line.

The dependence of the characteristics of the structure on the position of the strip center with the slot center located at the E-plane center of the waveguide is shown in Fig. 4.3. As the strip center deviates from the slot center, the effective dielectric constant of the c-mode first increases and then decreases. On the contrary, the effective dielectric constant of the π-mode first decreases and then increases. $|m_c|$ initially rises sharply and then drops slowly, while m_π changes insignificantly. Z_{stc} remains unchanged, whereas $Z_{st\pi}$ decreases from a very large value to a value slightly smaller than Z_{stc}.

The variations of the effective dielectric constant, the transadmittance, and the strip impedance with the position of the slot center for a centered strip line is plotted in Fig. 4.4. As the slot center deviates from the strip center, the changes in the effective dielectric constants and the strip impedances are similar to those in the case shown in Fig. 4.3. m_c initially decreases drastically and then increases slightly. The value of m_π is negative and very small.

Fig. 4.5 shows that the dependence of the characteristics on the position of the strip and slot centers when the strip and the slot deviate from the E-plane center with the same distance in the same direction. As the offset S is increased, the effective dielectric constant changes slightly. m_c decreases rapidly, while m_π remains very small. Z_{stc} changes slightly, whereas $Z_{st\pi}$ decreases from infinity to a large value. Part

of $Z_{st\pi}$ is not shown due to its relatively large value, which is beyond the scale of the figure.

In addition, the dependence of the characteristics on the separation between the strip and slot centers when the strip and the slot deviate from the E-plane center with the same distance but in the opposite directions is shown in Fig. 4.6. As the offset S is increased, the effective dielectric constant of the c-mode first increases and then decreases, whereas that of the π-mode first decreases and then increases. m_c first falls rapidly and then rises, while m_π remains very small. Z_{stc} changes insignificantly, whereas $Z_{st\pi}$ decreases sharply from infinity to a value smaller than Z_{stc}.

Fig. 4.7 shows that the influence of the strip width on the characteristics. As the strip width is increased, the effective dielectric constant increases. m_c first increases and then decreases, while m_π decreases slightly. Both Z_{stc} and $Z_{st\pi}$ decrease.

The effect of the slot width on various characteristic parameters of the structure is illustrated in Fig. 4.8. It can be seen that as the slot width is increased, the effective dielectric constant of the c-mode has only a slightly variation and that of the π-mode decreases monotonously. m_c first decreases and then increases, whereas m_π changes insignificantly. Z_{stc} increases slightly, while $Z_{st\pi}$ increases rapidly.

The variations of the effective dielectric constant, the transadmittance, and the strip impedance with a lateral displacement of the substrate are plotted in Fig. 4.9. In general, the displacement has only a little effect on the characteristics. When the substrate is laterally displaced close to a side wall, the c-mode effective dielectric constant only has a small change and the change in the π-mode effective dielectric constant is relatively larger. Although m_π shows no significant change, m_c has a small increase. Z_{stc} decreases when the strip is closer to the side wall and it has almost no change when the slot is closer to the side wall. $Z_{st\pi}$ increases when the slot is closer to the side wall and decreases when the strip is closer to the side wall.

4.3 SUMMARY

The coupled strip-slot structure is characterized with the assumption which ensures that the resultant impedance matrix of the structure is symmetric in a lossless, linear, and isotropic medium. The impedance and propagation characteristics of the structure are illustrated through the numerical results.

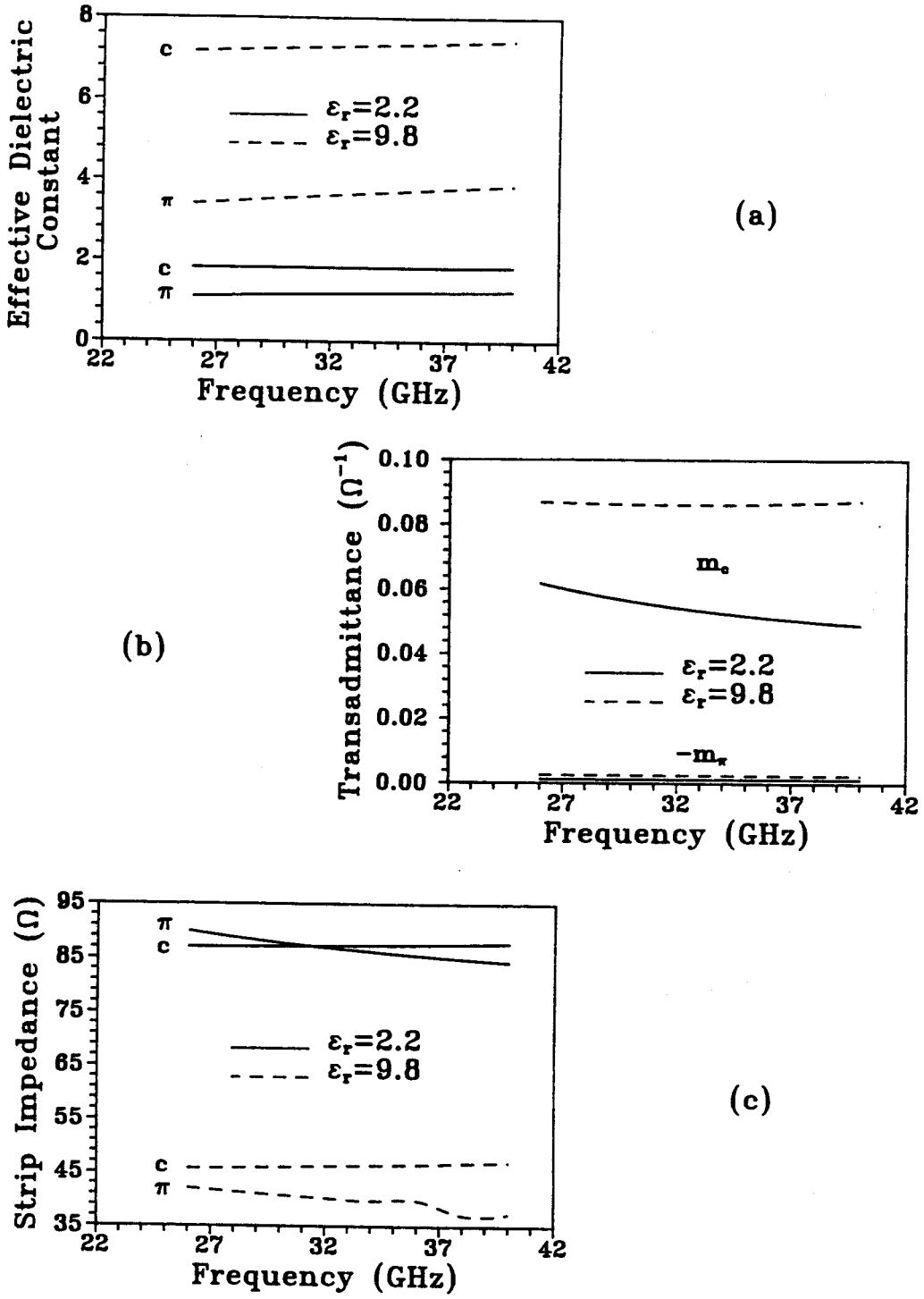

Fig. 4.1 (a) Effective dielectric constant, (b) transadmittance, and (c) strip impedance of a coupled strip-slot structure as a function of frequency with ε_r as a parameter (h_1=3.429, d=0.254, w_l=0.2, w_t=0.3, p_l=1.478, p_t=2.078, length unit: mm).

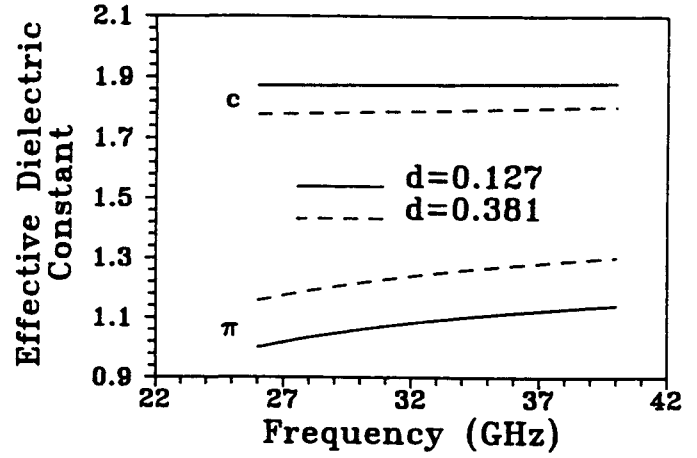

(a)

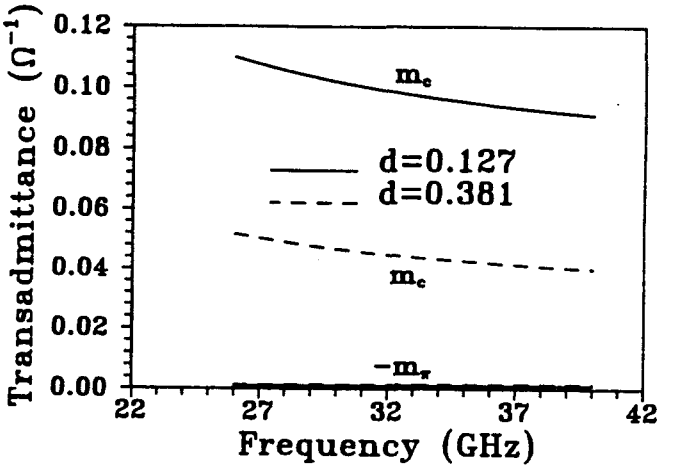

(b)

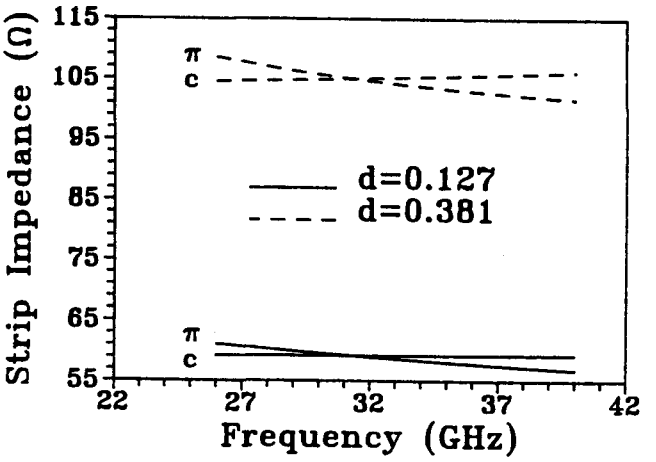

(c)

Fig. 4.2 (a) Effective dielectric constant, (b) transadmittance, and (c) strip impedance of a coupled strip-slot structure as a function of frequency with d as a parameter (ε_r=2.2, h_1=3.556-0.5d, w_l=0.2, w_t=0.3, p_l=1.478, p_t=2.078, length unit: mm).

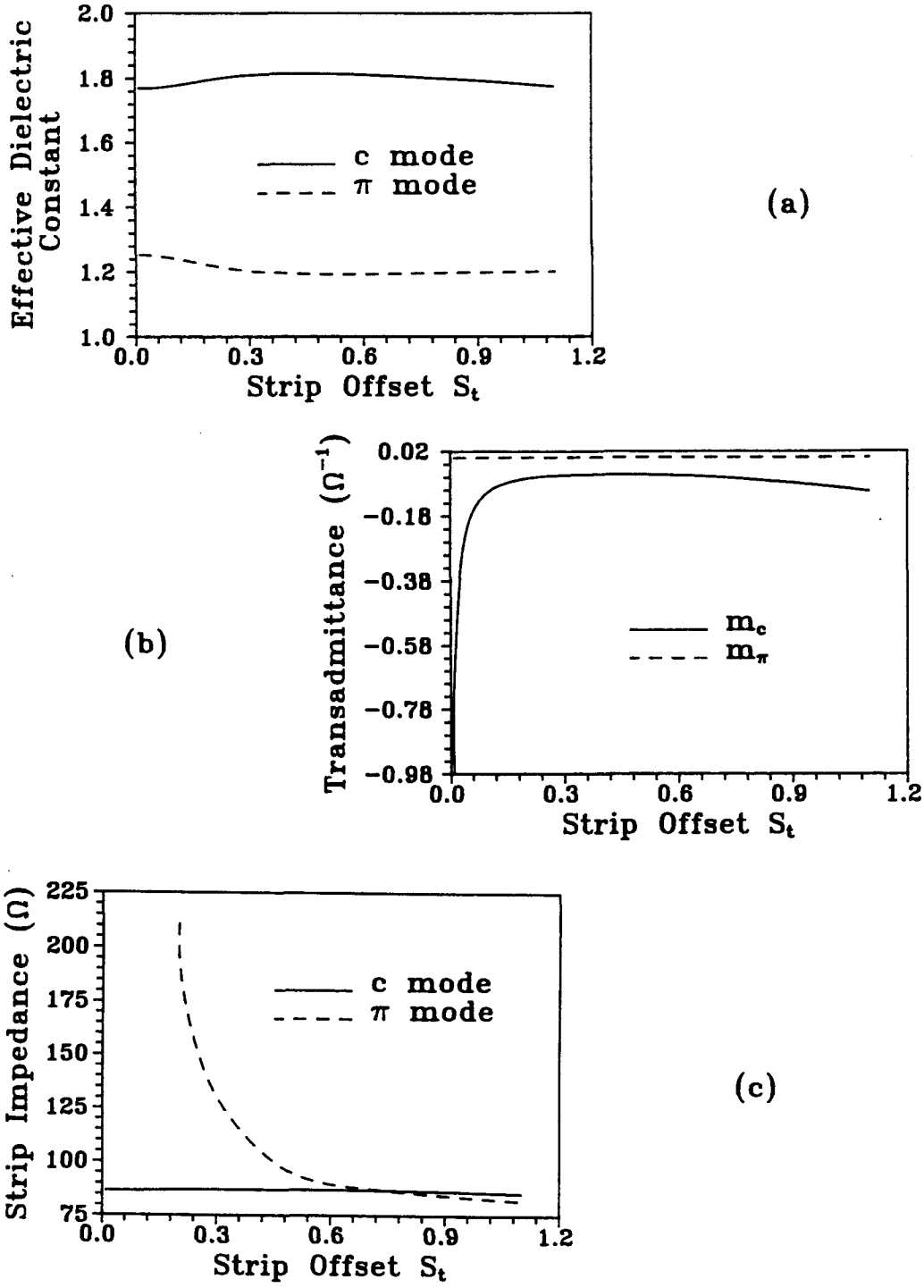

Fig. 4.3 (a) Effective dielectric constant, (b) transadmittance, and (c) strip impedance of a coupled strip-slot structure as a function of the strip offset S_t (ε_r=2.2, h_1=3.429, d=0.254, w_l=0.2, w_t=0.3, p_l=1.778, p_t=1.778-S_t, f=33GHz, length unit: mm).

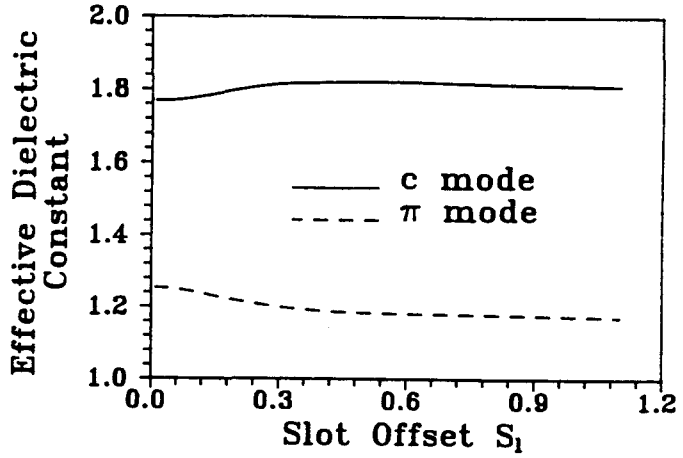

(a)

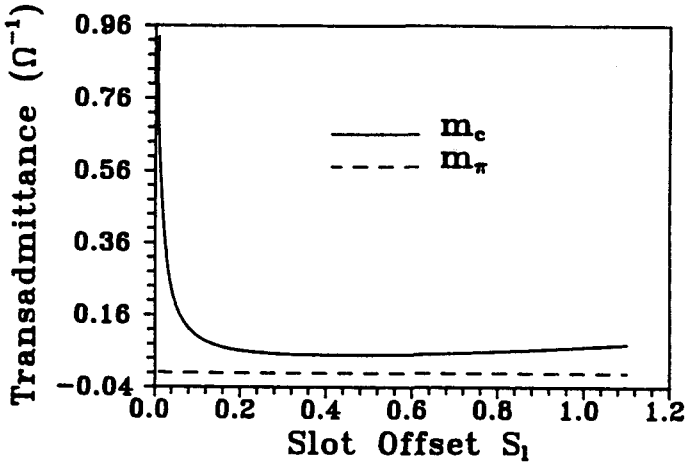

(b)

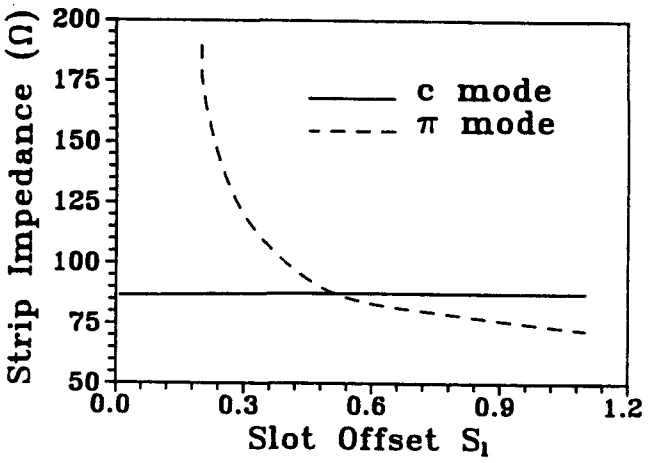

(c)

Fig. 4.4 (a) Effective dielectric constant, (b) transadmittance, and (c) strip impedance of a coupled strip-slot structure as a function of the slot offset S_l (ε_r=2.2, h_l=3.429, d=0.254, w_l=0.2, w_t=0.3, p_l=1.778-S_l, p_t=1.778, f=33GHz, length unit: mm).

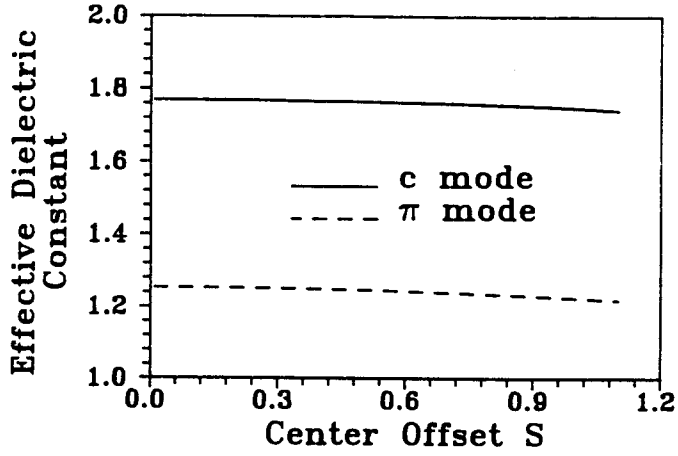

(a)

(b)

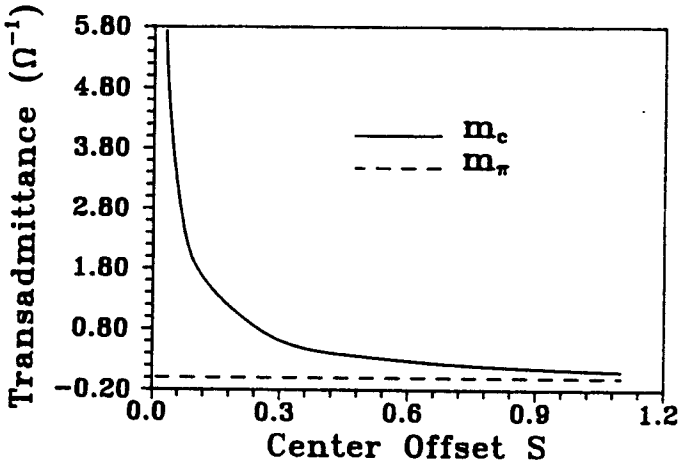

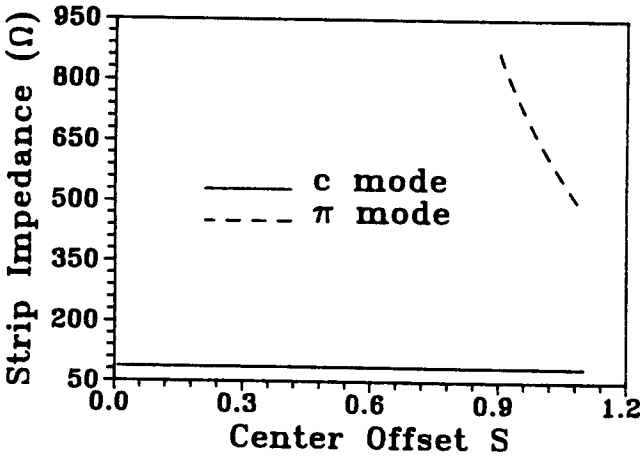

(c)

Fig. 4.5 (a) Effective dielectric constant, (b) transadmittance, and (c) strip impedance of a coupled strip-slot structure as a function of the slot and strip offset S (ε_r=2.2, h_1=3.429, d=0.254, w_l=0.2, w_t=0.3, p_l=p_t=1.778-S, f=33GHz, length unit: mm).

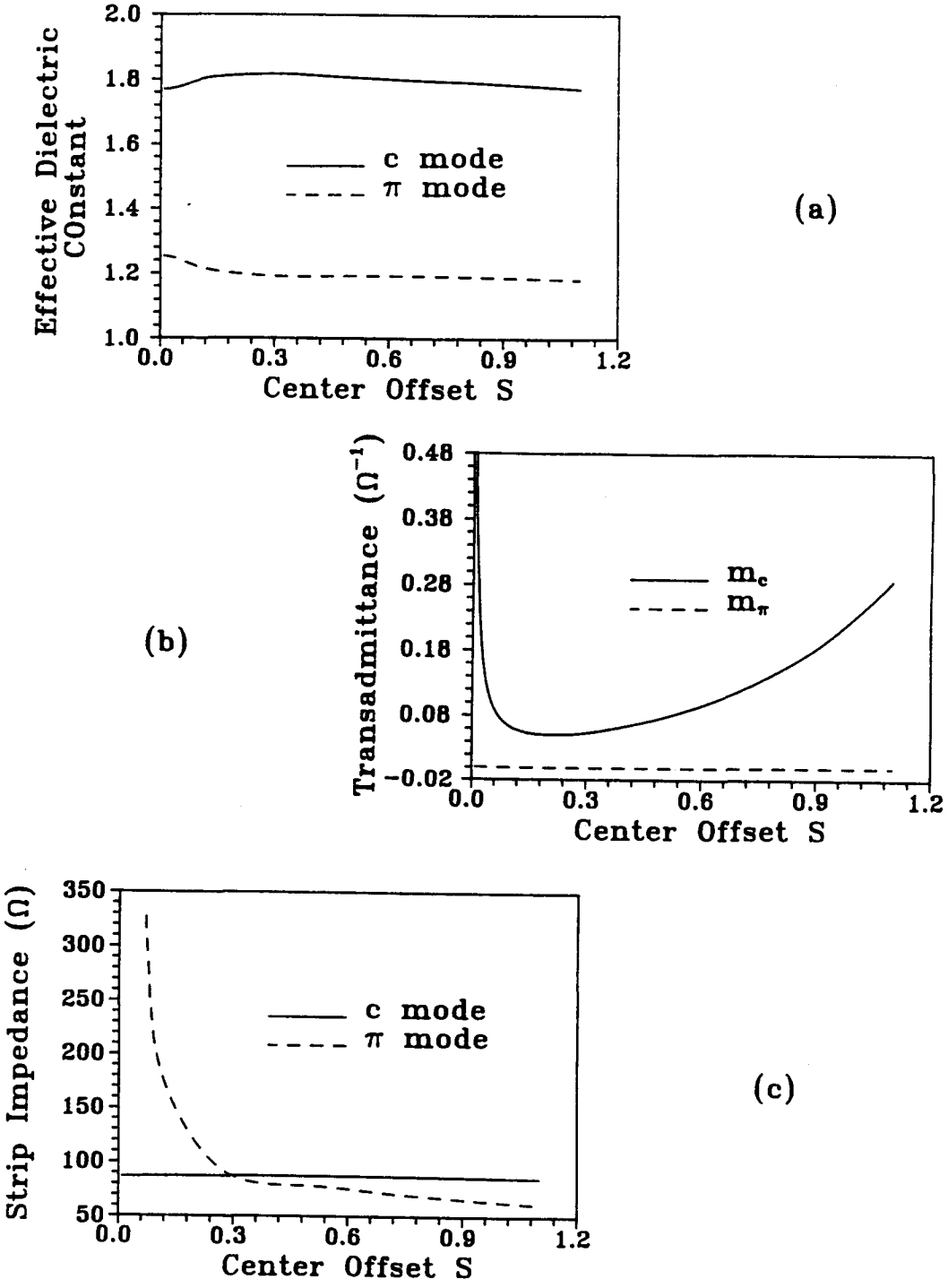

Fig. 4.6 (a) Effective dielectric constant, (b) transadmittance, and (c) strip impedance of a coupled strip-slot structure as a function of the slot and strip offset S in the opposite directions (ε_r=2.2, h_1=3.429, d=0.254, w_l=0.2, w_t=0.3, p_l=1.778-S, p_t=1.778+S, f=33GHz, length unit: mm).

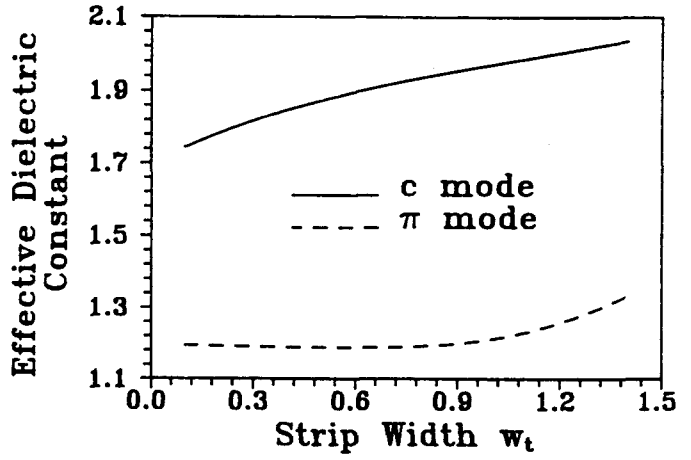

(a)

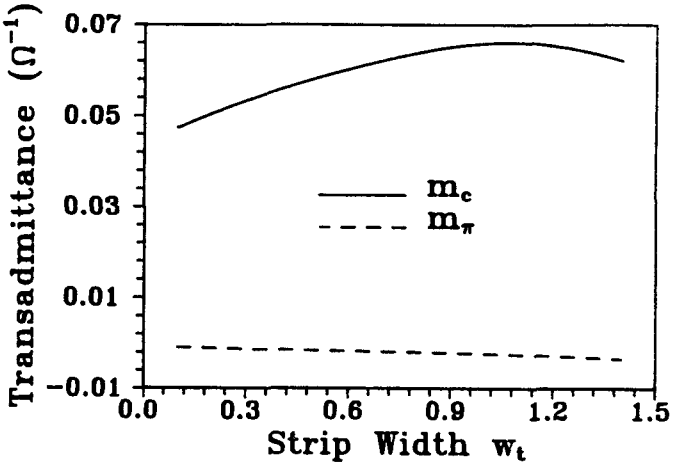

(b)

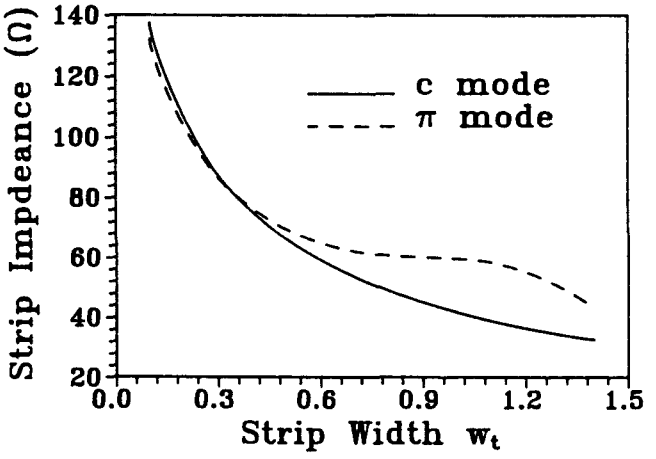

(c)

Fig. 4.7 (a) Effective dielectric constant, (b) transadmittance, and (c) strip impedance of a coupled strip-slot structure as a function of the strip width (ε_r=2.2, h_1=3.429, d=0.254, w_l=0.2, p_l=1.478, p_t=2.078, f=33GHz, length unit: mm).

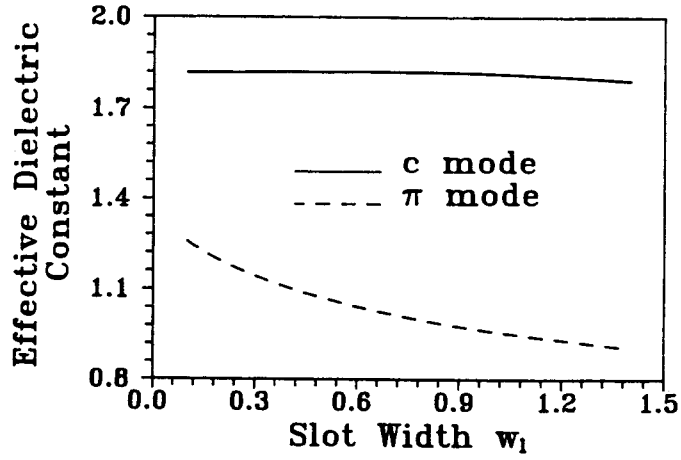

(a)

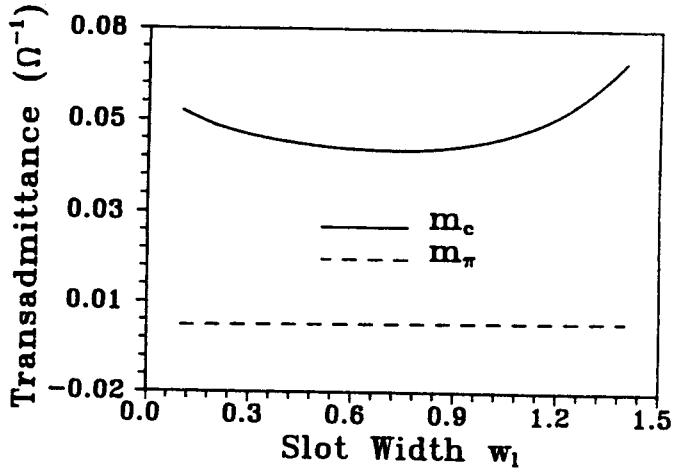

(b)

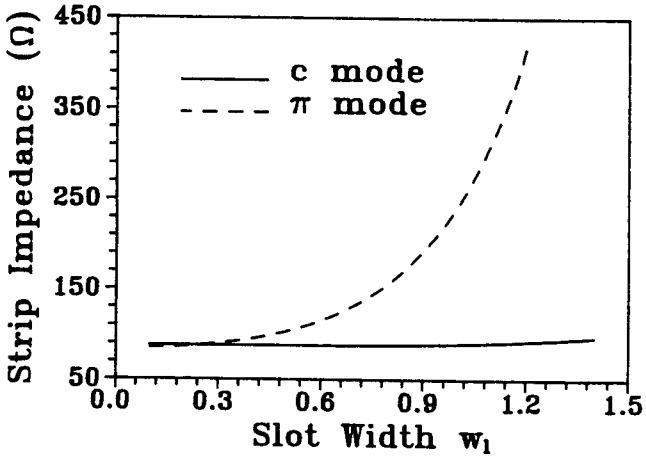

(c)

Fig. 4.8 (a) Effective dielectric constant, (b) transadmittance, and (c) strip impedance of a coupled strip-slot structure as a function of the slot width (ε_r=2.2, h_1=3.429, d=0.254, w_t=0.3, p_l=1.478, p_t=2.078, f=33GHz, length unit: mm).

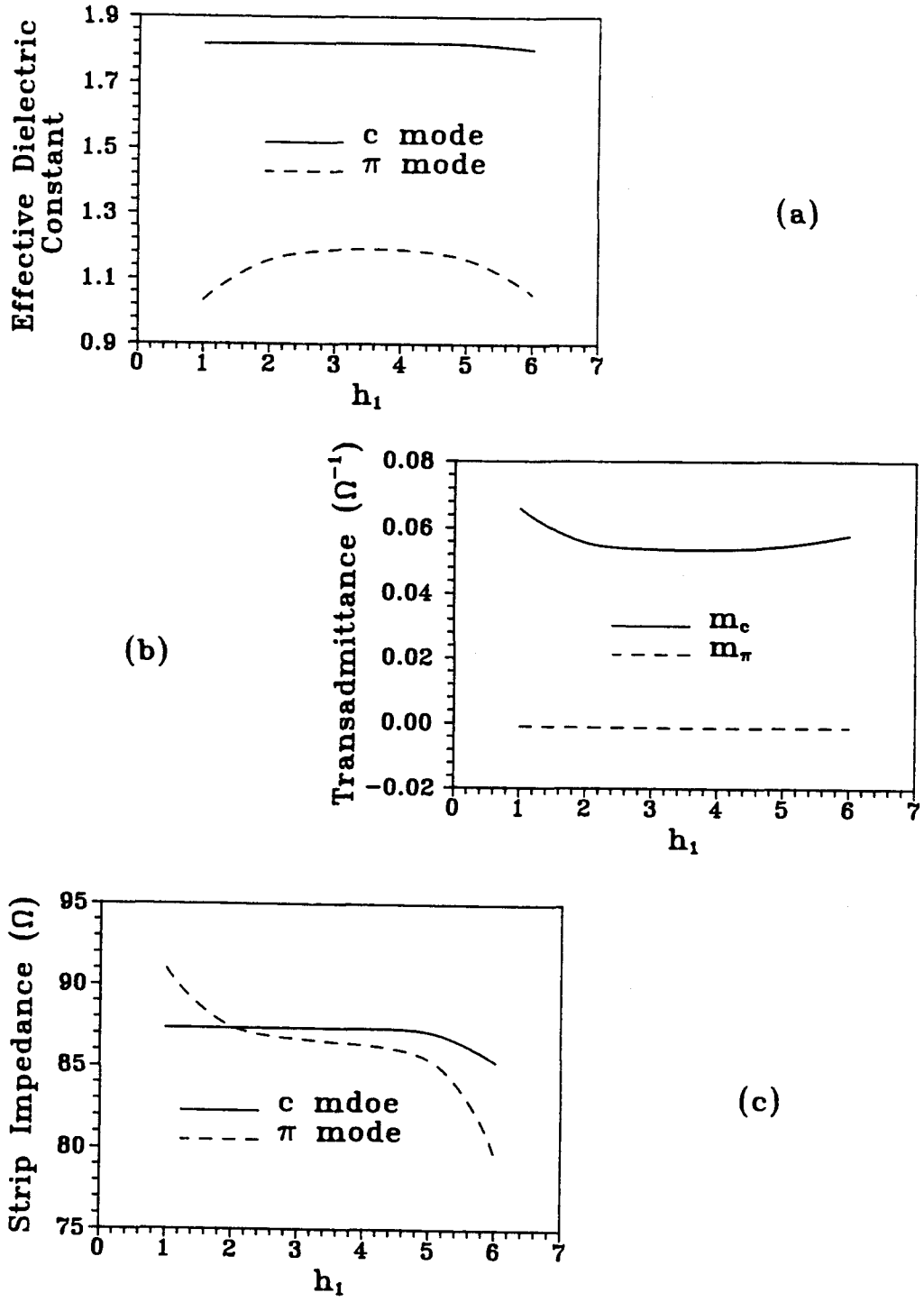

Fig. 4.9 (a) Effective dielectric constant, (b) transadmittance, and (c) strip impedance of a coupled strip-slot structure as a function of the lateral displacement of the substrate h_1 (ε_r=2.2, d=0.254, w_l=0.2, w_t=0.3, p_l=1.478, p_t=2.078, f=33GHz, length unit: mm).

5. QUASI-TEM CHARACTERISTICS OF LAYERED MULTICONDUCTOR STRIP-SLOT STRUCTURES

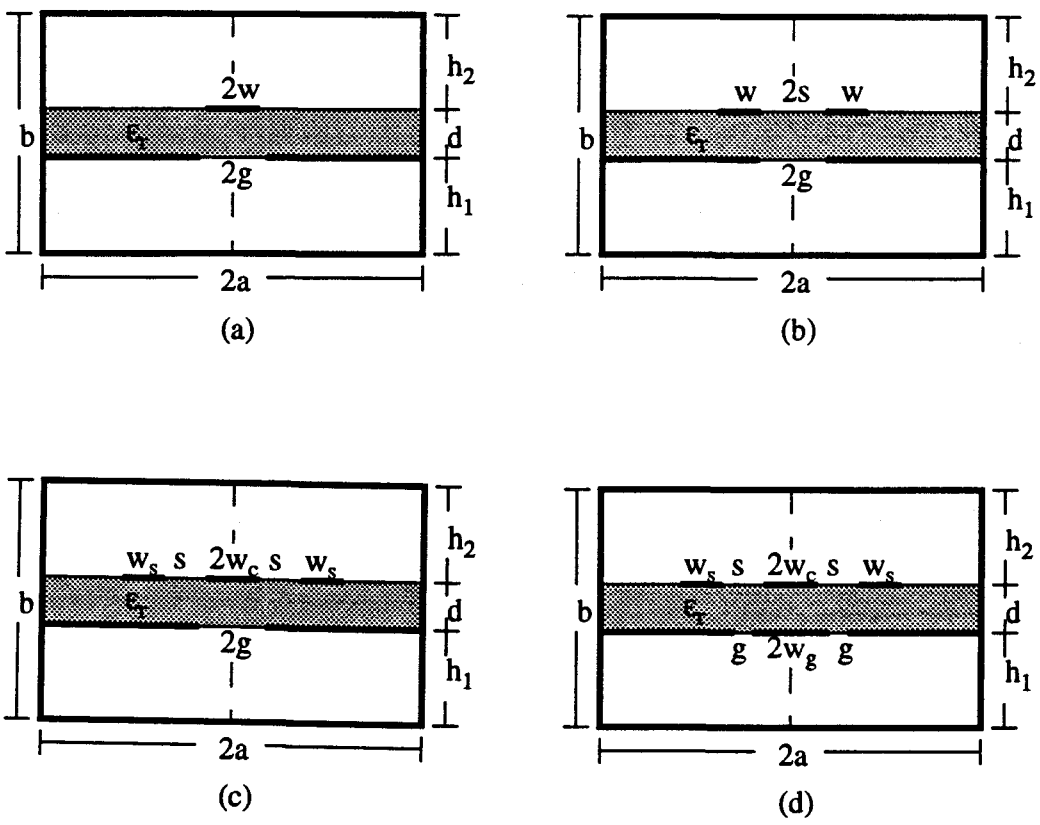

Fig. 5.1 Cross sections of some symmetric strip-slot structures: (a) strip-slot, (b) two-strip one-slot, (c) three-strip one-slot, and (d) three-strip two-slot structures.

The layered multiconductor strip-slot structures such as those shown in Fig. 5.1 have not only been used in microwave circuits [28, 45, 46], but are increasingly used in electronic packagings and VLSI interconnections [47]. Due to the inherent difficulties in the analysis of the structures, a full-wave analysis can only provide solutions for the propagation characteristics of the structures, which alone is not sufficient to develop an equivalent circuit model for their applications in VLSI and

microwave circuits. Since a frequency dependent circuit model of the structures is not available to date, a quasi-TEM, though approximate, circuit model for the structures will be invaluable for the applications in VLSI and microwave circuits. The quasi-TEM solutions yield quite accurate results at low microwave frequencies.

In this chapter, the characteristics of various layered multiconductor strip-slot structures are presented on the basis of the quasi-TEM spectral domain analysis formulated in Chapter 2. First, the effects of the basis functions representing the charge distributions on the strips and the ground plane conductors and of the summation terms used in the analysis on the accuracy of the computational results are discussed. Second, the effect of the shielding case is studied. Then, the results of the coupled strip lines with one and two slots on the ground plane are shown in various figures. Later, the characteristics of double-sided strip lines with a slot on the common ground are presented. Finally, some examples are given to illustrate the applications of the structures in the far-end crosstalk reduction in digital circuit systems.

5.1 BASIS FUNCTIONS AND SUMMATION TERMS

The singularity of the charge distribution in the vicinity of sharp edges makes it necessary to consider the edge conditions in selecting basis functions, which approximate the true charge distributions, to speed up the convergence of the calculation. The same basis functions used in the full-wave analysis for the electric fields on the slots are used with a modification which guarantees that the charge distribution at the corner of the ground plane and the shielding case equals to zero. More specifically, the odd functions which are only defined in half of the space region are used for the charge distributions on the ground conductors connected to the shielding case.

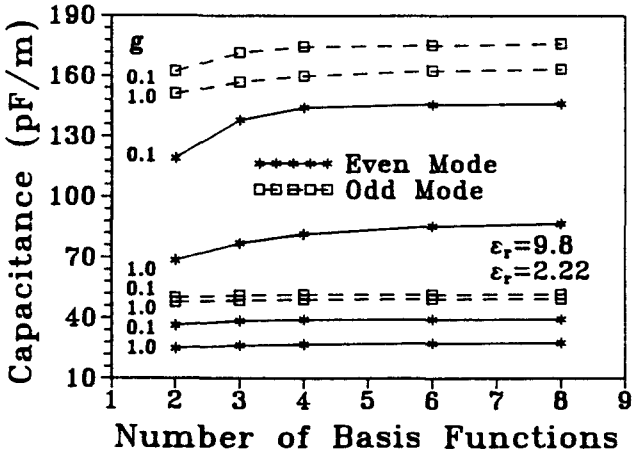

Fig. 5.2 Effect of the number of basis functions on capacitance with g and ε_r as parameters (a=14.4, b=21d, d=0.635, h_1=10d, w=0.6, s=0.3, length unit: mm).

Since all other parameters in the quasi-TEM analysis are derived from the capacitances, it is sufficient to examine the convergence of the capacitance calculation. Fig. 5.2 indicates that as the number of the basis functions increases, the capacitance asymptotically approaches the upper bound of the true capacitance when 1,500 summation terms are used in the calculation. The difference between the results of using six basis functions and those of using eight basis functions is negligibly small. The use of more basis functions will not significantly improve the accuracy of the results, while it reduces the computational efficiency. Therefore, the use of six basis functions in the capacitance will yield an accurate result.

The dependence of the convergence of the capacitance calculation on the summation terms used in the spectral domain analysis is illustrated in Fig. 5.3 for the substrate with ε_r = 9.8. It can be seen that the effect of the summation terms on the convergence is trivial when more than 600 summation terms is used.

In the following calculations, six basis functions and 1,500 summation terms are used to guarantee a sufficient accuracy in the capacitance calculation.

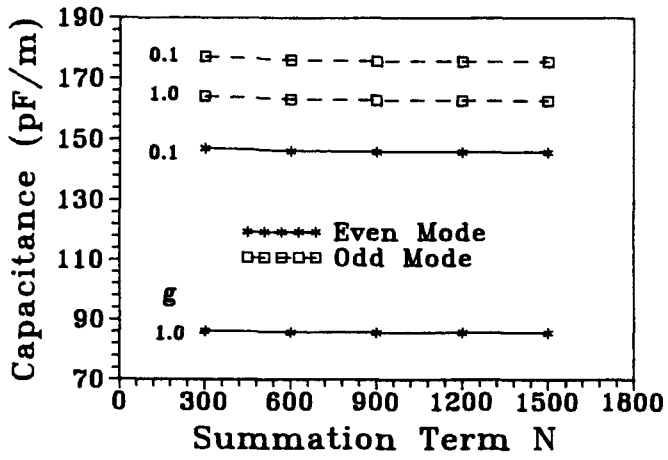

Fig. 5.3 Effect of summation terms on capacitance with g as a parameter (ε_r=9.8, a=14.4, b=21d, d=0.635, h_1=10d, w=0.6, s=0.3, length unit: mm).

5.2 EFFECT OF THE SHIELDING CASE

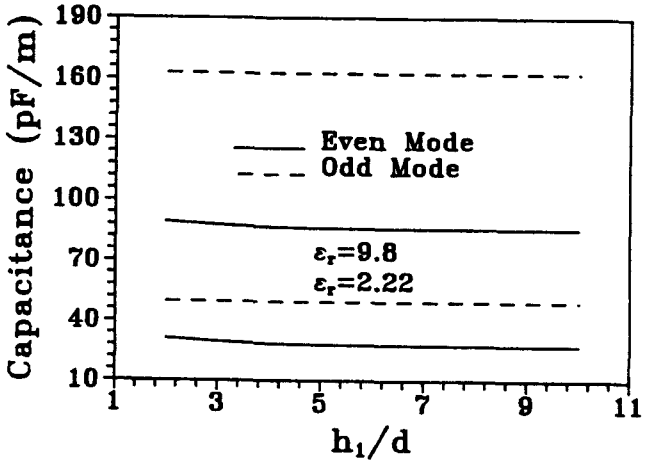

Fig. 5.4 Effect of top and bottom walls on capacitance with ε_r as a parameter (a=14.4, d=0.635, w=0.6, s=0.3, g=1.0, length unit: mm).

The effect of the walls of the shielding case on the capacitance calculations depends on the case dimension. If the case is too small, it interacts strongly with the strips and the ground plane slots. If it is too large, more expansion terms are needed to ensure an accurate results. The influence of the top and bottom walls on the capacitance is shown in Fig. 5.4, where the distance from the top wall to the strip lines and that from the bottom wall to the ground plane have been set equal. It is observed that as long as the distance is large enough, say, eight time larger than the substrate thickness, the effect from the top and bottom walls can be neglected. A similar effect from the side walls of the shielding case is demonstrated in Fig. 5.5 as a function of the ratio of the distance from the center of the broad wall to either of the side walls to the strip width. It is seen that the overall effect from the side walls is small.

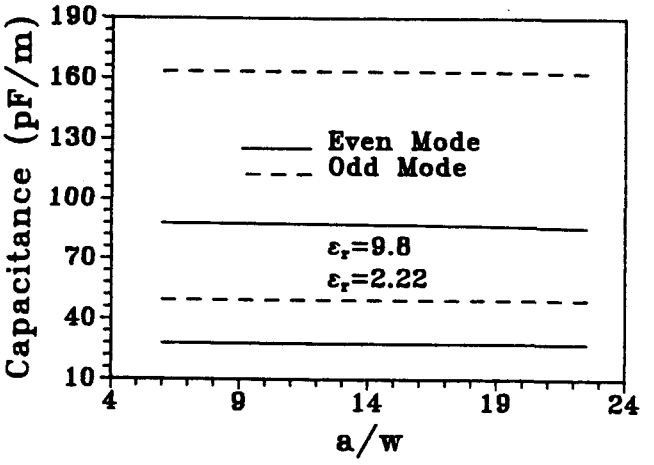

Fig. 5.5 Effect of side walls on capacitance with ε_r as a parameter (b=21d, d=0.635, h_1=10d, w=0.6, s=0.3, g=1.0, length unit: mm).

Therefore, it is concluded that the wall effect is insignificant with h_1 and $h_2 \geq$ 10d and a $\geq$ 22.5w, which will be used in the following calculations.

5.3 SYMMETRIC TWO STRIPS WITH A GROUND PLANE SLOT

The analysis of the coupled strip lines with a ground plane slot has been presented in [28], where the characteristic impedances and the normalized wavelengths were computed with the knowledge of the line capacitances. However, information on the line capacitances as well as inductances was not made available in [28]. The information on the line capacitances and inductances is of great interest in studying signal crosstalks and distortions in electronic packagings and interconnections used in VLSI digital circuits. One way to reduce crosstalk between interconnects is to increase the distance between them. However, the limited area available on a circuit chip or chip module makes it almost impractical to increase the distance between interconnects. Hence, there is a necessity to find an alternative to reduce the crosstalk. Introducing ground plane slots is one of possible choices.

Shown in Fig. 5.6 is the effect of the ground plane slot on the capacitance, inductance, effective dielectric constant, and impedance. As the slot width is increased, C_{11} first decreases and then increases and finally decreases again, while L_{11} changes in a way just opposite to C_{11}. Both $|C_{12}|$ and L_{12} increase. The change in capacitances for a substrate with a large value of ε_r is more significant than that for a substrate with a small value of ε_r. The effective dielectric constant first decreases and then increases and finally decreases again. The change in the even mode effective dielectric constant is relatively large. The even and odd mode effective dielectric constant can be equalized by changing the slot width. Both even and odd mode impedances increase. The odd mode impedance has only a small variation, whereas the change in the even mode impedance covers a wide range.

The variations of the capacitance, inductance, effective dielectric constant, and impedance as a function of the substrate thickness is depicted in Fig. 5.7. As the substrate thickness is increased, C_{11} decreases monotonically, while $|C_{12}|$, L_{11}, and

L_{12} all increase. The effective dielectric constant first increases and then decreases for the substrate with $\varepsilon_r = 9.8$. In the case of $\varepsilon_r = 2.22$, the even mode effective dielectric constant first increases and then decreases, whereas that of the odd mode decreases. The even and odd mode impedances both increase, but the increase in the even mode impedance is much faster than that in the odd mode impedance.

The dependence of the capacitance, inductance, effective dielectric constant, and impedance on the strip width is illustrated in Fig. 5.8. As the strip width is increased, C_{11} and $|C_{12}|$ increase while L_{11} and L_{12} decrease. The effective dielectric constant increases slightly, whereas the impedance decreases.

Increasing the separation between the strips leads to a decrease in the mutual capacitance and inductance as shown in Fig. 5.9. As the separation is increased, C_{11} decreases while L_{11} increases. The effective dielectric constant first increases and then decreases. It is more pronounced in the case of $\varepsilon_r = 9.8$. The even mode impedance decreases, whereas the odd mode impedance increases. Both even and odd mode impedances converge to the impedance of a single strip line and the mutual terms will vanish for a large separation.

In general, the even mode effective dielectric constant and impedance are more sensitive to a change in the structural parameters than those of the odd mode.

5.4 SYMMETRIC THREE STRIPS WITH A GROUND PLANE SLOT

The capacitance, inductance, effective dielectric constant, and modal impedance [48] of the symmetric coupled three strips with a ground plane slot as a function of the slot width is shown in Fig. 5.10. As the slot width is increased, the self capacitance C_{11} and the self inductance L_{11} of the side strip behave in a similar manner as those in the symmetric coupled two strips with a ground plane slot. Whereas the self capacitance of the center strip C_{22} decreases, the self inductance of

the center strip L_{22} increases correspondingly. The mutual capacitance between the side and the center strips $|C_{12}|$ first decreases and then increases, while the mutual inductance between the side and the center strips L_{12} first increases and then decreases and finally increases again. The mutual capacitance $|C_{13}|$ and the mutual inductance L_{13} between the side strips experience three different changes: increase, decrease, and again increase. While the effective dielectric constants of both the even-even and the even-odd modes decrease continuously, that of the odd mode first decreases and then increases and finally decreases again. However, it is confined within those of the other two modes. The odd mode impedance initially increases and then decreases and again increases after reaching a local minimum. The even-even mode impedance, like the odd mode impedance, undergoes three regions: increase, decrease, and again increase. In addition, its variation covers a wide range of impedance values. The impedance curve of the even-odd mode looks like a bell-shaped one. It has intersection points with those of the odd and even-even modes.

The variations of the capacitance, inductance, effective dielectric constant, and modal impedance with the substrate thickness are indicated in Fig. 5.11. As the substrate thickness is increased, the self capacitances C_{11} and C_{22} decrease and the self inductances L_{11} and L_{22} increase correspondingly. All the mutual capacitances and inductances increase. The effective dielectric constant of the odd mode has only a slight change. The effective dielectric constant of the even-even mode decreases, while that of the even-odd mode increases. The impedances of both odd and even-even modes increase, whereas that of the even-odd mode decreases.

The dependence of the capacitance, inductance, effective dielectric constant, and modal impedance on the center strip width is shown in Fig. 5.12. As the center strip width is increased, C_{11} has a small decrease, whereas L_{11} has a slight increase. C_{22} rises due to the increase in the center strip width, which results in a decrease in

L_{22}. Here, all the mutual capacitances and inductances decrease. The effective dielectric constants of the odd and the even-odd modes decrease, while that of the even-even mode increases. The odd mode impedance increases, whereas those of the even-even and the even-odd modes decrease.

The effect of the side strip width on the capacitance, inductance, effective dielectric constant, and modal impedance is plotted in Fig. 5.13. As the side strip width is increased, C_{11} increases and L_{11} decreases. It is observed that the side strip width only slightly affects C_{22} and L_{22}. All the mutual terms except $|C_{13}|$ decreases. $|C_{13}|$ increases because of the increase in the coupling between two side strips. The effective dielectric constants of both the odd mode and the even-odd mode decrease, while that of the even-even mode increases. All the modal impedances decrease monotonically.

The influence of the separation between the center and side strips on the capacitance, inductance, effective dielectric constant, and modal impedance is shown in Fig. 5.14. As the separation is increased, the self capacitances decrease while the self inductances increase correspondingly. All of mutual capacitances and inductances decrease. The overall change in the effective dielectric constant is relatively small. The odd and even-odd mode impedances increase, while the even-even mode impedance decreases.

5.5 SYMMETRIC THREE STRIPS WITH TWO GROUND PLANE SLOTS

For the symmetric coupled three strip structure, there is a conducting strip on the ground plane when two symmetric slots are introduced on the ground plane. If the length of the ground plane strip is much longer than that of the other strips, the ground plane strip can be considered as a floating conductor, which has a zero-sum charge [49]. Otherwise, it should be treated as a strip line instead of a ground

conductor due to its inability of being connected to the ground without altering the physical structure.

The effect of a floating conductor in the symmetric three strip lines with two ground plane slots on the capacitance, inductance, effective dielectric constant, and modal impedance is shown in Fig. 5.15. When the slot width is zero, that is, there is no slot on the ground plane, it is just simply a symmetric coupled three strip lines. As the slot width is increased, C_{11} first decreases and then increases slightly and finally decreases again after it reaches a maximum. However, the overall change in C_{11} is relatively small. C_{22} has a relatively large decrease. On the other hand, both L_{11} and L_{22} increase. The mutual capacitances and inductances also increase. The effective dielectric constants of the even-even and the even-odd modes decrease first rapidly and then slowly, whereas that of the odd mode first decreases quickly and then increases slowly and later decreases again. The odd and even-even mode impedances first increase and then decrease and finally increase again. The change in the odd mode impedance is relatively small, while that in the even-even mode is more drastic. The even-odd mode impedance first rises and then drops. It is seen that there are intersection points where the even-odd mode and the odd or the even-even mode impedances are equal. When the inner edges of the two slots merge together, it becomes a symmetric coupled three strip lines with one ground plane slot, which has been discussed in the previous section.

The influence of a ground plane strip line in the symmetric coupled three strip line structure with two ground plane slots on the capacitance, inductance, effective dielectric constant, and modal impedances is illustrated in Fig. 5.16, where C_{44} and L_{44} are the self capaciatance and inductance of the ground plane strip, C_{14} and L_{14} are the mutual capaciatance and inductance between the side and the ground plane strips, and C_{24} and L_{24} are the mutual capacitance and inductance between the center and the

ground plane strips. Since the structure is a four line system, there are four fundamental modes associated with it. Modes a, b, and c correspond to the odd, even-even, and even-odd modes in the structure with a floating conductor, whereas mode d is due to the existence of the ground plane strip line. As the slot width is increased, the self capacitances decrease while the self inductances increase. $|C_{12}|$ and $|C_{13}|$ increase, whereas $|C_{24}|$ decreases. $|C_{14}|$ first increases and then decreases. All the mutual inductances increase. The effective dielectric constants of modes a and c first increase and then decrease. The effective dielectric constant of mode b just simply decreases, while that of mode d first decreases and then increases. The impedances of modes a and b first decrease and then increase, while those of modes c and d both increase. The changes in the impedances of modes a, b, and c are small, but the change in the impedance of mode d is quite large.

5.6 DOUBLE-SIDED STRIP LINES WITH A GROUND PLANE SLOT

Two different double-sided strip line structures with a ground plane slot are illustrated in Fig. 5.17. One is symmetric to the ground plane (GPS); the other symmetric to the slot center (SCS). These structures could be useful in microwave filter, VLSI interconnection, and PCB applications.

Fig. 5.18 shows the capacitance, inductance, effective dielectric constant, and modal impedance of the two different structures as a function of the distance between the strip and the slot centers, i.e., the strip offset s. It can be seen that as s is increased, the self capacitances increase and self inductances decrease for both structures. The difference between the self capacitances is relatively small, so is that between the self inductances. The mutual capacitances and inductances decrease. However, the mutual capacitance and inductance of the SCS structure drop much faster than those of the GPS structure. The differences between the mutual capacitances and between the

mutual inductances are quite significant as s is further increased. The odd mode effective dielectric constant of the GPS structure is a constant, while that of the even mode first increases and then decreases and eventually increases again. On the other hand, the odd mode effective dielectric constant of the SCS structure first increases and then decreases and later increases again, whereas its even mode counterpart experiences a similar change as that in the GPS structure. One thing is worth noting that there is an intersection point where the even and the odd mode effective dielectric constants are equal in the SCS structure. The even mode impedances decrease for both structures. The odd mode impedance of the GPS structure is a constant, while that of the SCS structure first increases and then decreases. The even and the odd mode impedances converge to each other as s becomes very large.

Since their self capacitances as well as self inductances are very close to each other and the mutual capacitance and inductance of the SCS structure are smaller than those of the GPS structure, the former should be favored in the VLSI interconnection and PCB applications for the crosstalk reduction.

5.7 APPLICATIONS

The layered multiconductor strip-slot structures can be used in electronic packagings and VLSI interconnections for reducing far-end crosstalk. Crosstalk is an increasingly important factor in high-speed circuit interconnection design due to the increases in the clock frequency and integration density in VLSI circuits [1, 47, 50]. The crosstalk can be reduced by increasing the separation between the interconnects, i.e., the transmission lines. However, difficulties arise in the design when the area used by the interconnects is limited. The far-end crosstalk reduction in the coupled interconnects is obtainable by introducing ground plane slots, which add more

freedom in the interconnection design without increasing the area used by the interconnects and without significantly increasing the near-end crosstalk.

The capacitances and inductances calculated in the proceeding sections can be used in a SPICE model [48] to study the crosstalk reduction in coupled interconnects with ground plane slots. In the following examples, an non-ideal input step signal with the magnitude of one volts and the rise time of 100 ps is employed as an input. In addition, a substrate of $\varepsilon_r = 9.8$ is used. The length of the interconnects is chosen to be 5 cm long and all of the interconnects are terminated with resistors of 50 Ω as shown in Fig. 5.19.

The near- and far-end crosstalks of the symmetrically coupled two interconnects with a ground plane slot are plotted in Fig. 5.20 as a function of the slot width. As the slot width is increased, the magnitude of the far-end crosstalk decreases from a large negative value to a small negative value. A further increase in the slot width results in a positive far-end crosstalk, which suggests that a zero far-end crosstalk is achievable with the width of an appropriate value. On the other hand, the near-end crosstalk increases with the slot width. However, the increase in the near-end crosstalk is relatively small. If the near-end crosstalk is of less concern in the high-speed digital circuits, a zero far-end crosstalk is naturally the best choice. Otherwise, a trade-off between the far- and the near-end crosstalks is needed. A 50% reduction in the far-end crosstalk is obtainable with the ground plane slot, while the relatively small near-end crosstalk has no significant increase. It is also possible to equalize the magnitude of the near-end crosstalk with that of the far-end crosstalk by changing the slot width.

The reason for the far-end crosstalk to change from a negative value to a positive value is due to the fact that the even mode travels faster than the odd mode with a large slot on the ground plane, while it travels slower than the odd mode with a

small slot or without any slot on the ground plane. This is indicated in Fig. 5.6(b) where the effective dielectric constants of the even and odd modes are plotted as a function of the slot width. When the even and odd modes travel at an equal speed, a zero far-end crosstalk can be realized if the interconnects are terminated with a matched impedance $Z_0 = \sqrt{Z_{0o}Z_{0e}}$, where Z_{0o} and Z_{0e} are the odd and even mode impedances of the structure.

For the symmetric three-strip interconnects shown in Fig. 5.1(d), two symmetric ground plane slots are introduced to reduce the far-end crosstalk. The ground plane strip between the slots can be treated as either a floating conductor or a short-circuited transmission line. The ground plane strip is considered as a floating conductor when it is much longer than the interconnect length, otherwise it has to be treated as a transmission line with its two terminals connected to the ground. The input signal can be connected to either one of the side interconnects or the center one. When the input is connected to a side interconnect, all three modes are excited. When it is linked with the center interconnect, only the even-even and the even-odd mode are excited.

First, consider that a side interconnect is excited and the ground plane strip as a floating conductor. The near- and far-end crosstalks as a function of the slot width are shown in Fig. 5.21. As the slot width is increased, the peak of the center line far-end crosstalk changes from a large negative value to a small positive one, while that of the center line near-end crosstalk has a relatively small increase. The side line far-end crosstalk changes from a small negative value to a significantly large positive value, whereas the side line near-end crosstalk initially increases slightly and then changes from a small positive value to a small negative value. A further increase in the slot width worsens the center line crosstalk.

It is reasonable to reduce the center line far-end crosstalk by at least 30% without significantly increasing the center line and the side line near-end crosstalks. When the center interconnect is excited, the near- and the far-end crosstalks on the side interconnects are found to be same as those on the center interconnect with the input connected to a side interconnect. Time domain responses from the SPICE simulation are shown in Fig. 5.22 for the coupled two interconnects with a ground plane slot with g = 0 and 0.9 mm and in Fig. 5.23 for the coupled three-strip interconnects with two ground plane slots and with the input connected to a side interconnect for g = 0 and 0.6 mm, respectively.

Now, let the ground plane strip be treated as an additional transmission line with its terminals short-circuited and the input be connected to a side interconnect. Shown in Fig. 5.24 are the peak values of the near- and far-end crosstalks. As the slot width is increased, the peak values of the far-end crosstalks decrease. While the center line near-end crosstalk has a relatively small increase, the side line near-end crosstalk initially increases and then decreases slightly. When the two slots merge to become a large slot, the center line far-end and the side line near-end crosstalks reach their minimums while the center line near-end and the side line far-end crosstalks reach their maximums. A 45% reduction in the center line far-end crosstalk can be realized, whereas the near-end crosstalks are still kept at relatively low levels. When the center line is excited, the corresponding crosstalks are again same as those on the center line with the input connected to a side line.

The effect of an extra length ΔL on both sides of the ground plane strip with the open- and short-circuited terminations on the crosstalks is shown in Fig. 5.25. When $\Delta L = 0$, the far-end crosstalks in the open-circuited case are better than those in the short-circuited case. When $\Delta L \geq 2L$ the open- and short-circuited ground plane strips have the same effect on the crosstalks for the given example. This is due to the

fact that ΔL introduces a long delay so that the reflected signals from the open- and short-circuited ends can be negligible in the digital system. On the other hand, it is seen that the crosstalks are far different from those shown in Fig. 5.21. This could be partly due to the discontinuity in the ground plane strip.

The SPICE simulation results for $\Delta L = 0$ are shown in Fig. 5.26 for $g = 0$ and 1.0 mm. It is observed that a small ringing effect appears in all of the responses due to the presence of the short-circuited ground plane strip.

Fig. 5.27 shows some experimental results of the coupled two strips with a ground plane slot and the coupled three strips with two ground plane slots and a short-circuited ground plane strip. The step input signal with the magnitude of 250 mV and the rise time of 30 ps was connected to the center interconnect for the three-strip two-slot structure. The experimental results indicate that the ground plane slots can indeed reduce the far-end crosstalk.

The mechanism for the far-end crosstalk reduction in the symmetric coupled two strip lines with one ground slot is different from that in the symmetric coupled three strip lines with two ground plane slots. While the far-end crosstalk reduction in the former is realized by controlling the wave propagation velocities of the odd and the even mode with the ground plane slot, the reduction in the latter is obtained by mainly changing the polarities of the modal voltages or currents on the lines with the ground plane slots. As can be seen in Figs. 5.10, 5.15, and 5.16, the velocities of the even-even and the even-odd modes cannot be equalized by just simply changing the ground plane slot width.

5.8 SUMMARY

The capacitances, inductances, effective dielectric constants, and modal impedances of various strip-slot structures are calculated by the quasi-TEM spectral technique. The calculated results are used in the SPICE model to study the crosstalk reduction in digital systems. The simulation results show that slots on the ground plane can reduce the far-end crosstalk in the coupled interconnects, which are validated by the experimental results.

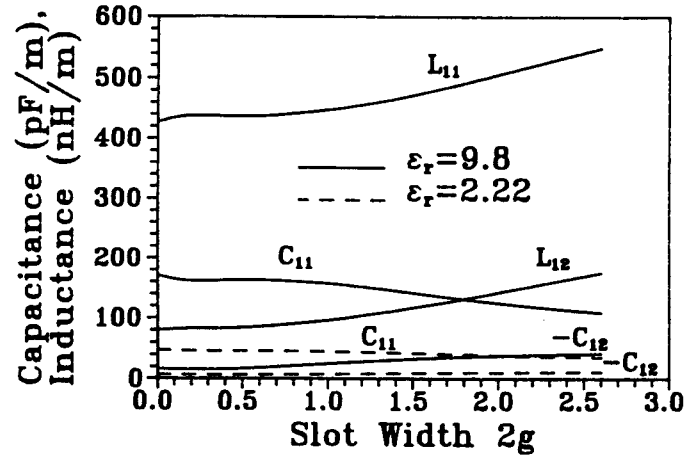

(a)

(b)

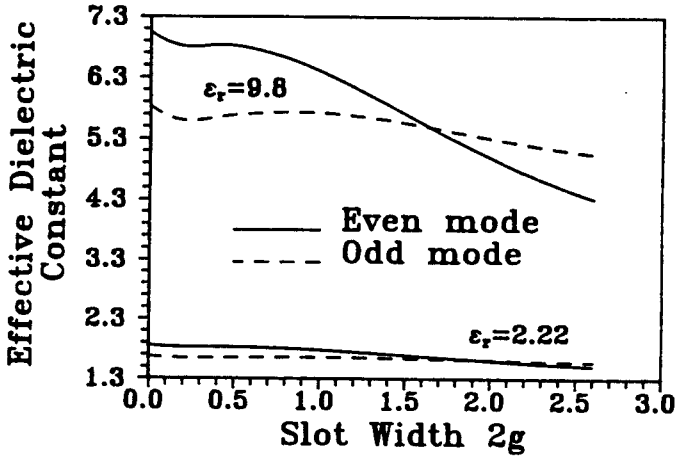

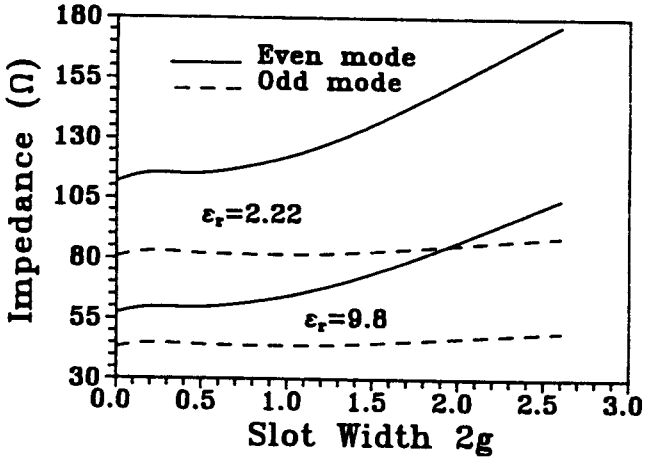

(c)

Fig. 5.6 (a) Capacitance and inductance, (b) effective dielectric constant, and (c) impedance of a coupled two-strip structure with a ground plane slot as a function of the slot width with ε_r as a parameter (a=14.4, b=21d, d=0.635, h_1=10d, w=0.6, s=0.3, length unit: mm).

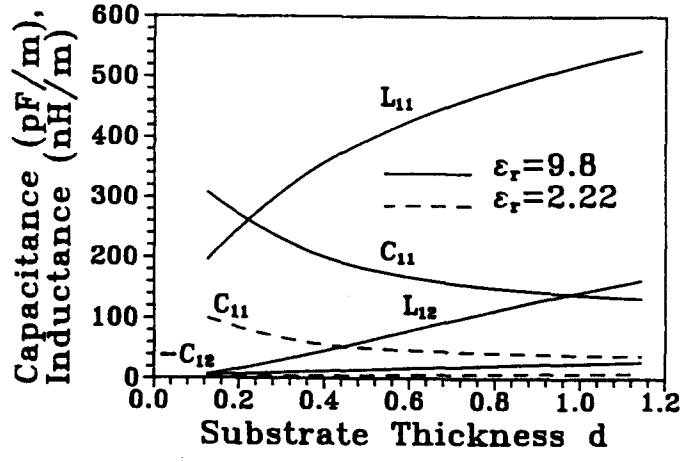

(a)

(b)

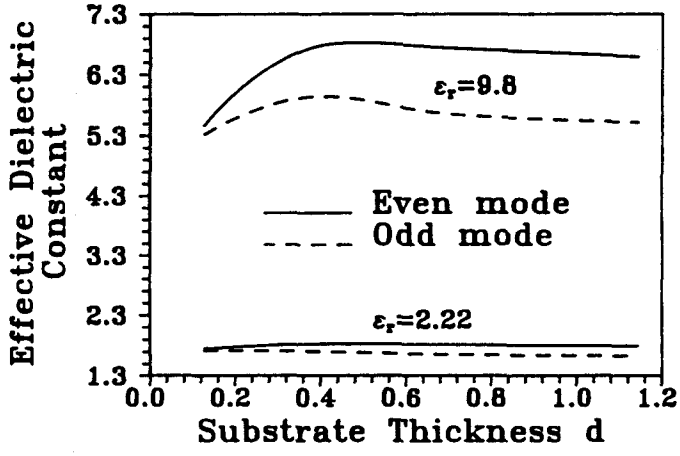

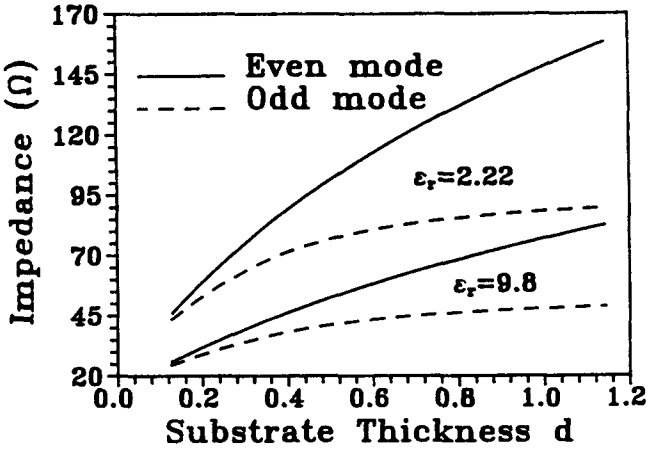

(c)

Fig. 5.7 (a) Capacitance and inductance, (b) effective dielectric constant, and (c) impedance of a coupled two-strip structure with a ground plane slot as a function of the substrate thickness with ε_r as a parameter (a=14.4, b=21d, h_1=10d, w=0.6, s=0.3, g=0.3, length unit: mm).

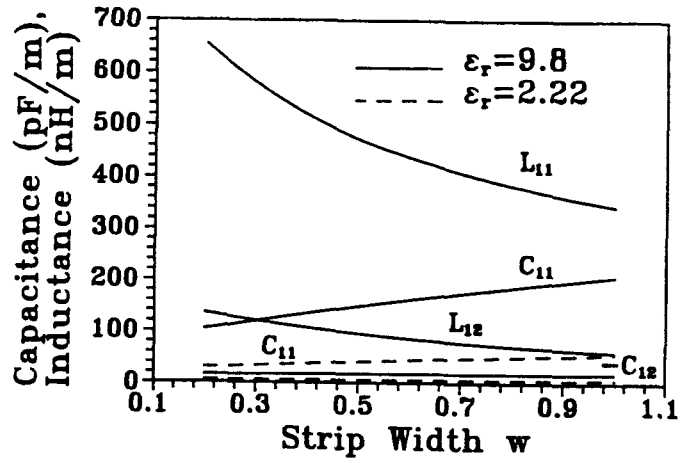

(a)

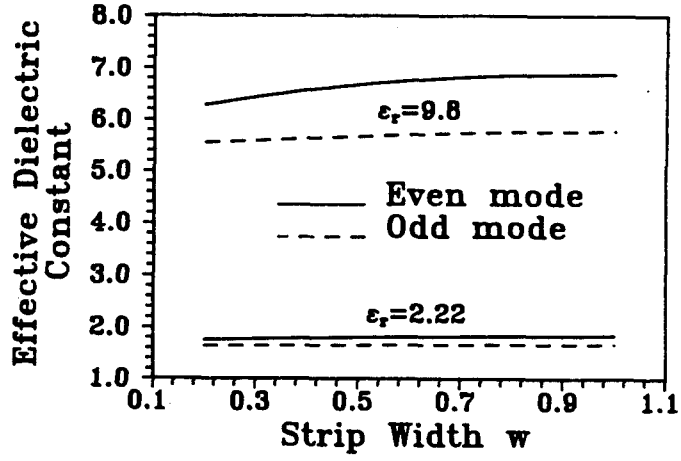

(b)

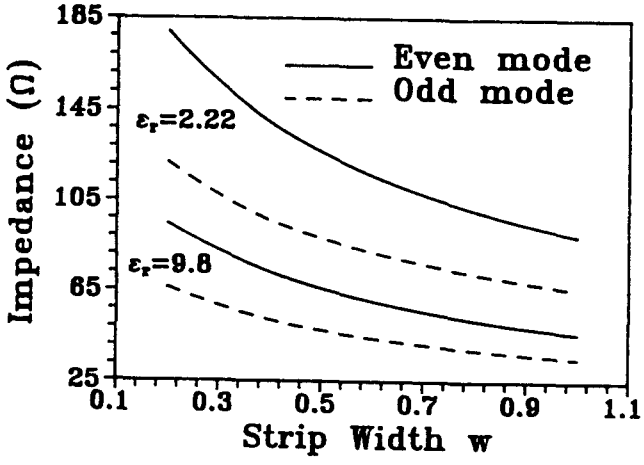

(c)

Fig. 5.8 (a) Capacitance and inductance, (b) effective dielectric constant, and (c) impedance of a coupled two-strip structure with a ground plane slot as a function of the strip width with ε_r as a parameter (a=24w+s, b=21d, h_1=10d, d=0.635, s=0.3, g=0.3, length unit: mm).

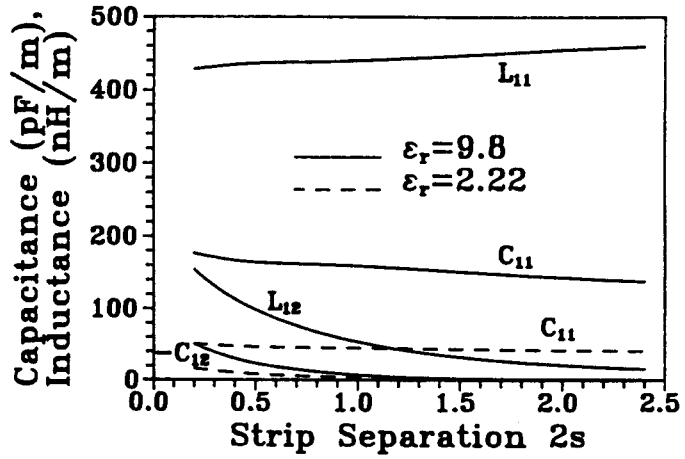

(a)

(b)

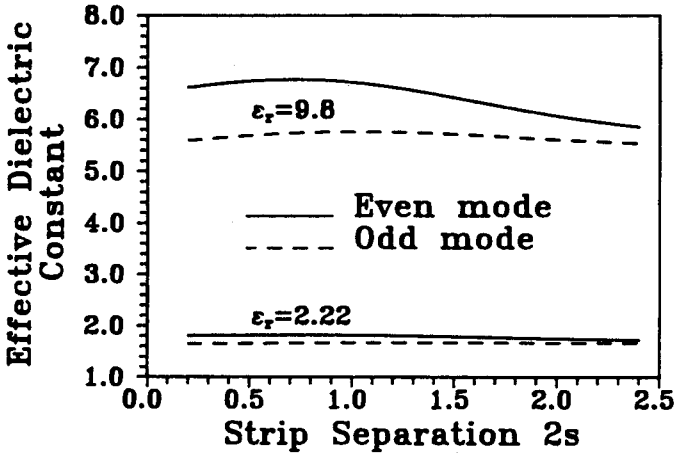

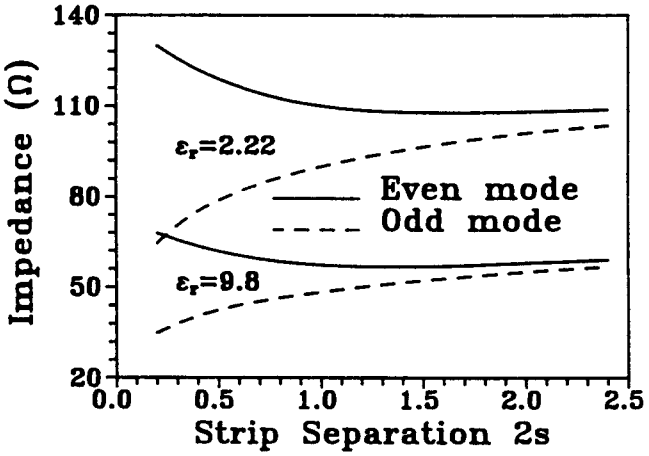

(c)

Fig. 5.9 (a) Capacitance and inductance, (b) effective dielectric constant, and (c) impedance of a coupled two-strip structure with a ground plane slot as a function of the separation between strips with ε_r as a parameter (a=24w+s, b=21d, h_1=10d, d=0.635, w=0.6, g=0.3, length unit: mm).

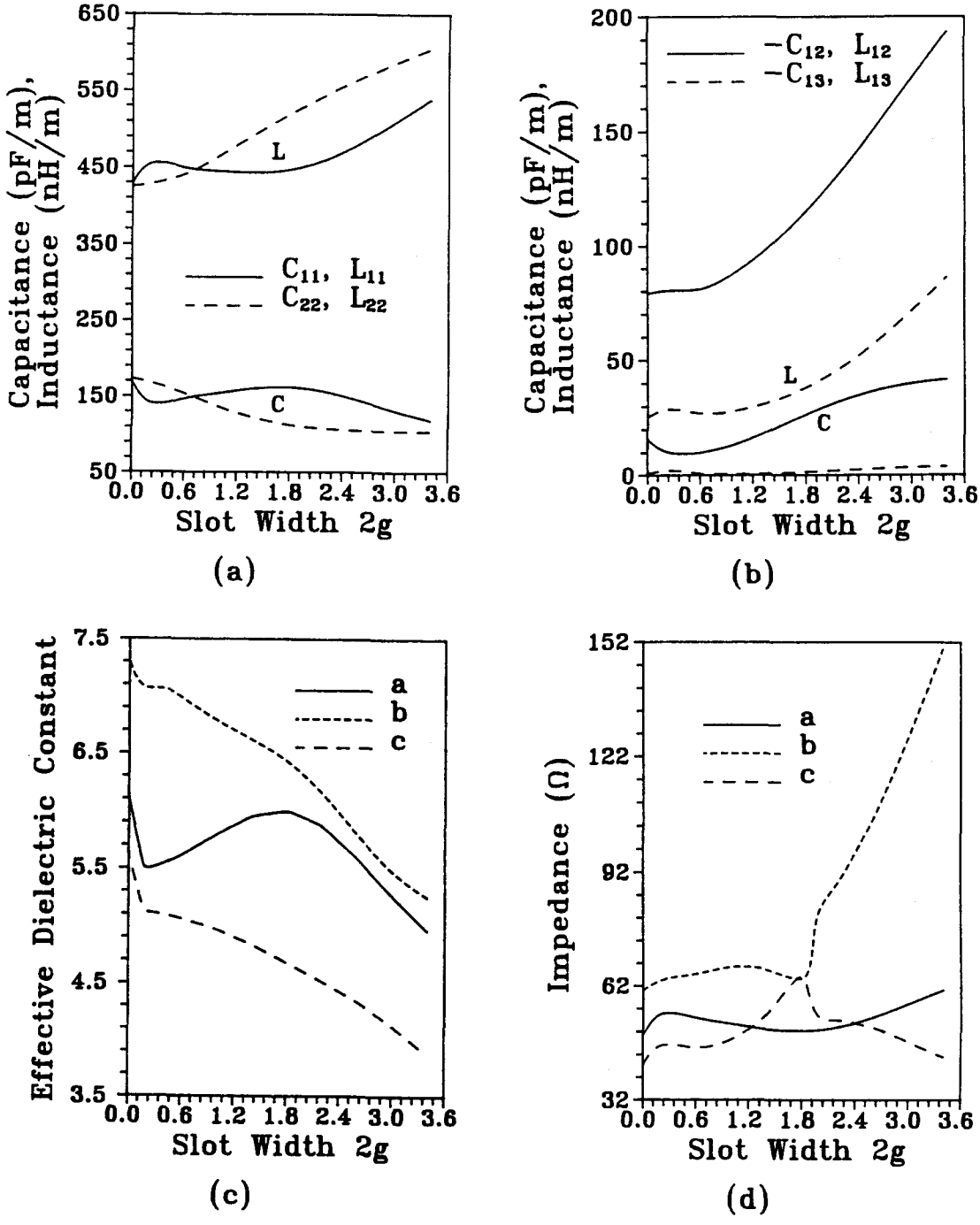

Fig. 5.10 (a) Self capacitance and inductance, (b) mutual capacitance and inductance, (c) effective dielectric constant, and (d) impedance of a coupled three-strip structure with a ground plane slot as a function of the slot width (ε_r=9.8, a=14.4, b=21d, d=0.635, h_1=10d, w_s=0.6, w_c=0.3, s=0.6, length unit: mm).

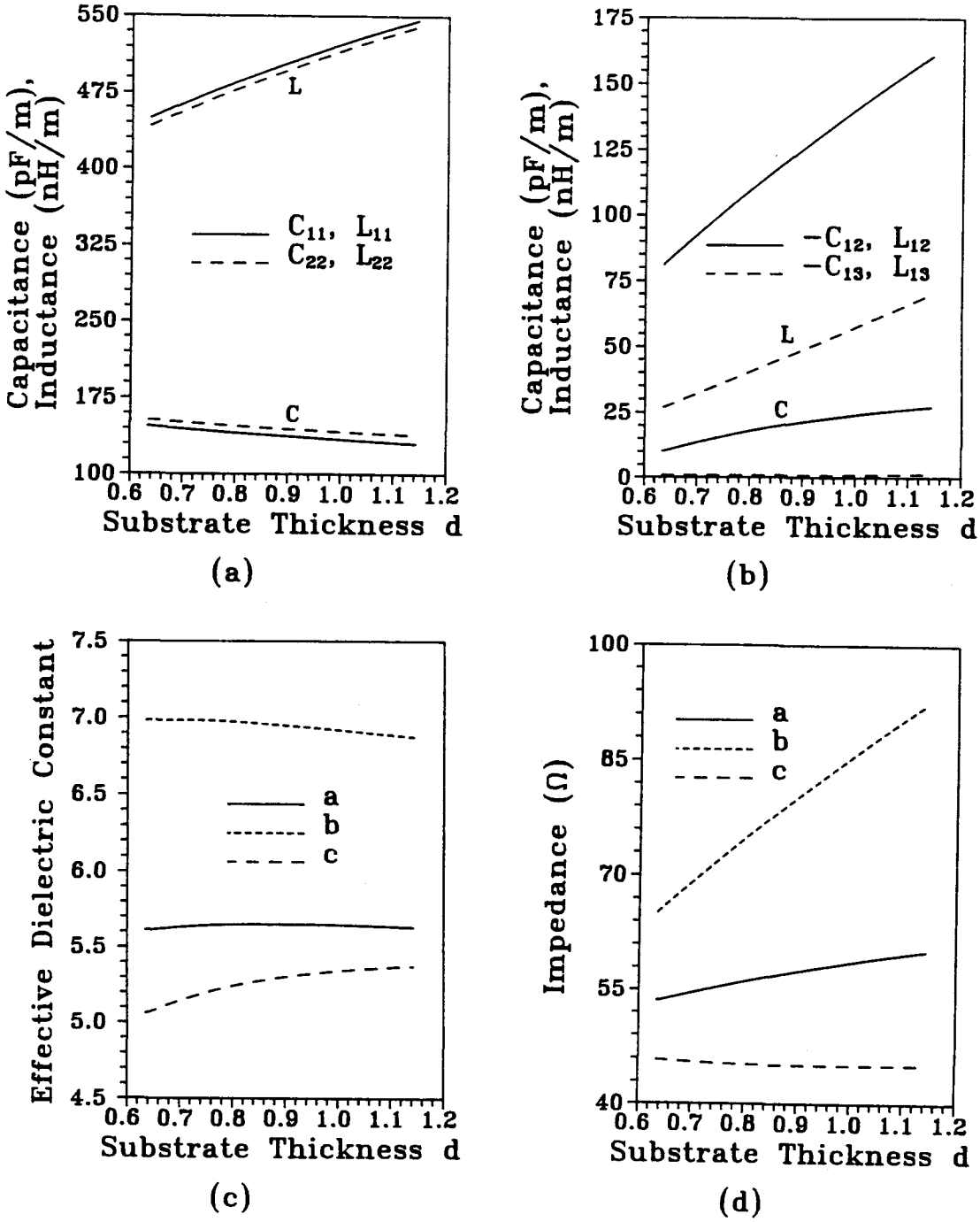

Fig. 5.11 (a) Self capacitance and inductance, (b) mutual capacitance and inductance, (c) effective dielectric constant, and (d) impedance of a coupled three-strip structure with a ground plane slot as a function of the substrate thickness (ε_r=9.8, a=14.4, b=21d, h_1=10d, w_s=0.6, w_c=0.3, s=0.6, g=0.3, length unit: mm).

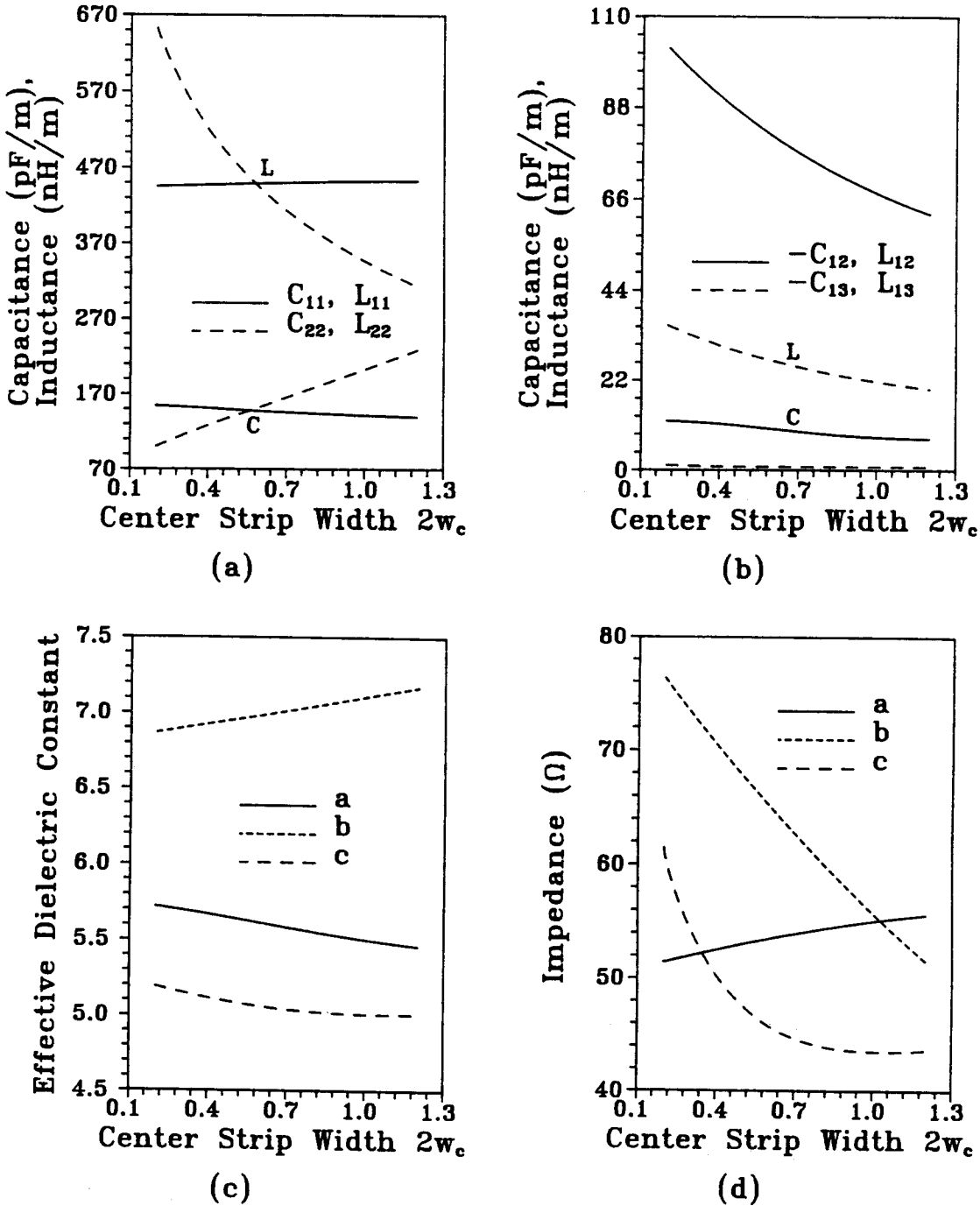

Fig. 5.12 (a) Self capacitance and inductance, (b) mutual capacitance and inductance, (c) effective dielectric constant, and (d) impedance of a coupled three-strip structure with a ground plane slot as a function of the center strip width (ε_r=9.8, a=23.5w_s+s+w_c, b=21d, d=0.635, h_1=10d, w_s=0.6, s=0.6, g= 0.3, length unit: mm).

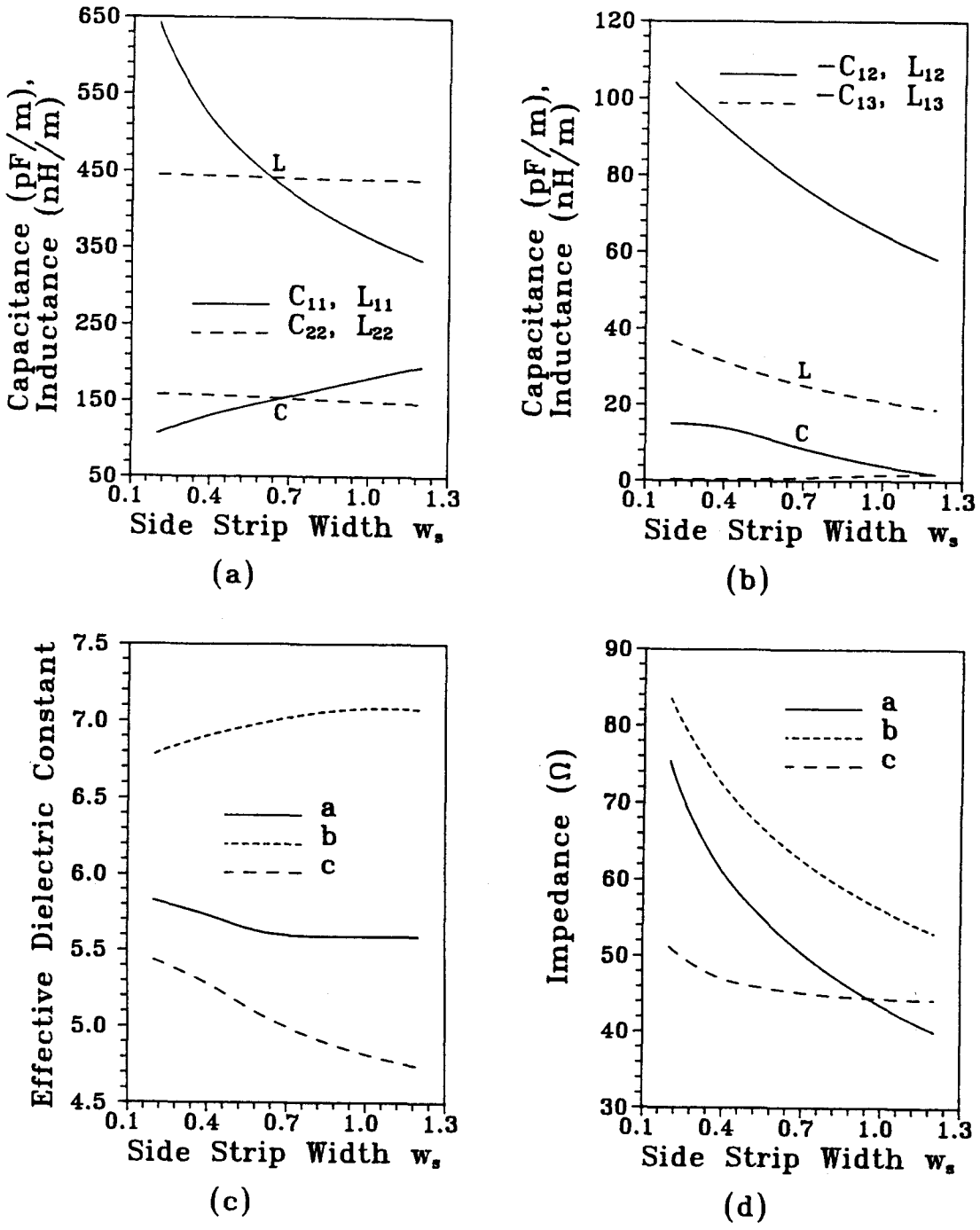

Fig. 5.13 (a) Self capacitance and inductance, (b) mutual capacitance and inductance, (c) effective dielectric constant, and (d) impedance of the coupled three strip structure with a ground plane slot as a function of the side strip width (ε_r=9.8, a=22.5w_s+s+w_c, b=21d, d=0.635, h_1=10d, w_c=0.3, s=0.6, g=0.3, length unit: mm).

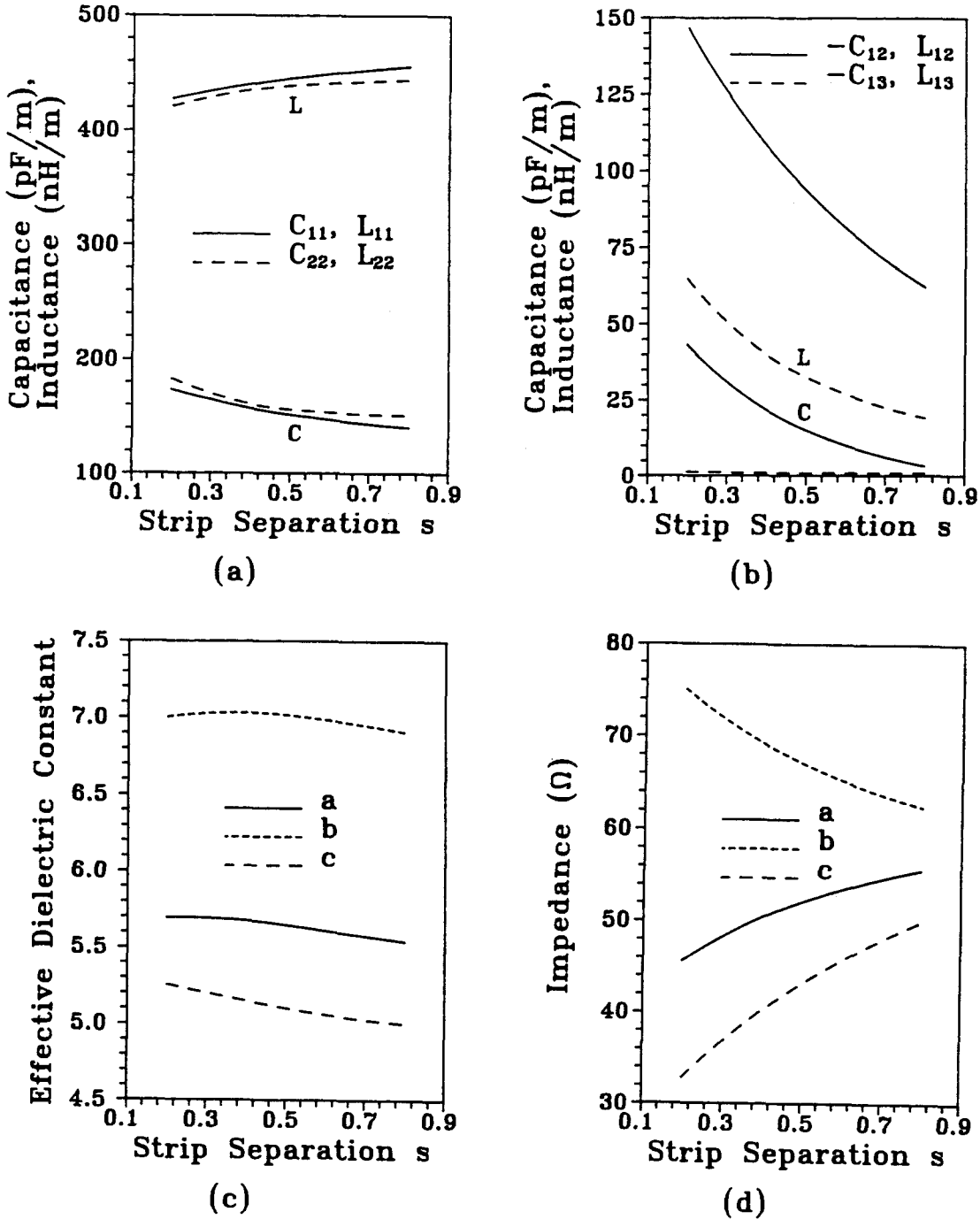

Fig. 5.14 (a) Self capacitance and inductance, (b) mutual capacitance and inductance, (c) effective dielectric constant, and (d) impedance of the coupled three strip structure with a ground plane slot as a function of the separation between the center and the side strips (ε_r=9.8, a=23.5w_s+s+w_c, b=21d, d=0.635, h_1=10d, w_s=0.6, w_c=0.3, g=0.3, length unit: mm).

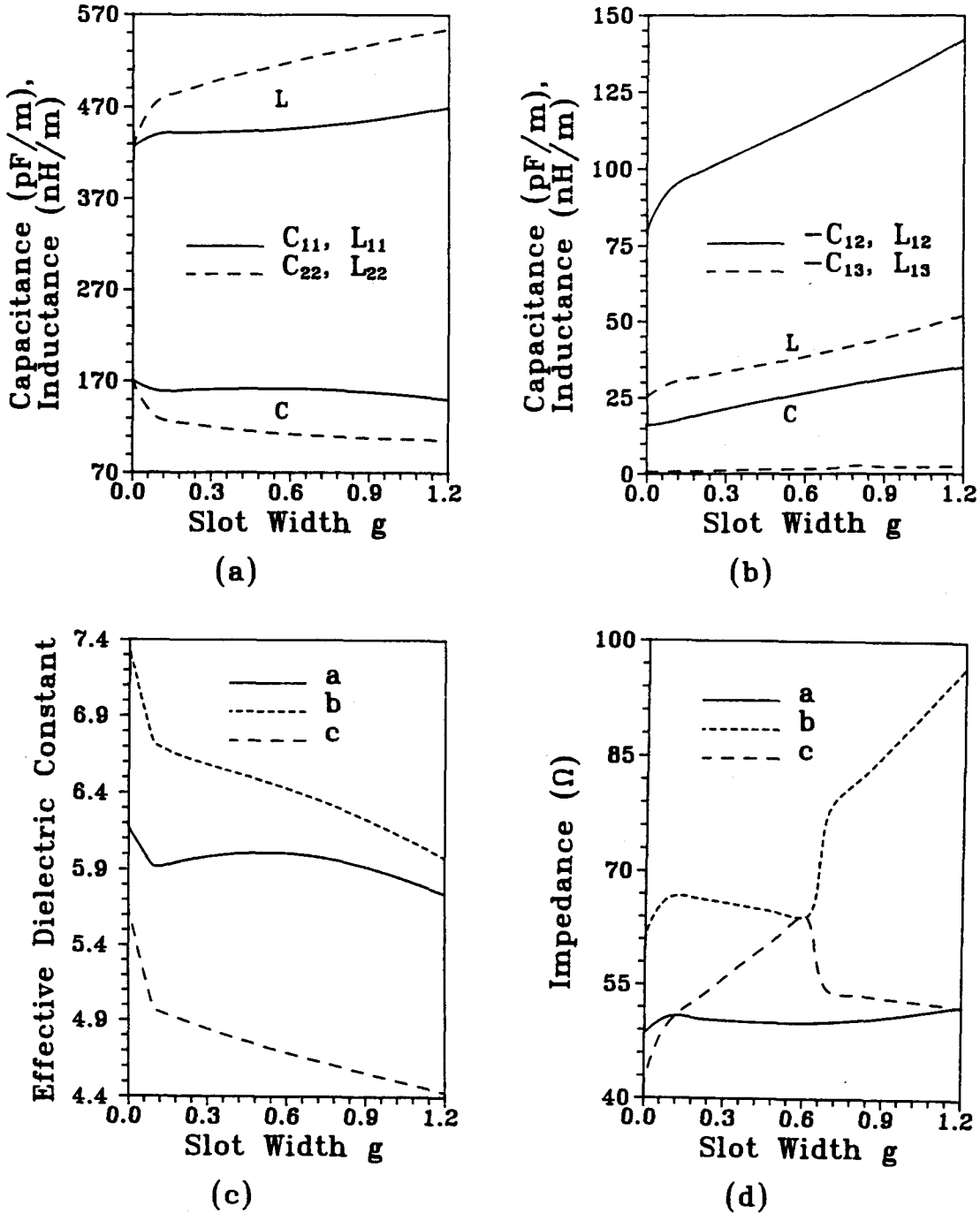

Fig. 5.15 (a) Self capacitance and inductance, (b) mutual capacitance and inductance, (c) effective dielectric constant, and (d) impedance of the coupled three strip structure with two slots and a floating conductor on the ground plane as a function of the slot width (ε_r=9.8, a=23.5w_s+s+w_c, b=21d, d=0.635, h_1=10d, w_s=0.6, w_c=0.3, s=0.6, w_g=w_c+0.5(s-g), length unit: mm).

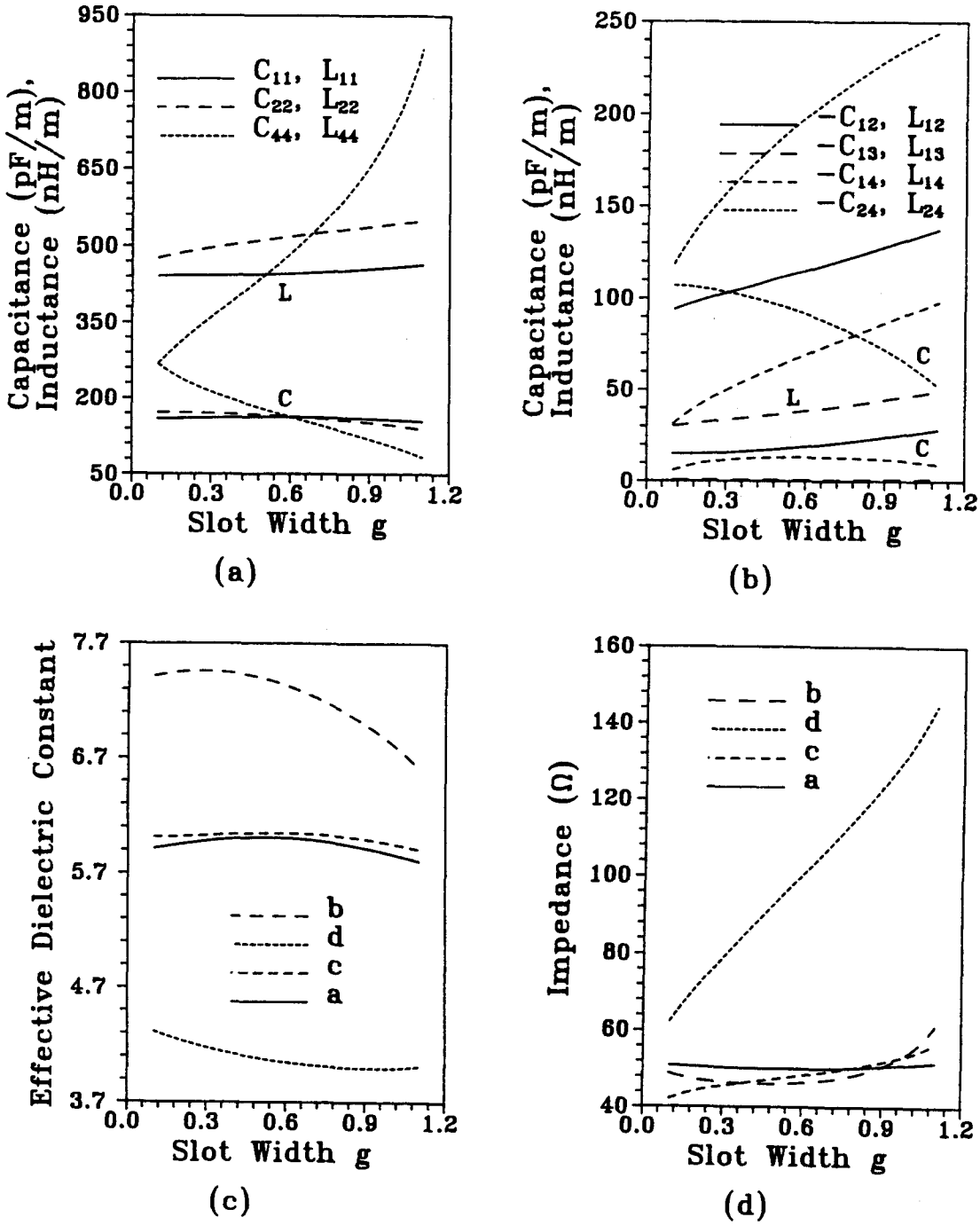

Fig. 5.16 (a) Self capacitance and inductance, (b) mutual capacitance and inductance, (c) effective dielectric constant, and (d) impedance of the coupled three strip structure with two slots and a strip on the ground plane as a function of the slot width (ε_r=9.8, a=23.5w_s+s+w_c, b=21d, d=0.635, h_1=10d, w_s=0.6, w_c=0.3, s=0.6, w_g=w_c+0.5(s-g), length unit: mm).

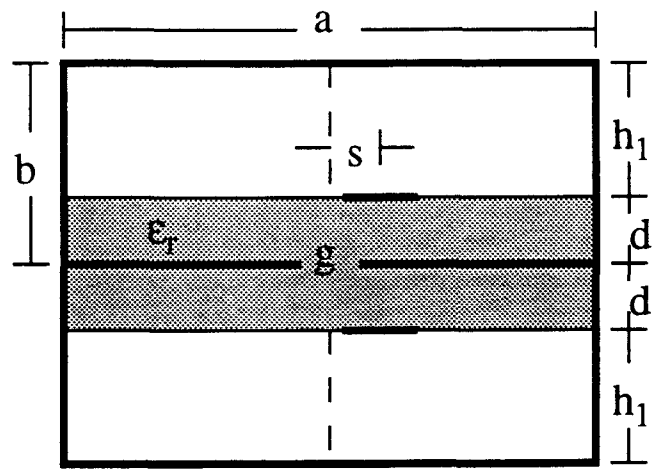

(a)

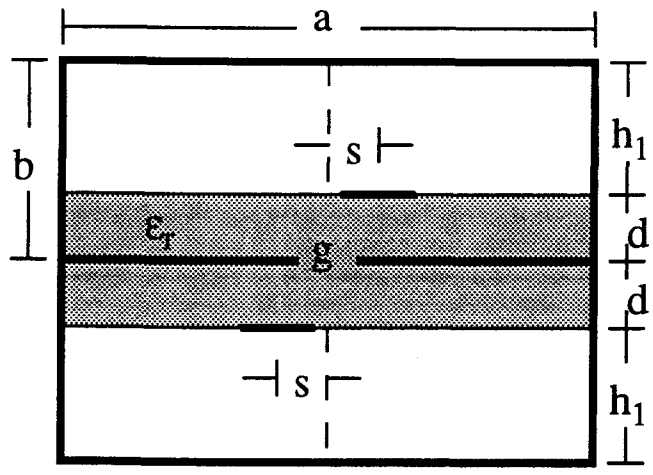

(b)

Fig. 5.17 Double sided strip line structures with a ground plane slot: (a) symmetric to the ground plane (GPS) and (b) symmetric to the slot center (SCS).

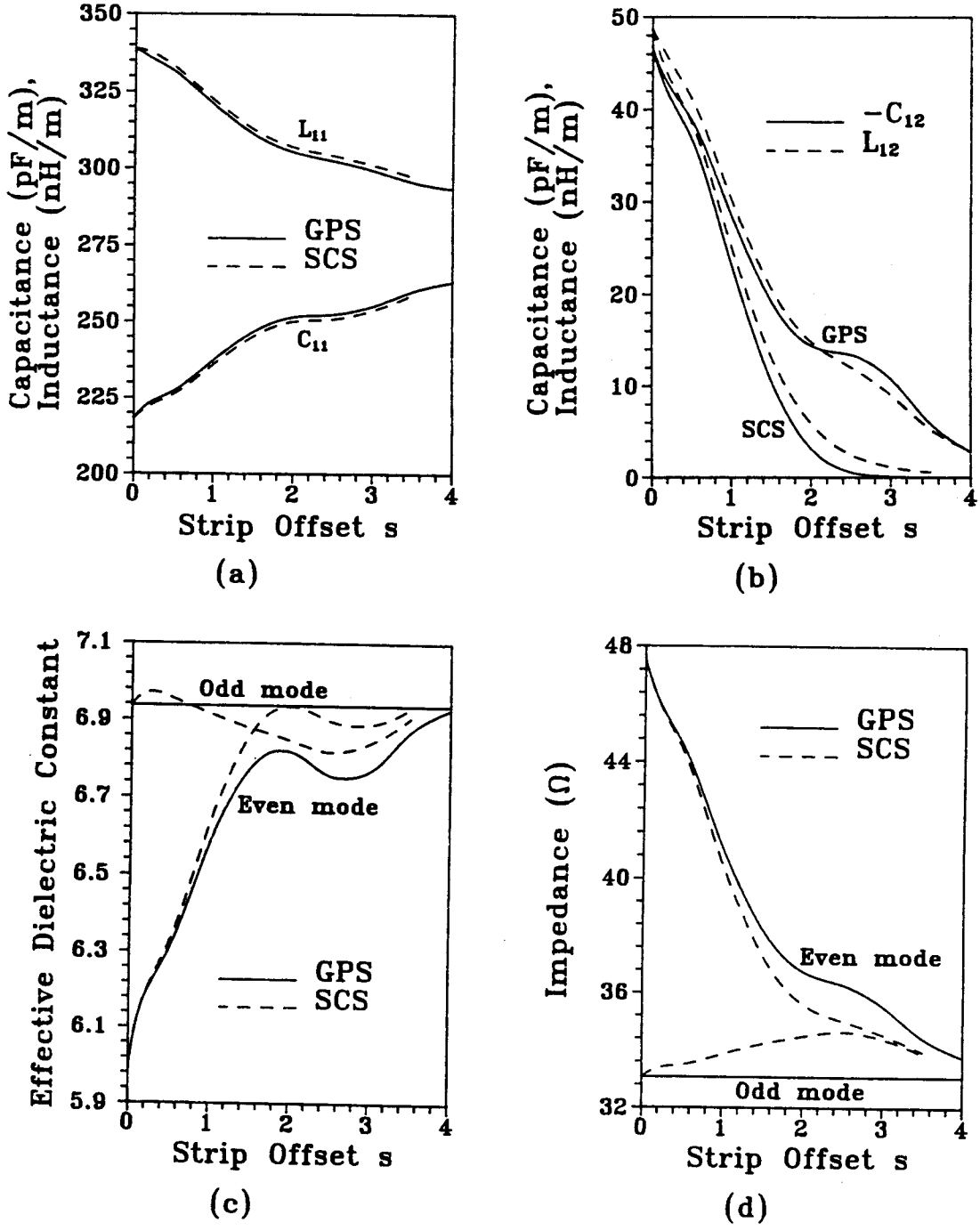

Fig. 5.18 (a) Self capacitance and inductance, (b) mutual capacitance and inductance, (c) effective dielectric constant, and (d) impedance of the double-sided strip structure with a ground plane slot as a function of the separation between the strip and the slot centers s (ε_r=9.8, a=46 b=11d, d=1, h_1=10d, w=g=2, length unit: mm).

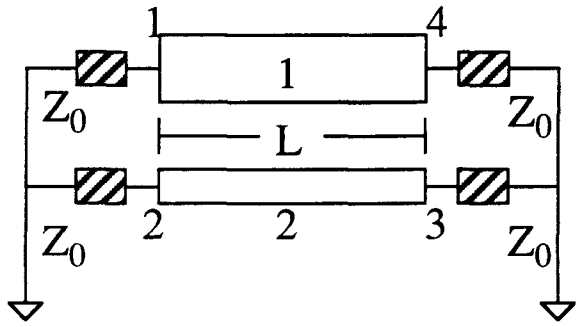

(a)

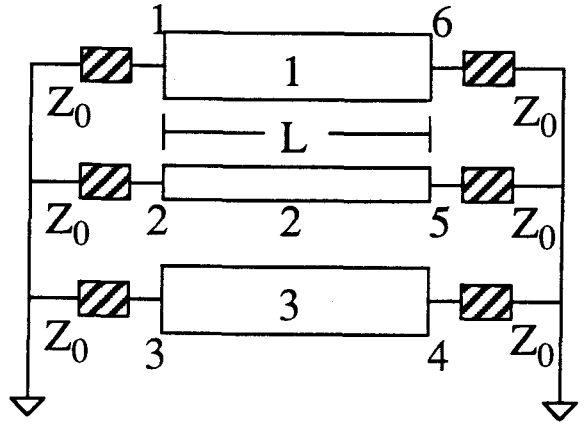

(b)

Fig. 5.19 Schematic of coupled (a) four-port and (b) six-port interconnects.

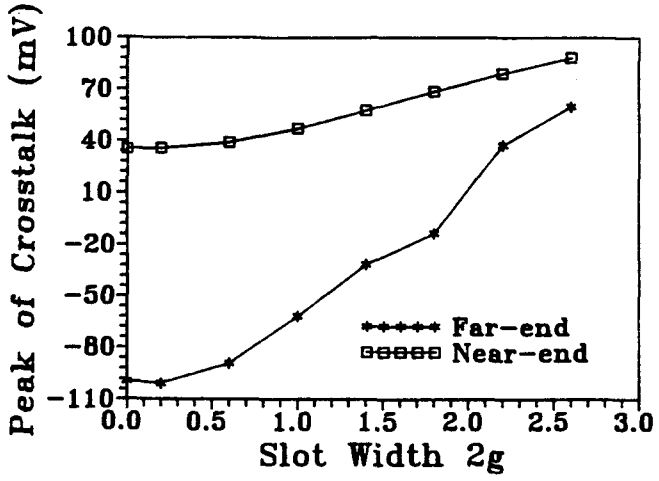

Fig. 5.20 Crosstalk in the coupled two-strip one-slot structure as a function of the slot width 2g (ε_r=9.8, a=14.4, b=21d, d=0.635, h_1=10d, w=0.6, s=0.3, L=50, length unit: mm).

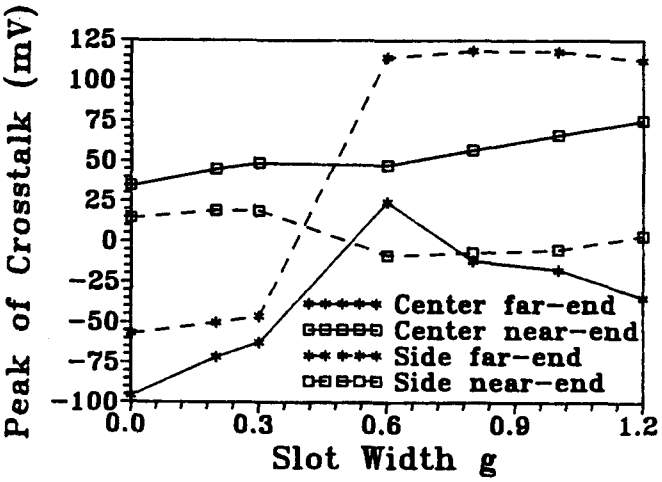

Fig. 5.21 Crosstalk in the coupled three-strip two-slot structure with a floating conductor on the ground plane as a function of the slot width g (ε_r=9.8, a=24, b=21d, d=0.635, h_1=10d, w_s=2w_c=0.6, s=0.6, w_g=w_c+0.5(s-g), L=50, length unit: mm).

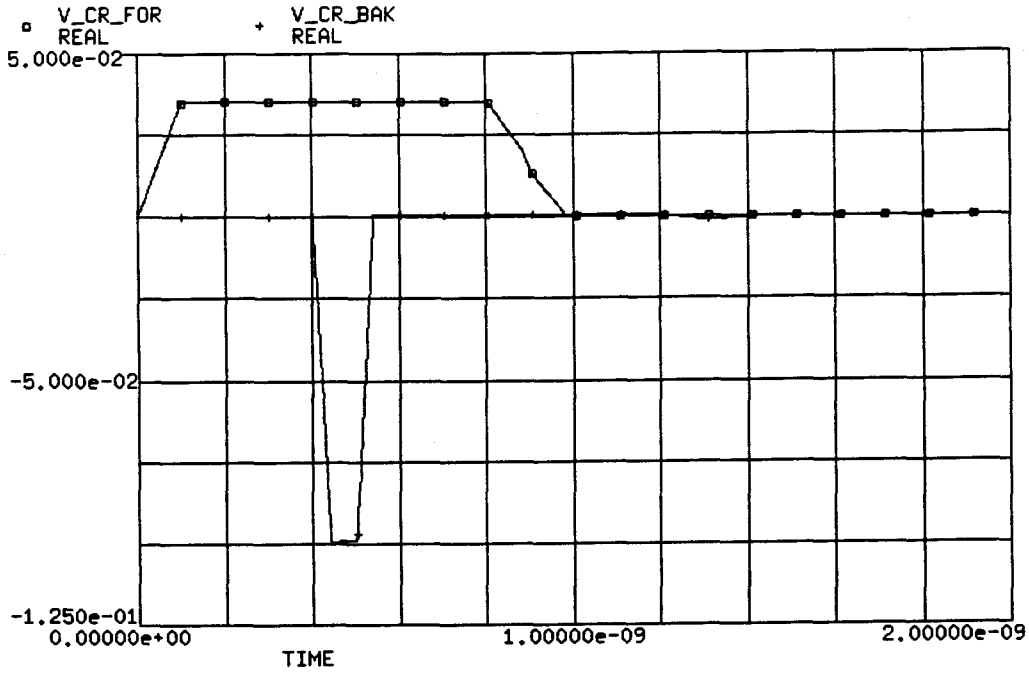

(a)

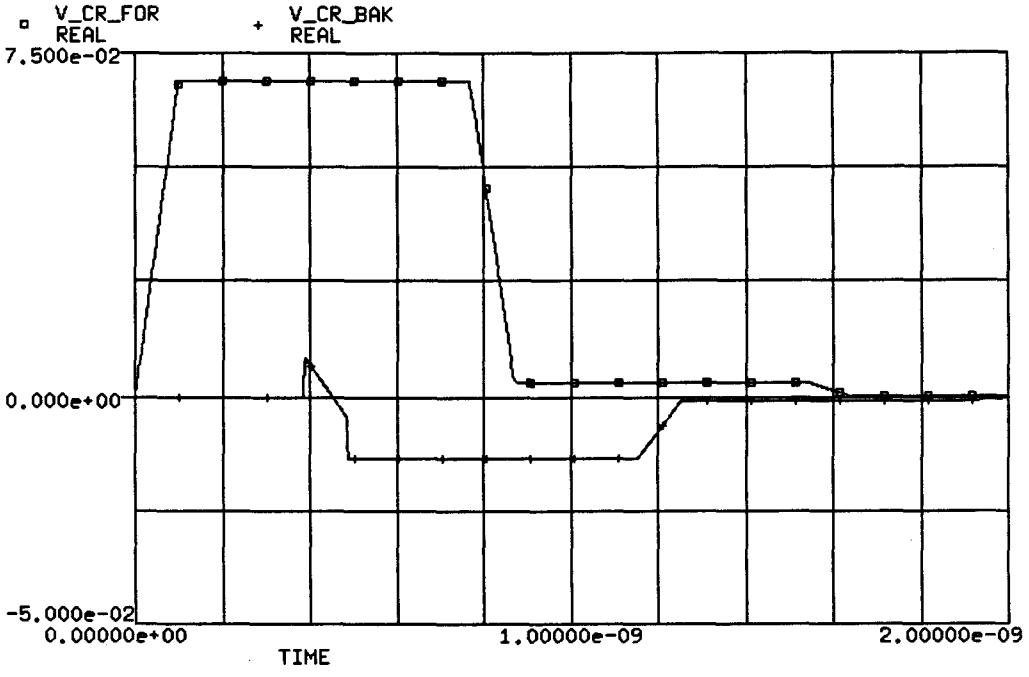

(b)

Fig. 5.22 Time domain simulation of the crosstalk shown in Fig. 5.20: (a) g=0 and (b) g=0.9mm (V_CR_BAK: near-end crosstalk, V_CR_FOR: far-end crosstalk, time unit: second, voltage unit: volt).

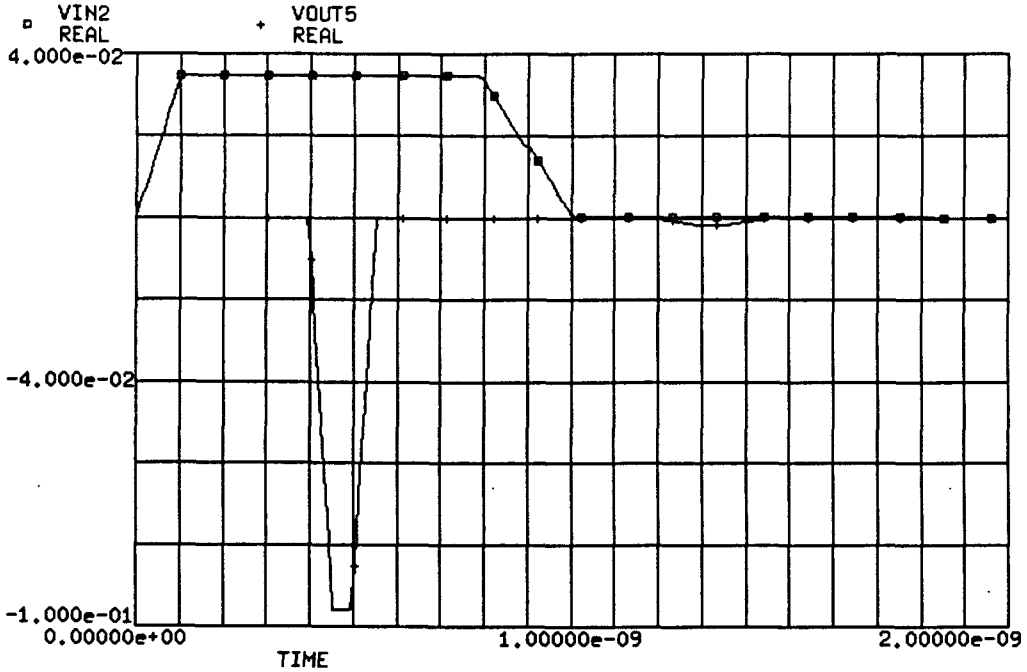

(a)

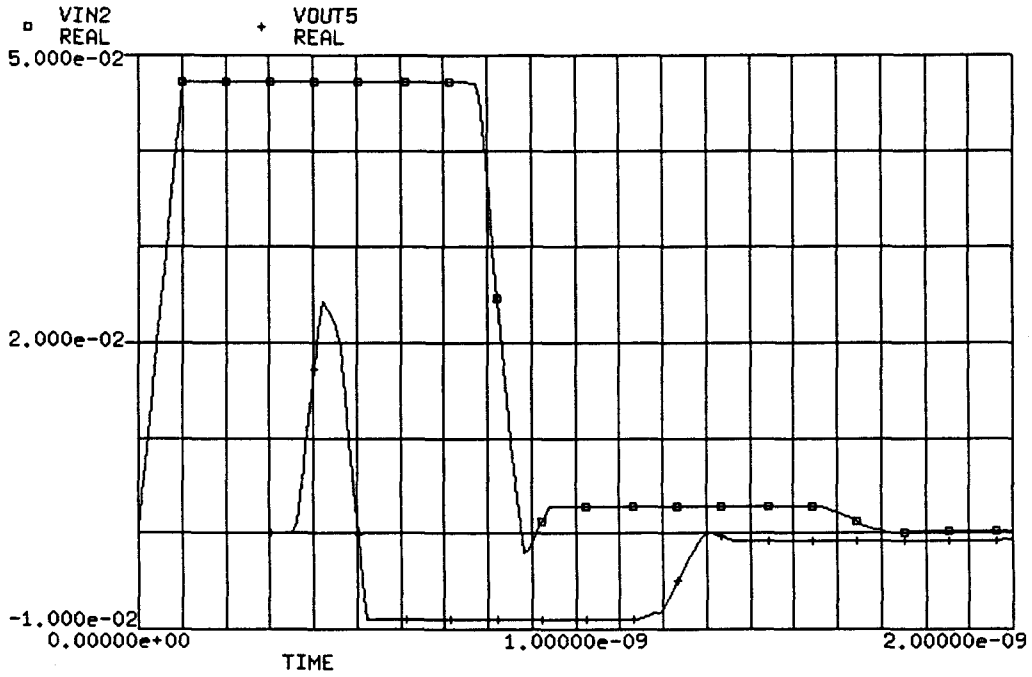

(b)

Fig. 5.23 Time domian simulation of the crosstalk on the center interconnect shown in Fig. 5.21: (a) g=0 and (b) g=0.6mm (VIN2: center near-end crosstalk, VOUT5: center far-end crosstalk, time unit: second, voltage unit: volt).

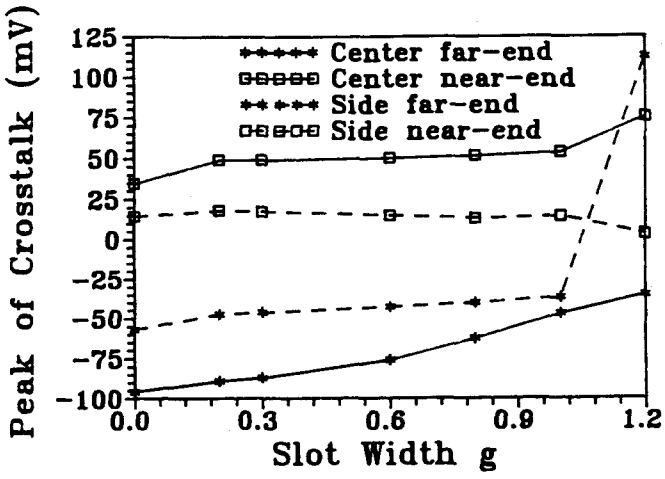

Fig. 5.24 Crosstalk in the coupled three-strip two-slot structure with a short-circuited ground plane strip as a function of the slot width g (ε_r=9.8, a=24, b=21d, d=0.635, h_1=10d, w_s=2w_c=0.6, s=0.6, w_g=w_c+0.5(s-g), L=50, length unit: mm).

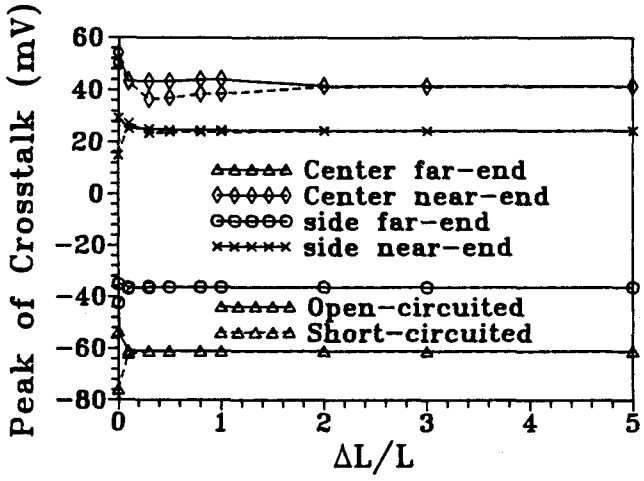

Fig. 5.25 Effect of an extra length ΔL of the ground plane short- or open-circuited strip on the crosstalk in the coupled three-strip two-slot structure (ε_r=9.8, a=24, b=21d, d=0.635, h_1=10d, w_s=2w_c=0.6, s=0.6, g=0.6, w_g=0.3, L=50, length unit: mm).

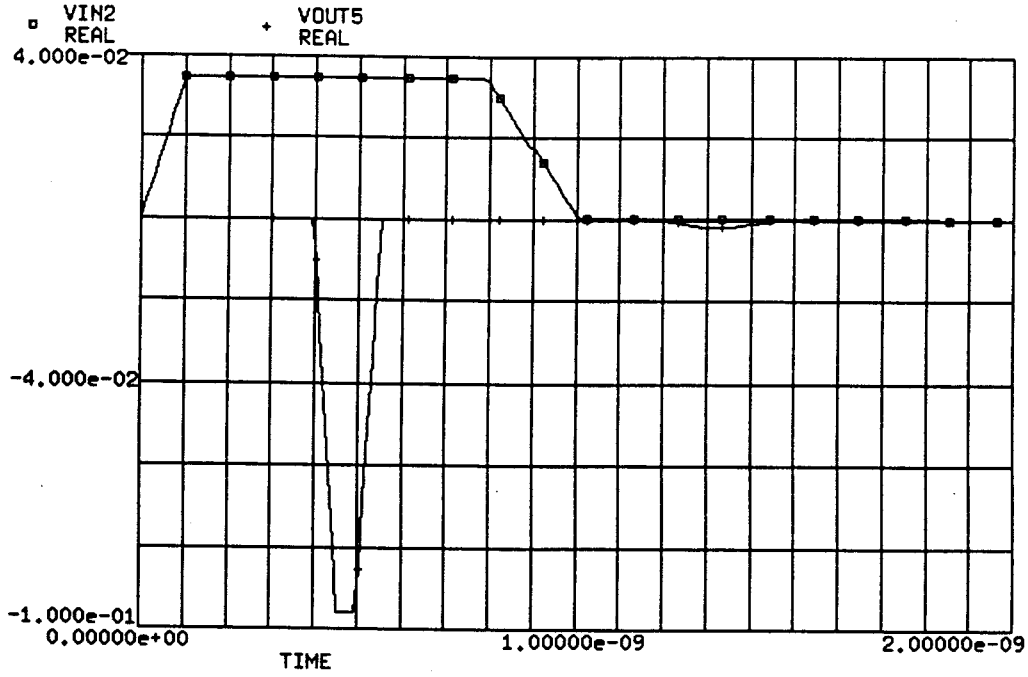

(a)

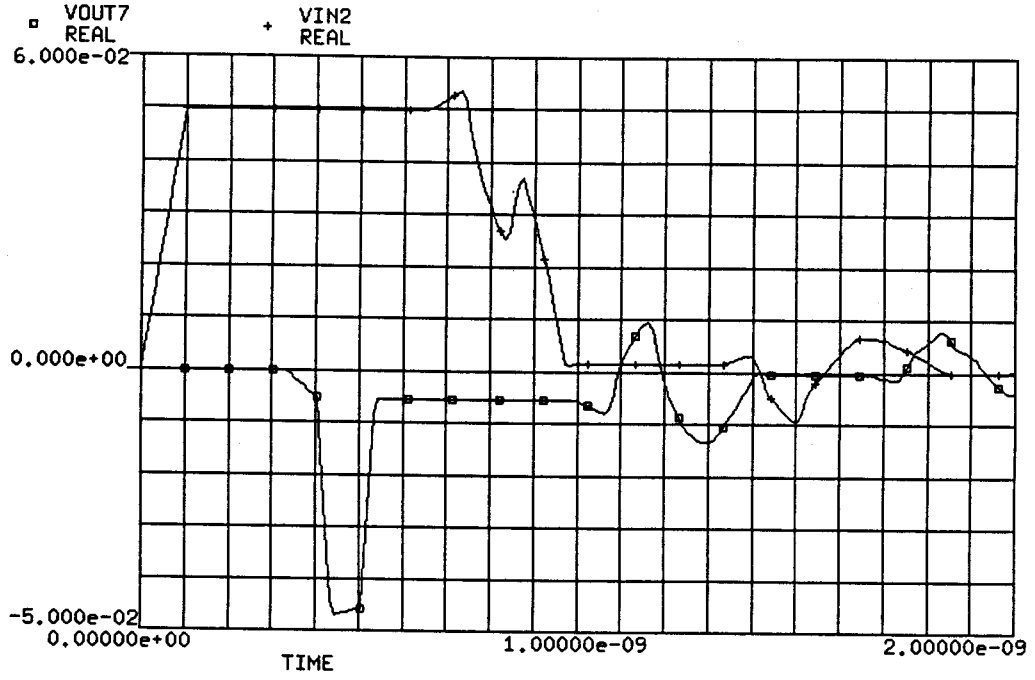

(b)

Fig. 5.26 Time domain simulation of the crosstalk on the center interconnect shown in Fig. 5.24: (a) g=0, VIN2: center near-end crosstalk, VOUT5: center far-end crosstalk and (b) g=1.0mm, VIN2: center near-end crosstalk, VOUT7: center far-end crosstalk (time unit: second, voltage unit: volt).

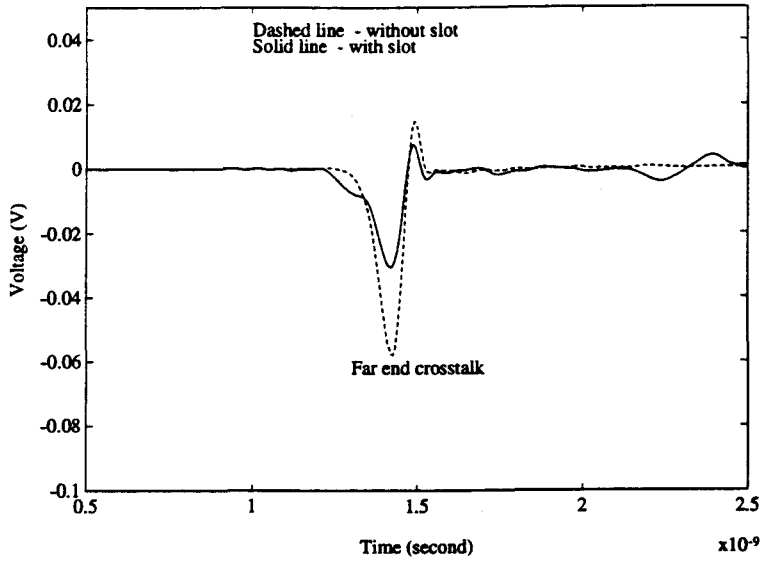

(a)

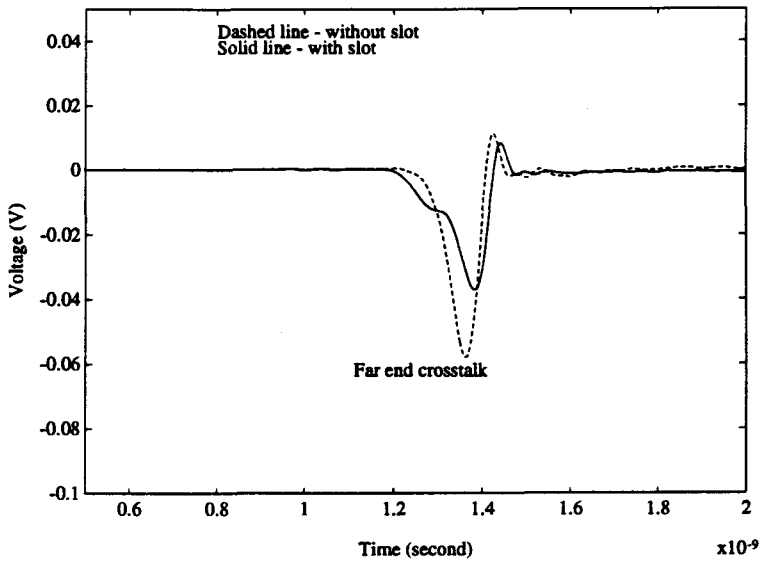

(b)

Fig. 5.27 Measured crosstalks in (a) the coupled two-strip one-slot open structure (ε_r=4.7, w=2s=2g=1.8d, d=1.5mm, L=90mm) and (b) the coupled three-strip two-slot open structure with a short-circuited ground plane strip (ε_r=4.7, w_s=2w_c=s=g=2w_g=1.8d, d=1.5mm, L=90mm).

6. CONCLUSIONS AND FUTURE WORK

The full-wave modal analysis and quasi-TEM spectral domain technique have been introduced to characterize the layered multiconductor coupled slot and strip-slot structures. The solutions for the differential equations (the Helmholtz equation in the full-wave analysis and the Laplace equation in the quasi-TEM analysis) together with the boundary conditions lead to sets of algebraic equations interrelating the sources ($\mathbf{J}$ and ρ) to the resultant field and potential ($\mathbf{E}$ and ϕ) at the interfaces of the layered structure. Implementation of the Galerkin method to these equations yields the results for the propagation constants in the full-wave analysis or for the unknown coefficients of the charge distributions in the quasi-TEM analysis. Once the propagation constants or the charge distribution coefficients are found, all the other characteristics of the structures can be readily derived. One of the advantages of using the modal analysis lies in its ability to incorporate finite metal thickness and waveguide grooves, which play a significant role in the design of fin line circuits [6]. The application of the spectral domain technique is primarily confined to the structures with infinitesimal metal thickness, though it can be extended to the structures with moderate metal thickness [45].

For a multiple coupled line structure in a lossless, linear, and isotropic medium, a resultant impedance matrix of the structure must be symmetric. The usefulness of different impedance definitions proposed for the multiple coupled line structures in the literature has been examined. It is found that the impedance matrix derived from the modal impedance definition given in [32] for multiple coupled strip lines satisfies the symmetry. Therefore, it is used to study the impedance characteristics of the unilateral and as well as bilateral coupled two-slot and symmetric three-slot fin line structures. The calculated results are used to design the

coupled fin line directional couplers as illustrated in the examples, which demonstrate the applications of the coupled line structures. Effects of the finite metal thickness and waveguide grooves on the impedance characteristics of the multiple coupled fin line structures are of interest in practical applications and should be included in any future study of these structures.

In the full-wall analysis of the coupled strip-slot line structure, the symmetry of the resultant impedance matrix is ensured by assuming that the ratio of the coupling power contributed by the strip line to the total coupling power in the strip mode is equal to that of the coupling power contributed by the slot line to the total power in the slot mode. Before a useful circuit model can be built for the applications of such structure in microwave circuits, a rigorous proof of the assumption needs to be done. Otherwise, new definitions for the voltages and currents in the coupled strip-slot structure have to be introduced. Once this simplest form of the coupled strip-slot structure is fully characterized, its natural extension to the multiple coupled strip-slot structures should be explored.

The quasi-TEM calculations of the capacitances, inductances, effective dielectric constants, and modal impedances for various strip-slot structures are presented, which are used to study the far-end crosstalk reduction in digital systems. The SPICE simulation of the coupled multiport and measured results show that the ground plane slots reduce the far-end crosstalk in the interconnects. While the velocities of the even and odd modes in the coupled two strip lines can be equalized with the ground plane slot, those of even-even and even-odd in the symmetric coupled three strip lines cannot be made equal by simply changing the slot width. However, the difference in mode velocities can be reduced. In the three strip line structure with two ground plane slots, the ground plane strip between the slots is treated as either a floating conductor or a transmission line short-circuited at its both

terminals. The short-circuited transmission line results in a ringing effect in the time domain response. One way to reduce the ringing effect is to open meshes on ground plane instead of slots [51]. Additional experimental and theoretical work in this area is warranted because of its applications in multichip module and other high performance packaging technologies.

BIBLIOGRAPHY

[1] H. B. Bakolu, *Circuits, Interconnections, and Packaging for VLSI.* Reading, MA: Addison-Welsey, 1990.

[2] D. Mirshekar-Syahkal, *Spectral Domain Method for Microwave Integrated Circuits.* Taunton, Somerest, England: Research Studies Press, 1990.

[3] T. Itoh, Ed., *Numerical Techniques for Microwave and Millimeter-Wave Passive Structures.* New York: Wiley, 1989.

[4] V. K. Tripathi, R. T. Kollipara, and L. A. Hayden, 'Quasi-TEM spectral domain analysis of thick microstrip for microwave and digital integrated circuits,' Electron. Lett., vol. 25, pp. 1253-1254, 1989.

[5] R. T. Kollipara and V. K. Tripathi, 'Dispersion characteristics of moderately thick microstrip line by the spectral domain method,' IEEE Microwave Guided Wave Lett., vol. 2, pp.100-101, 1992

[6] B. Bhat and S. K. Koul, *Analysis, Design and Applications of Fin Lines.* Norwood, MA: Artech House, 1987.

[7] R. K. Hoffmann, *Handbook of Microwave Integrated Circuits.* Norwood, MA: Artech House, 1987.

[8] B. C. Wadell, *Transmission Line Design Hand book.* Boston: Artech House, 1991.

[9] P. J. Meier, 'Integrated fin-line millimeter wave components,' IEEE Trans. Microwave Theory Tech., vol. MTT-22, pp. 1209-1216, Dec. 1974.

[10] P. J. Meier, 'Two new integrated-circuit media with special advantage at millimeter wavelengths,' IEEE MTT-S Int'l Microwave Symp. Digest, 1972, pp. 221-223.

[11] H. Hofmann, 'Dispersion of planar waveguides for millimeter-wave application,' Arch. Elek. Übertraung., vol. 31, no. 1, pp. 40-44, Jan. 1977.

[12] J. B. Knorr and P. M. Shayda, 'Millimeter-wave fin-line characteristics,' IEEE Trans. Microwave Theory Tech., vol. MTT-28, pp. 737-743, July 1980.

[13] A. Beyer, 'Analysis of the characteristics of an earthed fin line,' IEEE Microwave Theory Tech., vol. MTT-29, pp. 676-680, July 1981.

[14] D. Mirshekar-Syahkal and J. B. Davis, 'An accurate, unified solution to various fin-line structures, of phase constant, characteristic impedance, and attenuation,' IEEE Microwave Theory Tech., vol. MTT-30, pp. 1854-1861, Nov. 1983.

[15] R. Vahldieck, 'Accurate hybrid-mode analysis of various finline configurations including multilayered dielectrics, finite metalization thickness, and substrate

holding grooves,' IEEE Trans. Microwave Theory Tech., vol. MTT-32, pp. 1454-1460, Nov. 1984.

[16] J. Bornemann and F Arndt, 'Calculating the characteristic impedance of finlines by transverse resonance method,' IEEE Trans. Microwave Theory Tech., vol. MTT-34, pp. 85-92, Jan. 1986.

[17] P. Espes, P. F. Combes, J. -M. Goutoule, and B Theron, 'Asymmetric finline for space applications using millimeter waves,' IEEE Trans Microwave Theory Tech., vol. MTT-37, pp.289-298, Feb. 1989.

[18] L. P. Schmidt, T. Itoh, and H. Hofmann, 'Characteristics of unilateral finline structures with arbitrarily located slots,' IEEE Trans. Microwave Theory Tech., vol. MTT-29, pp. 352-355, Apr. 1981.

[19] A. K. Sharma and W. J. R. Hoefer, 'Propagation in coupled unilateral and bilateral finl-lines,' IEEE Trans. Microwave Theory Tech., vol. MTT-31, pp. 498-502, June 1983.

[20] J. Bornemann, 'Rigorous field theory analysis of quasi planar waveguides,' IEE Proc. vol. 132, pt. H, no. 1, pp. 1-6, Feb. 1985.

[21] A. Biswas, and V. K. Tripathi, 'Analysis and design of asymmetric and multiple coupled finline couplers and filters,' IEEE MTT-S Int'l Microwave Symp. Digest, 1990, pp. 403-406, 1990.

[22] F. C. de Ronde, 'A new class of microstrip directional couplers,' IEEE MTT-S Int'l Microwave Symp. Digest, 1970, pp. 184-186.

[23] H. Callsen and L. P. Schmidt, 'Quaisplanar 3 dB hybrid for millimeter-wave integrated circuits,' Electron. Lett., vol. 18, pp.161-163, 1982.

[24] R. Hoffmann and J. Sigel, 'Microstrip-slot coupler design - part I: S-parameters of uncompensated and compensated couplers,' IEEE Trans. Microwave Theory Tech., vol. MTT-30, pp. 1205-1210, Aug. 1982.

[25] T. Tanaka, K. Tsunoda and M. Aikawa, 'Slot-coupled directional couplers on a both-sided substrate MIC and their applications,' IEEE Trans. Microwave Theory Tech., Electronics and Communications in Japan, pt. 2, vol. 72, no. 3, pp. 91-99, 1989.

[26] M. -F. Wong, V. F. Hanna, O. Picon, and H. Baudrand, 'Analysis and design of slot-coupled directional couplers between double-sided substrate microstrip lines,' IEEE Trans. Microwave Theory Tech., vol. 39, pp. 2123,2129, 1991.

[27] M. Schoenberger, A. Biswas, A. Mortazawi, and V. K. Tripathi, 'Coupled slot-strip coupler in finline,' IEEE MTT-S Int'l Microwave Symp. Digest, 1991, pp.751-753.

[28] T. Itoh and A. S. Hebert, 'A generalized spectral domain analysis for coupled suspended microstriplines with tuning septums,' IEEE Trans. Microwave Theory Tech., vol. MTT-26, pp. 820-826, Oct. 1978.

[29] S. Luo, M. Thorburn, and V. K. Tripathi, 'Modelling of multiple coulped concentric open and closed microstrip ring structure,' IEE Proc.-H, vol. 138, pp.573-576, Dec. 1991.

[30] T. Itoh, Ed., *Planar Transmission Line Structures.* New York: IEEE Press, 1987.

[31] R. H. Jansen, 'Unified user-oriented computation of shielded, covered and open planar microwave and millimeter-wave transmission-line characteristics,' IEE Proc.. Microwave, Opt. Acoust., vol. 3, pp. 14-22, Jan. 1979.

[32] V. K. Tripathi and H. Lee, Spectral-domain computation of characteristic impedances and multiport parameters of multiple coupled microstrip lines,' IEEE Trans. Microwave Theory Tech., vol. 37, pp.215-221, Jan. 1989.

[33] V. K. Tripathi and A. Biswas, 'Coplanar and broadside coupled finline six port hybrids,' Proc. 20th Europ. Microwave Conf., 1990, pp.1033-1038.

[34] V. K. Tripathi, 'Asymmetric coupled transmission lines in an inhomogeneous medium,' IEEE Trans. Microwave Theory Tech., vol. MTT-23, pp. 734-739, 1975.

[35] V. K. Triapthi, 'On the analysis of symmetrical three-line microstrip circuits,' IEEE Trans. Microwave Theory Tech., vol. MTT-25, 726-729, Sept. 1977.

[36] R. Mittra and S. W. Lee, *Analytical Techniques in the Theory of Guided Waves.* New York: Macmillan, 1971.

[37] L. -P. Schmidt and T. Itoh, 'Characteristics of a generalized finline millimeter wave integrated circuits,' Int'l J. of Infrared and Millimeter Waves, vol. 2, pp. 427-436, 1981.

[38] A. Beyer, D. Kother, and I. Wolff, 'Development of a coupler in fin-line modulator,' IEEE MTT-S Int'l Microwave Symp. Digest, 1985, pp. 139-143.

[39] E. Kpodzo, K. Schunemann, and G. Begemann, 'A quadriphase fin-line modulator,' IEEE Trans. Microwave Theory Tech., vol. MTT-28, pp. 747-752, July, 1980.

[40] D. J. Gunton and E. G. S. Paige, 'An analysis of the general asymmetric directional coupler with non mode inverting terminations,' IEE Proc. Microwave, Opt. Acoust., vol. 2, pp. 31-36, Jan. 1978.

[41] V. K. Tripathi and Y. K. Chin, 'Analysis of the general nonsymmetric directional coupler with arbitrary terminations,' IEE Proc. -H, vol. 129, no. 6, pp. 360-362, Dec. 1982.

[42] J. Choma, Jr., *Electrical Networks.* New York: Wiley, 1985.

[43] R. K. Hoffmann and J. Siegl, 'Microstrip-slot coupler design - part II: practical design aspects,' IEEE Trans. Microwave Theory Tech., vol. MTT-30, pp. 1211-1216, Aug. 1982.

[44] L. -P. Schmidt, 'A comprehensive analysis of quasiplanar waveguides for millimeter-wave application,' Proc. 11th Europ. Microwave Conf., 1981, pp. 315-320.

[45] M. Aikawa and H. Ogawa, 'Double-sided MIC's and their applications' IEEE Trans. Microwave Theory Tech., vol. 37 pp. 406-413, Feb. 1989.

[46] C. Nguyen, 'Broadside-coupled coplanar waveguides and their end-coupled band-pass filter applications,' IEEE Trans. Microwave Theory Tech., vol. 40, pp.2181-2189., Dec. 1992.

[47] S. Luo and V. K. Tripathi, 'Crosstalk reduction in coupled interconnects with ground plane slots,' Proc. Progress in Electromagnetics Research Symp., July 1993.

[48] V. K. Tripathi and J. B. Retting, 'A SPICE model for multiple coupled microstrips and other transmission lines,' IEEE Trans. Microwave Theory Tech., vol. MTT-33, pp. 1513-1518, Dec. 1985.

[49] M. Karam, Y. Demers, Y. Xu, and R. G. Bosisio, 'Theory and design of wideband 3-dB suspended microstrip couplers with floating conductor,' Microwave Opt. Tech. Lett., vol. 3, pp. 181-191, May 1990.

[50] S. I. Long and S. E. Butner, *Gallium Arsenide Digital Integrated Circuit Design.* New York: McGraw-Hill, 1990.

[51] S. Luo, J. M. Jong, and V. K. Tripathi, 'Spectral domain quasi-TE computation of the propagation characteristics of single and coupled interconnects with meshed ground plane,' accepted by IEEE 2nd topical meeting on Electrical Performance of Electronic Packaging (1993).